POTENTIAL OF WIND AND SOLAR ENERGY GENERATION OVER WEST AFRICA IN A CHANGING CLIMATE

BY

SAWADOGO WINDMANAGDA

(BSC, MSC)

MET/15/5749

A Thesis submitted in the Department of Meteorology and Climate Science, Earth and Mineral Sciences, in partnership with the West African Science Service Centre on Climate Change and Adapted Land Use (WASCAL), submitted to the School of Postgraduate Studies in partial fulfilment of the requirements for the award of Doctor of Philosophy in Meteorology and Climate Science of the Federal University of Technology, Akure, Nigeria

September 2019

DECLARATION

I hereby declare that this Thesis was written by me and is a correct record of my own research work. It has not been presented in any previous application for any degree of this or any other University. All citations and sources of information are clearly acknowledged by means of references.

Candidate's name: SAWADOGO Windmanagda

Signature: ……………………… Date: ………………………

CERTIFICATION

We certify that this Thesis entitled “Potential of Wind and Solar Energy Generation Over West Africa in a Changing Climate” is the outcome of the research carried out by SAWADOGO Windmanagda in the Department of Meteorology and Climate Sciences, the Federal University of Technology, Akure, Nigeria, in partnership with the West African Science Service Center on Climate and Adapted Land Use (WASCAL)

Supervisor’s Name: Prof. OKOGBUE Emmanuel Chilekwu

Signature: ……………………………… Date: ……………………………………….

Co-supervisor’s Name: Dr. ABIODUN Babatunde Joseph

Signature: ……………………………… Date: ……………………………………….

Head of Department: Prof. Balogun Ahmed

Signature: ………………………… Date: ……………………………………….

ACKNOWLEDGEMENTS

I gratefully acknowledge the scholarship and financial support provided to me by the Bundesministerium für Bildung und Forschung (BMBF), which is the Federal Ministry of Education and Research of Germany, through the West African Science Service Centre on Climate Change and Adapted Land Use (WASCAL).

I would like to express my thanks to my supervisor Prof. OKOGBUE Emmanuel Chilekwu for his advice, guidance as a father to write this thesis. I do appreciate his contribution and comments throughout this thesis.

I would also like to express my sincere gratitude to my co-supervisor Dr. Babatunde Joseph Abiodun who helped me to overcome the many challenges of my PhD journey and his excellent hospitality at the University of Cape Town, South Africa. Also, I learnt much from him during my visit.

I would like to express my appreciation to Prof Kehinde Ogunjobi, Director of the Graduate Research Program in West African Climate Systems (GRP-WACS) and Dr Vincent Ajayi, Deputy Director of the GRP-WACS and Dr Ademola Akinbobola Coordinator for their availability during the coursework and during the PhD fieldwork.

I also thank Prof. Ahmed Balogun the Head of Department of Meteorology and Climate Science for his suggestions, encouragement during my PhD research. I express profound gratitude to all lectures at the Department and the panel for their valuable contribution to this thesis during my progress report.

My regards go to Dr. Savadogo Moumouni, Executive Director of WASCAL and all the WASCAL staff in Accra for providing all requests and information regarding my scholarship. I deeply thank Dr. Bamba Sylla, Senior scientist at the WASCAL Competence Center in Ouagadougou, Burkina Faso for advices and suggestions for this thesis title.

My regards also go to the Climate System Analysis Group (GSAG) at the University of Cape Town, South Africa for hosting me during my visit. I take this opportunity to thank Mr. Phillip Mukwenha for its assistance in installing the climate tool software on my computer and troubleshooting computer issues for me. Also, I thank all the students belonging to CSAG, especially to Myra Naik, Michelle Gore, Mariam Nguvava, Koketso Molepo, and Sabina Omar, Roland Taking for their inputs during the "Tuesday Peer Review Meeting" of this work.

We thank the meteorological agencies of Burkina Faso and Ghana for providing the station data, CORDEX project for giving access to the simulation data, and ECMWF for providing the reanalysis data. The computing facilities were provided by the Climate System Analysis Group (CSAG) at University of Cape Town (UCT, South Africa) and the Computation Centre for High Performance Computing (CHPC, South Africa).

.

I also thank my GRP-WACS fellows – Naomi Kumi, Abdoulaye Ballo, and Abdoulatif Bonkaney who were with me in Cape Town, for their moral support and the social life in Cape Town. I thank also the Anhouse's warden Carol Hatley who has been more than a grandmother to me during my stay in Anhouse.

My regards to other GRP-WACS colleagues – Aissatou Faye, Alima Dajuma, Ezekiel Imoleayo Gbode, Ifeanyi Achibu, Mayeul Quenum and Abel Akammah.

My appreciation to Dr Ulrich Diasso, Dr Romaric Odoulami and Dr Michel Nikiema for their moral support, expertise and contribution to this thesis.

My gratitude to my family – Timbila Sawadogo, Jean-Baptiste Sawadogo, Pascaline Sawadogo, Abel Bagamzanre and Josue Bagamzanre for their prayers for me to achieve this PhD. Also, I am deeply grateful to my wife Aoua Traore who had to endure my absence during my PhD; I thank her for her moral support, motivations and prayers.

Above all, I thank the Almighty for what He has done for me for this thesis.

DEDICATION

To my lovely and wonderful wife TRAORE Aoua and my family

ABSTRACT

Many West African countries are plagued with a poor electricity supply. However, an abundance of solar irradiance and sufficient wind speed over the region makes solar and wind energy attractive solutions to the problem, but there is a dearth of information on how ongoing global warming may alter the solar energy potential and wind power density over the region in the future. Moreover, there is a lack of information on how accurately numerical weather prediction models simulate the shortwave radiation flux over the region. This study thus investigates, on the one hand, the impact of climate change on photovoltaic power generation potential (PVP) and on wind power density (WPD) over West Africa under various global warming levels (1.5°C; 2.0°C; 2.5°C and 3.0°C) under the RCP8.5 climate change scenario. On the other hand, this study assesses the shortwave radiation flux over West Africa.

For the PVP study, fourteen regional climate model simulations from the Coordinated Regional Climate Downscaling Experiment (CORDEX) were analysed. Eleven multi-model multi-ensemble simulation datasets, also from the CORDEX project, were analysed for the WPD study. The model simulations for the reference climate (1971-2000) were compared with surface wind speed from weather stations data: Accra (1986 - 2000), Bobo-Dioulasso (1986 - 2016), Ouagadougou (1986 - 2016) and Tamale (1986 - 2000) and two examples of reanalysis data (ERA-INTERIM and ERA20C). In addition, this study also investigated how the Weather Research and Forecasting (WRF) model radiation schemes (Cam, Dudhia, Goddard, New Goddard and rrtmg) simulate the surface downwelling solar radiation (Rs) over West Africa. We modified the Dudhia shortwave radiation physics by making the water vapour absorption varies with temperature and pressure according to levels. Furthermore, we run a short-term simulation (one-year) with WRF different shortwave radiations schemes and a long-term simulation (thirty-years) with the WRF Dudhia shortwave radiation scheme and the modified one. All the WRF output were compared with satellite data (SARAH).

The results show that the CORDEX simulation ensemble correctly captures the spatial distribution of climate variables (surface downwelling solar radiation, air temperature, wind speed and relative humidity) and PVP over West Africa, albeit with a few biases. The simulations and observations agree that PVP over West Africa varies from 8% along the Guinean zone to 25% over the Sahel zone and that the annual cycle of PVP is influenced by the seasonal variation of the monsoon system. The simulation ensemble projects a decrease (up to 3.8%) in PVP over West Africa in the future and indicates that the magnitude of the decrease grows with warming levels. The decrease in PVP is attributed to a decrease in Rs (solar dimming; up to 3 W/m^2) and an increase in ambient temperature (up to 3.5°C) induced by global warming. A decrease in projected PVP is also projected over all the West African countries. Nevertheless, the spatial and temporal distribution of the PVP changes are more influenced by Rs changes than by Ts changes, such as at GWL1.5, an increase in PVP is projected over all zones during the rainy season when an increase in Rs is projected. A decrease in projected PVP is also projected over all the countries. Nevertheless, the maximum decrease in PVP projected over any country or zone in the region is less than 3.8% even at GWL3.0. Hence, the study suggests that ongoing global warming may have an influence on PVP over West Africa.

Additionally, the results show that the model ensemble's mean gives a good simulation pattern of wind speed and WPD with high correlation values ($r = 0.9$ and $r = 0.95$ respectively) over West Africa, although it tends to overestimate them. In agreement with the reanalysis approach, the models indicate that the strongest winds and largest WPD are found in the Sahel zone, especially around Dakar. However, while the regional climate models (RCMs) show that 87% of the cities are viable for potential wind power generation in the historical climate, the reanalysis indicates that only four cities in the Sahel are suitable for it with a threshold of 39.2 W/m^2. The RCMs project an increase in monsoon wind speed and wind power potential over West African cities, and the magnitude of this increase grows with increasing global warming levels. Nevertheless, the increase is not sufficient to make the cities in the Guinean and Savannah zones viable for wind power generation in the warmer climate due to the small increase of surface wind speed over the region.

The study found that, for the short-term run, most of the different WRF shortwave radiation schemes simulate well the observed Rs over West Africa and its three different zones (Guinea, Savannah and Sahel). However, the Dudhia scheme performs better than the other schemes in simulating the Rs over Wes Africa with low mean square error (Cam, 100 W/m^2; Goddard, 99 W/m^2; New Goddard, 90 W/m^2; rrtmg, 80 W/m^2 and Dudhia, 61 W/m^2). Nonetheless, the modified Dudhia (DudhiaM) with the parameter n equal to 1 improves the simulation of the Rs over the region with a low mean square error of 45 W/m^2. The DudhiaM captures well the diurnal and annual variation of the observed Rs. Additionally, the long-term simulations (25 years) of the seasonal average and the annual average of the DudhiaM performs well than the Dudhia scheme in simulating the observed Rs over West Africa. The bias between the DudhiaM (3.21

W/m^2) and the observed are lower than the WRF Dudhia scheme (22.27 W/m^2) over West Africa. The DudhiaM also outdoes the Dudhia scheme in simulating the inter-annual variability, the annual cycle of the observed Rs over West Africa.

The results of this study show that most of the West African cities are not viable for wind energy in the present and future climate. We also showed the West Africa region has the potential to generate solar energy with the PV technology. However, the impact of global warming may reduce the potential but, this decrease in PVP may affect electricity production from the PV technology. Though, the results of the study may guide policymakers on how to harness wind power energy and photovoltaic (PV) power in order to meet the electricity demands of West Africa in the future.

TABLE OF CONTENT

CHAPTER FIVE: CONCLUSION AND RECOMMENDATIONS 148

LIST OF TABLES

LIST OF FIGURES

LIST OF ACRONYMS

AEJ	African Easterly Jet
AEWs	African Easterly Waves
AFWA	Air Force Weather Agency
AGL	above the ground level
AM	air mass
ARW	Advanced Research WRF
CAL	Cloud Albedo
COP	Conference of Parties
CFSR	Climate Forecast System Reanalysis
CM SAF	Satellite Application Facility on Climate Monitoring
CMIP5	Climate Model Intercomparison Project phase 5
CORDEX	Coordinated Regional Climate Downscaling Experiment
CRU	Climatic Research Unit
CSP	concentrated solar power
DJF	December–January–February
DNI	Direct normal irradiance
DOE	Department of Energy
ECMWF	European Centre for Medium-Range Weather Forecasts
ECOWAS	Economic Community of West African States
ECREEE	ECOWAS Centre for Renewable Energy and Energy Efficiency
EMC	Environmental Modeling Center
ERAINT	Era-Interim
ERA-20C	Era-Interim twentieth century
ESRL	Earth System Research Laboratory
FAA	Federal Aviation Administration
FPAR	Fraction of Photosynthetically Active Radiation
GFDL	Goddard Fluid Dynamics Laboratory
GCMs	General Climate Models
GFS	Global Forecast System
GHG	greenhouse gas
GHI	Global Horizontal Irradiance

GMT	global mean temperature
GODAS	global ocean data assimilation system
GWL	global warming level
ICOADS	International Comprehensive Ocean Atmosphere Data Set
IEA	International Energy Agency
IPCC	Intergovernmental Panel on Climate Change
ISPD	International Surface Pressure Databank
ITCZ	Intertropical Convergence Zone
JJA	June–July–August
LPG	liquefied petroleum gas
MAE	mean absolute error
MAM	March–April–May
MCSs	mesoscale convective systems
MM5	mesoscale model version 5
MODIS	Moderate Resolution Imaging Spectroradiometer
MOM3	Modular Ocean Model, version 3
MVIRI	Meteosat Visible and InfraRed Imager
NCAR	National Center for Atmospheric Research
NCEP	National Centers for Environmental Prediction
NMM	Nonhydrostatic Mesoscale Model
NOAA	National Oceanic and Atmospheric Administration
NWP	Numerical Weather Prediction
PBL	Planetary Boundary Layer
PNNL	Pacific Northwest National Laboratory
PSU	Pennsylvania State University
PV	photovoltaic
PVP	photovoltaic power generation potential
RCP	Representative Concentration Pathway
RCM	regional climate model
RE	renewable energy
RMSE	root mean square error
RRTMG	Rapid Radiative Transfer Model for GCM
SARAH-2	Surface Solar Radiation Data Set – Heliosat Edition 2
SDI	Surface Direct Irradiance

SDU	Sunshine Duration
SEVIRI	Spinning Enhanced Visible and Infrared Imager
SIS	Surface Incoming Shortwave radiation (Rs),
SON	September–October–November
SRES	Special Report on Emission Scenarios
SRI	Spectrally Resolved Irradiance
SST	sea surface temperature
STC	standard test conditions
SW	shortwave
TEJ	Tropical Easterly Jet
TREIA	Texas Renewable Energy Industry Alliance
UNFCCC	United Nations Framework Convention for Climate Change
UTC	Universal Time Coordinated
USGS	United States Geological Survey
WAM	West African Monsoon
WPD	wind power density
WRF	Weather Research and Forecasting
WSM	WRF single-moment

CHAPTER ONE: INTRODUCTION

1.1 Background

The second Assessment Report of the United Nations' Intergovernmental Panel on Climate Change (IPCC) in 1995 suggests that human activities are having a discernible impact on the world's climate. Based on that conclusion, many studies have been carried out to show the influence of human activities on the global climate (Dale, 1997; Smithers and Smit, 1997; Vitousek *et al*., 1997). In 2001, the third report of the IPCC confirmed that the climate is indeed changing due to human activities. The rate of such climate change in recent years has raised a red flag among researcher communities and led to a call to policymakers and politicians to take action to mitigate climate change. Most scientists believe that it is a consequence of greenhouse gas (GHG) emissions into the atmosphere (Oreskes, 2004), which contribute to the increase in the global mean temperature (GMT). During the last decades, the amount of GHGs has increased, especially in the case of carbon dioxide (CO_2), which is the highest amount of GHG emitted (Figure 1.1 a). For instance, the amount of CO_2 has increased by an average of 1.81 ppm per year over the past 39 years (1979 - 2017), against an average of about 1.6 ppm per year in the 1980s and 1.5 ppm per year in the 1990s; even worse, of growth rate of CO_2 emissions increased to 2.2 ppm per year during the last decade (2008 - 2017) (NOAA, 2018). To save the planet, the Conference of Parties (COP) of the United Nations Framework Convention for Climate Change (UNFCCC), meeting in Paris in 2015, has agreed to limit the increase of GMT (i.e. through a reduction of CO_2) to 2°C above pre-industrial levels and even further to 1.5°C (UNFCCC, 2015). To achieve this objective, the parties of the Paris Agreement must reduce the carbon footprint, mainly of the energy sector.

About 86% of primary power consumption of the world comes from fossil fuels, with oil accounting for 36%, coal for 23% and natural gas for 27% and the remaining of the primary power consumption hails from renewable energy (Abas *et al*., 2015). Moreover, the burning of oil, coal and natural gas for electricity and heat production are the major contributor (25%) to human-made GHG emissions; deforestation and agriculture (24%) are the second largest contribution to the increase of GHG (Figure 1.1 b). The release of CO_2 into the atmosphere is a result of the combustion of fossil fuel. There is no doubt that the burning of fossil fuels contributes to climate change and its impact is well known. In addition, there is a relationship between energy-related carbon emissions and urbanisation through infrastructure expansion (Madlener and Sunak, 2011; Wang *et al*., 2016). Currently, the population of the world is about 7.53 billion (The World Bank, 2018b); this is estimated to grow to 9 billion by 2050, and projected to reach 10 billion by 2100 (Lee, 2011). The increased population will contribute to greater CO_2 emissions into the atmosphere. From 1900 to 2014, the CO_2 emissions from fossil fuels increased significantly (Figure 1.2). This increase is attributed to industrialisation process, which has contributed about 78% of the total GHG emission from 1970 to 2011 (Boden *et al*. 2017). According to the International Energy Agency (IEA), it is expected to increase from 32.53 gigatonnes to 36 gigatonnes by 2040. However, climate change mitigation should not prevent us from using energy, because energy is the foundation of socio-economic development of any country. For this reason, the world needs another industrial revolution, albeit one in which our sources of energy are clean, accessible, affordable, and sustainable.

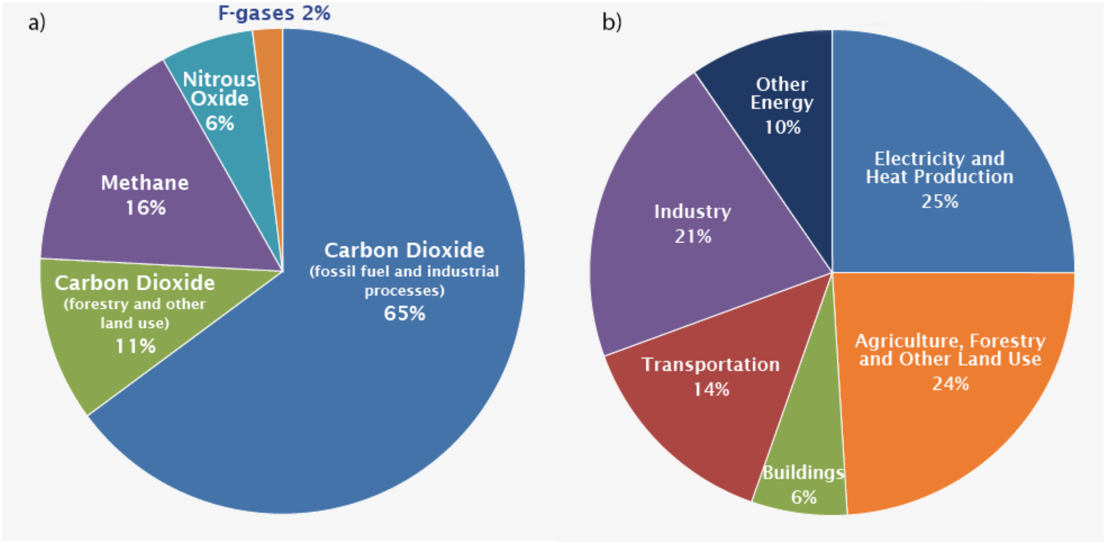

Figure 1.1: Global greenhouse gas emissions: (a) by type of gas; (b) by source (Edenhofer, 2015)

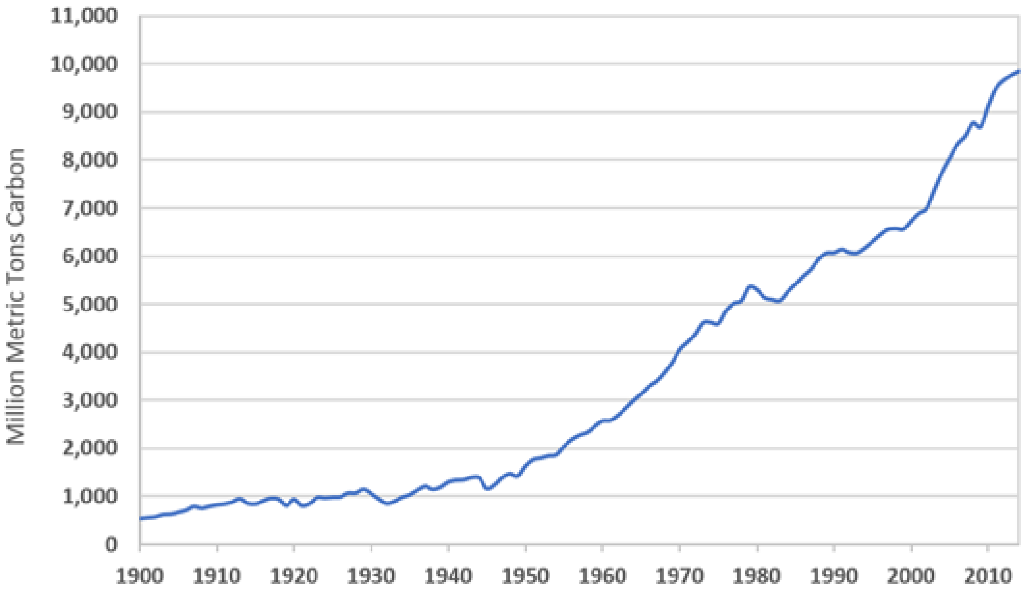

Figure 1.2: CO_2 emissions from fossil fuels from 1900 to 2014 (Boden *et al*., 2017)

Renewable energy is the best alternative form of energy for climate change mitigation. According to the Texas Renewable Energy Industry Alliance (TREIA), we can define renewable energy as: "Any energy resource that is naturally regenerated over a short time scale and derived directly from the sun (such as thermal, photochemical, and photoelectric), indirectly from the sun (such as wind, hydropower, and photosynthetic energy stored in biomass), or from other natural movements and mechanisms of the environment (such as geothermal and tidal energy). Renewable energy does not include energy resources derived from fossil fuels, waste products from fossil sources, or waste products from inorganic sources" (Walker and Swift, 2015, page 475). Moreover, renewable energy does not produce any harmful effects to the environment, unlike fossil fuel. Even though renewable energy is regarded as clean energy, there is a long road to its implementation for widespread energy generation. Currently, it makes up less than 17% of the total energy demand per person, and this percentage has only increased by 1.5% over the last 20 years until 2012 (Can Şener *et al*., 2018) because renewable technologies have not been fully developed or matured yet. Among the renewable sources of energy, hydropower and biomass remain the ones most used in developing countries. However, solar and wind energy are become competitive to hydropower and fossil fuel due to their advanced technology and low cost since the last decade. Therefore, there is a need for the West African region to start investing in the wind and solar energy.

1.2 Energy situation in West Africa

The energy situation in West Africa is built on two major sources, namely, biomass (78%) and fossil fuel (21%), with renewables making up only 1% (Figure 1.3). Traditional biomass in the form of wood is the main source of energy, accounting for

78% of total energy consumed, mainly for cooking. In the urban areas, charcoal remains the principal fuel despite the promotion of liquefied petroleum gas (LPG), while firewood is predominately used in the rural areas (Vilar, 2012). Fossil fuel (crude oil, natural gas) accounts for 21% of the energy sources in the region. At the end of 2013, the proven reserves were 65 billion barrels of oil and 5 trillion cubic metres of natural gas (IEA, 2017), which means that fossil fuel offers an important economic benefit for the region. Furthermore, in 2013, fossil fuel contributed to 70% of the electricity supply. Hydropower also contributed to 30% of electricity generation in the same year (ECREEE, 2016).

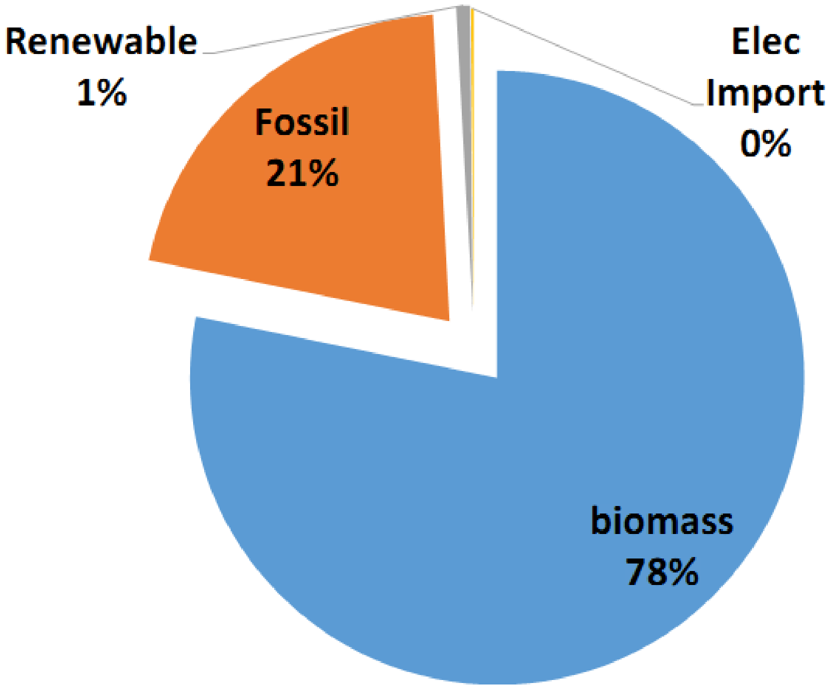

Figure 1.3: Energy sources in West Africa (ECREEE, 2013)

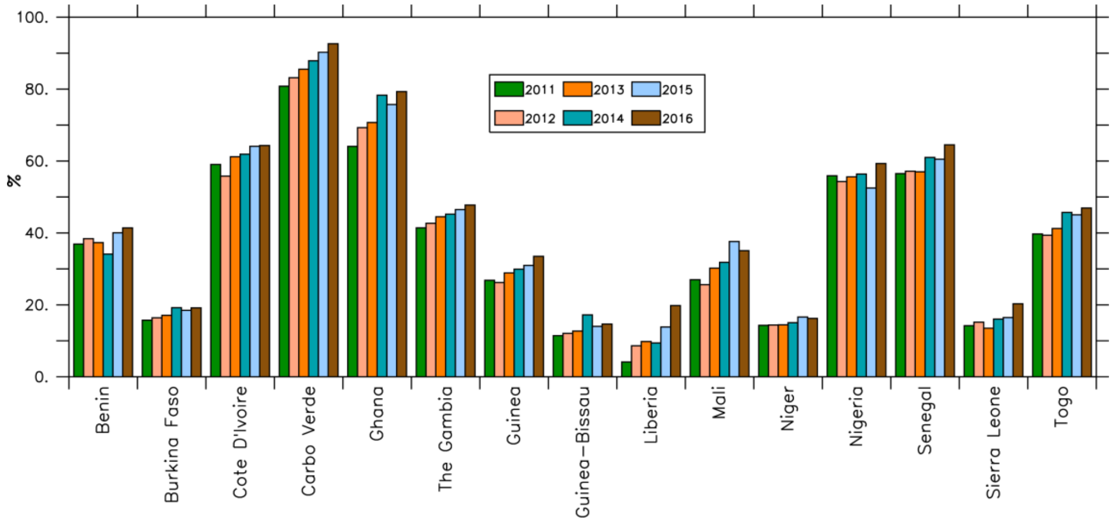

Figure 1.4: Electricity access in West Africa countries from 2011 to 2016. Data taken from (The World Bank, 2018a).

However, access to electricity remains a big challenge for most of the West African countries, with an average shortage of up to 80 hours per month and the region has the costliest kilowatt-hour of electricity ($0.25) in the world (The World Bank, 2018c). For example, more than 40% of the population in Nigeria (the most populous country in Africa) has no access to electricity (IEA, 2017). Similarly, in Senegal, more than 40% of the population are without electricity. The percentage is even higher in countries like Liberia, Sierra Leone, Niger and Burkina Faso (i.e. about 80%) (Figure 1.4). In some countries, like Ghana and Cape Verde, access to electricity is improving. The main reason for this lack of access is poor electricity production from hydropower and thermal power plants, which are the major sources of electricity generation in the region. Some hydropower plants have shut down due to a lack of water because of droughts. For instance, in 1998, the unavailability of water in the Akosombo Dam in Ghana led to electricity outages in Ghana as well as in neighbouring Togo and Benin. The same thing happened in Nigeria in 2001, when the largest dam in the country (the Kainji Dam) experienced drought. This was also a recurring problem in Senegal, Mali, and Guinea for several many years (Gnansounou, 2008). The West African countries that generate their electricity from thermal power such as Burkina Faso, Mali and Niger also experience power cuts due to difficulties with fuel procurement because there are inland countries (ECREE, 2013; Gnansounou, 2008). Poor access to electricity and lack of electricity affects the regional economies. Therefore, West African countries need to improve their electricity supply and their populations' access to electricity by using more reliable energy sources to produce electricity.

Renewable energy is seen as a more reliable energy source than fossil fuels and biomass, and one that can potentially provide a better quality of life for millions of people (Vilar, 2012). West Africa is blessed with abundant renewable resources, such as solar, wind, biomass. Nonetheless, the region still faces ongoing challenges with regard to meeting electricity demand. In 2010, in order to ensure the socio-economic development of the region, the Economic Community of West African States (ECOWAS) member states put in place a regional ECOWAS Centre for Renewable Energy and Energy Efficiency (ECREEE) to promote renewable energy and energy efficiency. ECREEE is also an institution that seeks financial support for renewable energy and energy efficiency projects throughout the region among project promoters, financial partners and potential investors (Vilar, 2012). To ensure trust between local and international investors in the energy sector, ECREEE developed an observatory for renewable energy and energy efficiency called ECOWREX in 2012 in other to obtain and share reliable and updated high-quality energy information and knowledge about energy systems and potential renewable energy resources in West Africa (ECREEE, 2013). Both institutions are contributing to improving access to energy services and awareness of the use of renewable energy in the region.

1.2.1 Solar energy

West Africa has significant solar resource potential for solar energy application. It is one of the sunniest regions in the world, with a daily average solar radiation of about 5-6 kWh m^{-2} throughout the year (ECREEE, 2015). Hence, to harness the potential solar energy for electricity, various countries are now building solar power plants using PV technology, which is a widely deployed and much-used solar energy technology, to power households, buildings, street lights and community centres. For instance, at the end of 2017, Burkina Faso inaugurated one of the largest PV solar power plants in West Africa with 33 MW, and Senegal has an installed capacity of 50 MW electricity from

PV solar power. Like Burkina Faso, Ghana and Senegal, most of the West African countries have set targets to increase their electricity production with PV technology by 2020-2030 (Table 1.1). Their agenda aims to increase electricity production in other to meet the electricity demand. Currently, only Burkina Faso, Ghana and Senegal have an installed capacity of 33, 22.5 and 50 MW of PV power respectively. With the biggest population over the region and to increase electricity production, Nigeria targets an installed capacity of 8,050 MW by 2030.

Table 1.1: Some West African countries with current PV power plant generation and their future targets.

Country	Installed capacity (MW)			References
	Current	2020	2030	
Benin	0	85	250	(ECREEE, 2016b)
Burkina Faso	33	65	205	(USAID, 2018a; SE4ALL, 2015)
Côte D'Ivoire	0	130	426	(ECREEE , 016h)
Gambia, The	0	15	35	(ECREEE, 2016a)
Ghana	22.5	200	500	(ECREEE, 2016f)
Guinea	0	100	500	(ECREEE, 2016e)
Guinea Bissau*	0	19	72	(ECREEE, 2017)
Liberia*	0	75	150	(ECREEE, 2016b)
Mali	0	308	528	(ECREEE, 16d)
Nigeria	0	2050	6000	(ECREEE, 2016c)
Niger	0	60	150	(ECREEE, 2016i)
Senegal	50	257	400	(ECREEE, 2016k; USAID, 2018)
Sierra Leone*	0	650	1200	(ECREEE, 2016d)
Togo	0	45	68	(ECREEE, 2016k)

Note: Those countries with * include other sources of renewable energy (wind and hydropower).

1.2.2 Wind energy

Unlike solar energy, wind energy is not well developed in West Africa. However, there is significant potential for wind power in the region. According to Vilar *et al*. (2012), the wind power potential in West Africa is especially strong in the coastal areas (Cape Verde, Senegal, and The Gambia). Moreover, some countries like Ghana, Mali and Nigeria are also viable for wind power projects. The potential of other countries with regard to wind power is not negligible but needs more investigations. ECREEE has also set a target to increase the electricity production in the region through wind power. For instance, by 2020, 318 MW of wind power will be added to the installed capacity of the region and by 2030, a further 993 MW (ECREEE, 2013).

1.3 Statement of the research problem

Renewable energy is the best option for alternative energy towards climate change mitigation. It does not include energy resources derived from fossil fuels, waste products from fossil sources, or waste products from inorganic sources (Ellabban et al., 2014). Though, its implementation for energy generation remains a long road to do. It shares less than 17% of the total energy demand per person and this percentage has only increased by 1.5% in 20 years (Şener et al., 2018). Apart from climate change mitigation, renewable energy technologies can contribute to energy security and development grows of a country. Among the renewable energy sources, solar and wind energy has been proposed to be the best energy option because it is not exhaustible and is abundant. It is in this perspective, the agenda of most of the West African countries have adopted the use of solar energy in their energy mix. However, solar and wind energy depend mainly on solar irradiation and surface wind speed respectively. So, any changes in those variables the future climate may alter their efficiency. In respond to that, our study examines the impact of climate on wind and solar energy over the West Africa region. We consider only the representative concentration pathway 8.5 (RCP 8.5) climate change scenario to project the possible changes in solar and wind energy under different warming levels over West Africa.

1.4 Justification of the study

The need to mitigate the impacts of climate change in relation to various socio-economic activities has led the UNFCCC to draft an agreement called the Paris Agreement. This aims to reduce the global carbon footprint and keep the GMT to 2°C, and perhaps even lower to 1.5°C, above the pre-industrial level (UNFCCC, 2015). Following the Paris Agreement where 195 UNFCCC members have signed the agreement by March 2019, the use of renewable energy becomes necessary to lower CO_2 emissions into the atmosphere. Apart from reducing climate change, renewable energy technologies can contribute to energy security and development growth. Solar and wind energy are the dominant sources of renewable energy, with advanced technologies and their relatively low costs making them competitive in relation to conventional energy sources. For this reason, most West African countries have adopted the use of solar and wind energy in their energy mix. For instance, the ECOWAS member states have decided to invest about 1,773 Million Euros in solar PV and 1,540 Million Euros in wind energy for electricity generation by 2030 to reduce the gap of access to electricity in the region (ECREEE, 2015). Unfortunately, however, climate change may affect the power output of those new energy sources.

Climate change may affect the PV power generation potential (hereafter PVP) and wind energy density (henceforth WPD) over the West African region. So far, no studies have investigated the impact of climate change on wind energy over West Africa, but a few studies have shown that climate change may reduce the PV power potential over the subcontinent (Huber et al., 2016; Bazyomo et al., 2016). Nevertheless, none of the previous studies have looked at the impact of climate change on PV power potential at specific global warming levels (GWLs). To obtain robust information for the implementation of the Paris Agreement, Hulme (2016) has advocated for more studies quantifying and comparing the impacts of global warming at 1.5 and 2°C GWLs. Furthermore, Bazyomo *et al*. (2016) projections are based on simulations from a regional climate, whereas robust information for policymakers requires multi-model multi-ensemble simulations. In addition, for accurate solar radiation forecasting, there is a dearth of information on the impact of different Weather Research and Forecasting (WRF) model radiation schemes to simulate the downward shortwave radiation (Rs) over the West African region.

The present study contributes to an understanding of how the increase in GMT may affect the potential of wind and solar energy under the different GWLs. It is envisaged that the results of this study will guide policymakers, stakeholders, partners of ECREEE, and local and international investors in renewable energy in the region on how to design those resources according to future climate characteristics and to meet future requirements. Also, this study will show how the WRF model can be used to monitor the Rs for the existing solar power plant for better forecasting.

1.5 Aims and objectives of the study

The study aims to examine how global warming of 1.5°, 2°, 2.5° and 3°C above pre-industrial levels may change the characteristics of WPD and PVP over West Africa under the climate change scenario Representative Concentration Pathway 8.5 (RCP8.5) by using multi-model multi-ensemble simulations; it also aims to assess how well WRF model simulates the Rs radiation flux over West Africa.

In setting out to achieve the aims of this study, the specific objectives are:

i. To project the possible changes in wind energy potential over West Africa under the global warming level of 1.5°C and above;
ii. To ascertain the impact of global warming at specific levels on PV power generation potential over West Africa;
iii. To improve the Dudhia shortwave radiation scheme in WRF with regard to solar energy over West Africa.

1.6 Research questions

This study considers the projections of climate change on WPD and PVP, focusing specifically on the impact of GWLs of 1.5°, 2°, 2.5° and 3°C above pre-industrial levels, and investigating how well the WRF model simulates the solar radiation flux over West Africa. To carry out this study, we have addressed the following research questions:

i. How may the increase in global warming alter the future potential for wind energy for electricity generation in West Africa?
ii. What are the impacts of climate change at specific GWLs on PVP in West Africa?
iii. How may the modification of the WRF Dudhia scheme enhance the simulation of the Rs over West Africa?

1.7 Thesis structure

The thesis is composed of five chapters. The introduction forms Chapter 1. The second chapter reviews the literature associated with the West African climate systems and the impact of climate change on wind and solar energy. The different WRF radiation schemes are also reviewed in Chapter 2. In Chapter 3, the methodology of the study is carefully explained. The model used for the projections and the data used to evaluate those models are described in detail. The subsequent chapter (Chapter 4) presents the results, using graphs and maps, and discusses the findings. Chapter 4 also analyses and discusses the capability of the multi-model multi-ensemble simulations to simulate the present climate vis-à-vis the observation data. The projection of wind and PV potential over West Africa is shown as well. Finally, Chapter 5, the last chapter of this thesis, presents the conclusions and gives a summary of the thesis. Limitations of the study and some recommendations for future work are also stated.

Having introduced the main topic of this thesis, the impact of climate change at specific GWLs on WPD and PVP and how WRF model may be used to simulate the Rs over West Africa, the next chapter reviews some of the relevant literature in this area of study.

CHAPTER TWO: LITERATURE REVIEW

This chapter reviews previous studies on the impacts of climate change on wind and solar energy, also on the WRF model radiation schemes. Firstly, we review the West African climate system dynamics. Then, we review the status of the current PV technology and some meteorological variables that influence the solar PV cells. In the third section, we look at the development of wind energy and the impact of climate change on the potential use of wind energy. Lastly, we examine how prior researchers have investigated the influence of radiation schemes to simulate the Rs across the world.

2.1 West African climate system dynamics

The various sources of income of the population in West Africa are dependent on the annual climate in that region. The weather and climate of West Africa have a major impact on food production, water resources and health, as well as other economic sectors, such as power generation, transportation and fisheries (Parker et al., 2017). Prior research suggests that the West African climate is dominated by the monsoon flow, called generally the "West African Monsoon (WAM)" (Afiesimama *et al*., 2006; Ramel et al., 2006; Cornforth, 2012). The word 'monsoon' (meaning 'season') is generally associated with seasonal rain in the tropics (Hall and Peyrillé 2006). In other words, the WAM controls the rainfall system over a region. This makes the WAM the most important event in the seasonal cycle, and local agriculture and water resources can be greatly affected by the onset and the strength of the WAM. The onset of the WAM results from the thermodynamic contrasts between the land (i.e., the Sahara) and the ocean (i.e., the equatorial Atlantic) (Nicholson, 2013). Literature reviews show that the seasonal cycle of the WAM can be divided into two periods: summer rainfall (boreal summer) and winter drought (boreal winter) (Cornforth, 2012; Doherty *et al*., 2014). The rainy phase of the WAM occurs during the boreal summer when the region expects significant rainfall with a maximum in August in the Sahel zone (Sultan and Gaetani, 2016). The rainy season takes place during June and September according to Cornforth (2012), and between May and September according to Sylla *et al*. (2013).

In contrast, during the boreal winter, there is no rainfall in the northern part of the West African region, and only a limited amount of rainfall along the coast. Most importantly, the Sahara region is dominated by dry, warm and often dusty north-easterly Harmattan winds (Knippertz *et al*., 2008) (see Figure 2.1). The boreal winter is not clearly documented in the literature, perhaps because the WAM is too weak to bring moisture inland. However, during this period, the cold air from the Sahara can cause health problems for local people (Parker et al., 2017).

There have been numerous studies to investigate the mechanism of the WAM during the boreal summer. The study of Lavaysse *et al*. (2009) reports that, during the boreal summer, the Western Sahara becomes an area of intense heat and low surface pressures due to high insolation and low evaporation, a phenomenon known as a Saharan heat low. Around the eastern side of the low, we have the south-westerly monsoon flow (wet air), while on the western side, we have the north-easterly Harmattan (dry air) (Figure 2.1). The cyclonic circulation associated with the Saharan heat low tends to increase the south-westerly and north-easterly winds. The convergence of these two trade winds is called the Intertropical Convergence Zone (ITCZ) or tropical belt (Holton et al., 1971; Zhang et al., 2006; Nicholson, 2009). It moves gradually northward, following the movement of the sun (Ramel et al., 2006). This movement of the rain belt results in two rainy seasons per year in the south and one in the north.

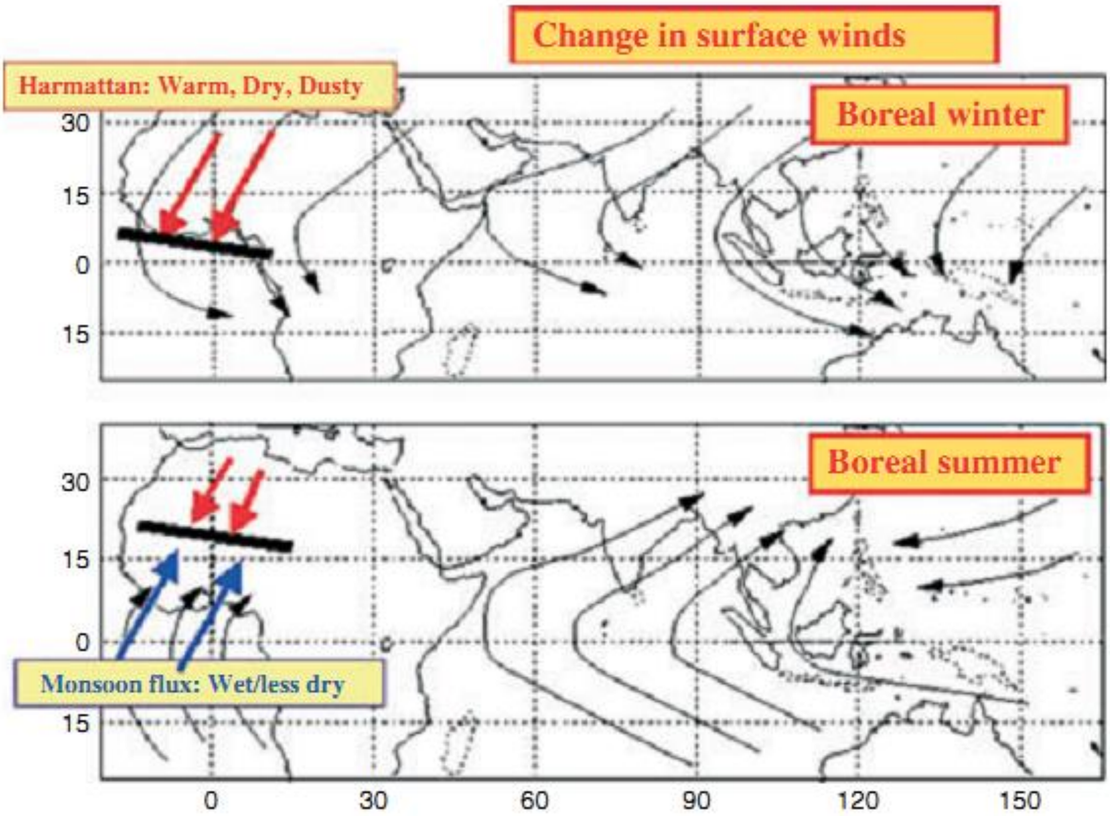

Figure 2.1: Schematic representation of the West African Monsoon (Cornforth, 2012)

A series of studies has identified the African Easterly Jet (AEJ) and the Tropical Easterly Jet (TEJ) as the key features of the WAM. The AEJ is defined as a region of strong zonal winds (up to ∼10 m/s) extending from East to West Africa, crossing the Atlantic Ocean, and located between 600 and 700 mb (Sylla et al., 2011) (see Figure 2.2). To understand the dynamics of the AEJ, Parker *et al*. (2005) used observed data from the JET2000 aircraft campaign during the last week of August 2000. Their study revealed that the thermodynamics of the structure of the AEJ can be categorised into two layers: the monsoon layer and the Saharan air layer. The monsoon layer is a humid zone connected to the land surface, extending northwards into the Sahel zone and increasing in depth towards the south, whereas the Saharan air layer can be seen as a layer of low static stability and low potential vorticity and also connected adiabatically to the land surface (Parker et al., 2005). Early studies have shown that the vertical shear of the AEJ is a key feature in the development of the mesoscale convective systems (MCSs) (Houze and Betts, 1981) and the development of the African Easterly Waves (AEWs) through its potential-vorticity and low-level-temperature contrasts (Burpee, 1972). AEWs can be seen as the disturbances around the EAJ. Diedhiou *et al*. (1998) have found that the AEWs are the main process involved in organising rainfall patterns over West Africa. The other feature, the TEJ, is also a zonal wind located in the upper troposphere near 150 mb (Figure 2.2). It has also been established that the TEJ plays an important role in the rainfall variability of the West African region (Nicholson and Grist, 2001).

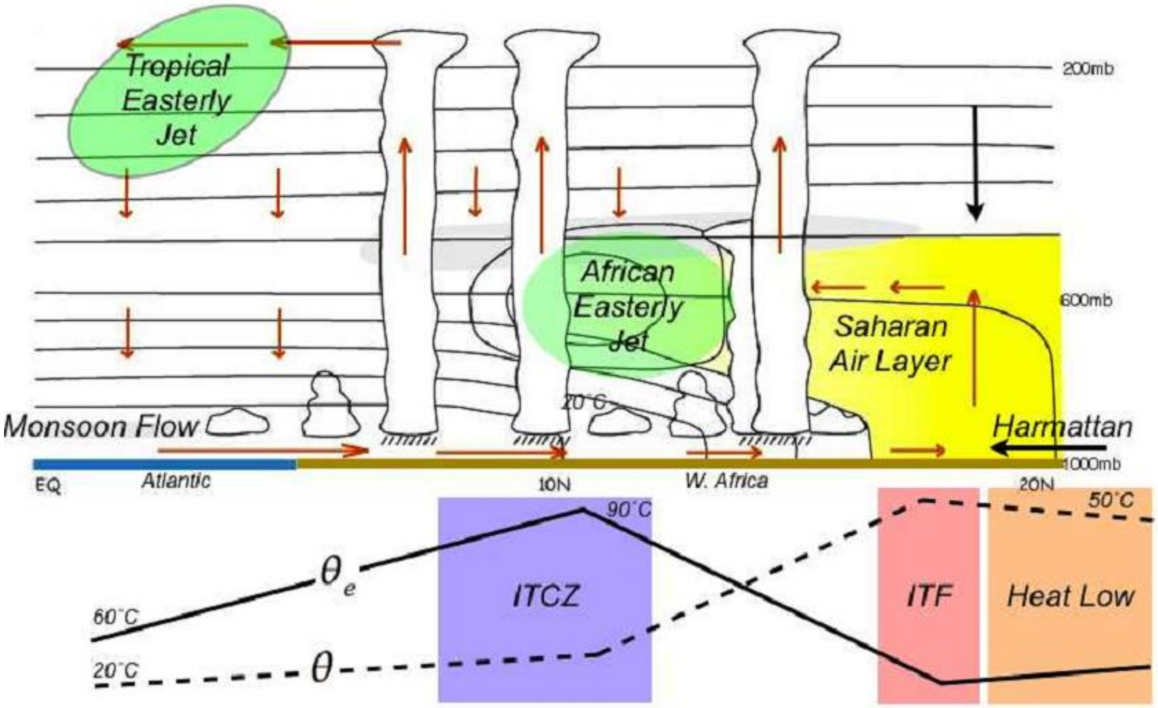

Figure 2.2: Schematic latitudinal section showing elements of a fully developed West African Monsoon, with typical meridional profiles of and θ_e and θ (Hall and Peyrillé, 2006).

2.2 Wind energy

In this sub-section, we review the historical background of the wind power and then review the impact of climate change on wind power potential over some regions of the world.

2.2.1 Historical background

The power of the wind has been exploited for at least the past 3000 years (Ackermann and Söder, 2000). The first application of using wind was for boat navigation on the Nile river around 5000 BC. After many centuries (by 700 BC), windmills with a horizontal axis for grinding grain and pumping water appeared in China and Persia (Hewson, 1975). Between the 12th and 19th centuries, the performance of the windmill was constantly improved in Europe and was widely used until at the end of the 19th century. The height of the typical European windmill at that time was about 30m, and it had a rotor with a diameter of 25 m. This new windmill could moreover drain lakes and marshes (Ackermann and Söder, 2000).

Professor James Blyth at Anderson's College in Glasgow built the first windmill for electricity production in the late 1880s (Price, 2005). He was able to power his home for many years. In 1888, in order to generate electricity at a larger scale, Charles F. Brush built a windmill in his backyard. He designed it with a rotor of 17m in diameter and with a height of 60 feet, and he was able to store the electricity from the windmill in a battery. Unfortunately, only 12 kilowatts were generated by this windmill (Dodge, 2015). Three years later, in 1891, the first wind turbine was constructed by Danish scientist Poul La Cour to generate electricity. Danish engineers subsequently improved the performance of this new device, which was used during World War I and II and to overcome energy shortages. The wind turbines built by the Danish company F.L. Smidth in Copenhagen in 1941 - 1942 can be considered a forerunner of modern wind turbine generators (Ackermann and Söder, 2000). The development of wind technology makes wind energy as the fastest growing renewable energy in the world. Since the last decades, various countries built their energy mix on wind energy. For instance, the largest operational onshore wind farm in the world is Gansu Wind Farm in China with a 6,800 MW and a target capacity of 20,000 MW by 2020. Among the European countries Germany remains the country with the largest installed capacity (45 GW), followed by Spain (23 GW), the UK (14 GW) and France (10 GW) (Konstantinidis and Botsaris, 2016).

2.2.2 Impact of climate change on wind energy potential

Several studies have discussed how ongoing global warming may alter winds speed and wind power potential over different regions of the world. For example, Tobin *et al*. (2015) projected a 5% increase in wind power over most European countries by the mid-century. Using EURO-CORDEX models, Davy *et al*. (2017) projected no changes in wind speed over the Black Sea. Silang *et al*. (2014) projected a 3% increase in wind speed and a 6% increase in wind power at 80 m over Phililla and Rizal in the Philippines. Rahim *et al*. (2012) projected a progressive increase in annual mean wind speed at a height ranging from 30 to 100 m in 2001 - 2099 in central Japan, while Breslow and Sailor (2002) projected a decrease in wind speed of 1.0 to 3.2% in the next 50 years and 1.4 to 4.5% over the next 100 years in the USA. Ren (2010) also projected a decrease in wind power over China in the period of 2071 to 2100. Fant *et al*. (2016) suggest a decrease in wind speed over South Africa. However, there is a dearth of information on how global warming may influence wind energy potential over West Africa in the future.

Most studies on projecting regional climate change over West Africa have focused only on rainfall and temperature (Diallo *et al*., 2012; Sylla *et al*., 2015; Sylla *et al*., 2016). Using CORDEX data, Sylla *et al*. (2016) predict a future increase in temperature, but also highlight uncertainties in precipitation changes over West Africa. Some studies (Abiodun *et al*., 2012; Monerie *et al*., 2013; Lee and Wang, 2014; Diallo *et al*., 2016) have explored the impacts of global warming on surface winds (e.g. monsoon flow). For example, over West Africa Abiodun *et al*. (2012) showed that global warming may enhance the monsoon flow because the land is projected to warm faster than the ocean; this may enhance the ocean-land temperature gradient that drives the West African monsoon flow. However, Abiodun *et al*. (2012) study only focuses on monsoon flow during the summer season, giving no information on how the flow may change in the winter period when the temperature gradient is reversed, or what over the annual changes may be. Also, the results of Abiodun *et al*. (2012) are only based on a single model simulation, whereas policy makers require robust information based on multi-model multi-ensemble simulations. Furthermore, it will be of interest to provide this information, especially as it relates to wind power potential, in the framework of the Paris Agreement of keeping global warming below 1.5° or 2°C (UNFCCC, 2015).

2.3 Solar PV technology

We review the historical background and the current development of solar energy. Then we assess the sensitivity of solar cell temperature to some meteorological variables and we also report some studies on the impact of climate change on PV energy output.

2.3.1 Historical background

The PV effect was discovered for the first time by Becquerel in 1839 (Penick and Louk, 1998). He found that, when a solid electrode in an electrolyte solution was exposed to light, a voltage is generated. In 1877, William Grylls Adams and his student, Richard Evans Day, observed the PV effect by exposing a semiconductor made of selenium to light. However, the voltage output from the PV effect was not good enough to consider as a new method of generating energy. In order to improve the output, in 1983, Charles Fritz coated the selenium semiconductor with an extremely thin layer of gold (Zweibel and Hersch, 1984). The efficiency of the energy conversion rate of the cell was between 1 and 2%. This experiment was considered as the first true PV cell. To enhance the efficiency of the cell, the German physicist Heinrich Hertz exposed free electrons to light to generate radio waves. Through this experiment, the first photoelectric effect was observed in 1887. Hertz observed that, when the same material was exposed to ultraviolet light, the cell produced more power. This process behind the photoelectric effect was difficult to explain at that time. It was only in 1904 that Albert Einstein explained the process of the photoelectric effect in a published paper, which earned him the Nobel Prize in Physics in 1921. Modern cells rely on this process. During the period of 1953-1956, in order to improve the efficiency of the cell, physicists at Bell Laboratories substituted selenium with silicon. This material gave an efficiency of up to 11%. PV cells were first used in 1958 in space to power the Vanguard satellite, the world’s first solar-powered satellite. Since 2008, solar energy has become widespread as renewable energy because of its affordable price and the improvement continue to make it more efficient and less expensive (Chu and Majumdar, 2012).

2.3.2 Worldwide status of solar PV technology

It has been reported by the International Energy Agency (IEA) that the price of PV systems has dropped by 70% for new utility-scale solar PV systems (IEA, 2018). Due to its low cost and clean energy, many countries have started to generate electricity based on PV technology. As a result, the market for PV technology has grown considerably during the past years. Between 2016 and 2017, the global installed capacity of PV technology was about 402 GW and the net installed capacity of PV technology in 2018 was more than the net capacity of the combined fossil fuels and nuclear power (REN21, 2018). The reason behind this exponential increase is the rapid growth of installed PV technology in China. According to the IEA, China's share of global PV demand grew dramatically from 10% to more than 55% in the five past years. China, the United States, Japan, Germany and Italy are the top countries in terms of global PV capacity (Figure 2.3). Unfortunately, the spread of PV technology in Africa remains unsatisfactory, despite it being the sunniest continent on Earth (Duah and Asamoah, 2018). Only South Africa and Algeria are leading the PV technology with a total cumulative capacity of about 1.8 GW and 0.4 GW respectively (REN21, 2018). Nevertheless, most African countries have begun building their energy mix on PV technology for the welfare of their population: 59 million Africans are using off-grid solar energy to power their homes, as well as solar lamps and mini-grids since 2016 (REN21, 2018).

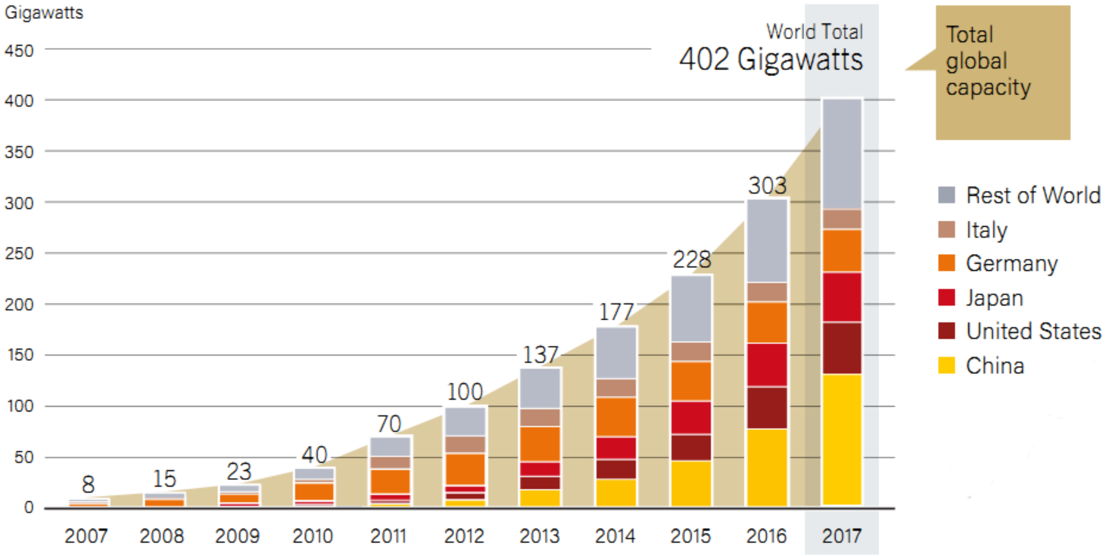

Figure 2.3: Solar PV Global Capacity, by Country or Region, 2007-2017 (REN21, 2018)

2.3.3 Sensitivity of PV cells

Several studies suggest that electricity production from natural resources such as solar energy is sensitive to weather conditions, climate variability and climate change (Ebinger and Vergara, 2011; Williamson *et al.*, 2009). This section thus reviews the sensitivity of PV cells vis-à-vis meteorological variables such as solar radiation, air temperature, wind speed and relative humidity.

2.3.3.1 Solar radiation

PV power output depends strongly on solar radiation (Lurwan et al., 2014; Clack, 2017). Solar radiation is the expression of the input of energy upon the Earth, and the engine for electricity generation from solar energy. Solar radiation emitted from the sun is a type of electromagnetic radiation. The literature agrees that the spectral distribution of solar radiation has a wavelength of between 200 - 2500 nm, which includes the total irradiance (96.3%), whereas the remaining solar radiation is at longer wavelengths (3.7%) (Sirisamphanwong and Sirisamphanwong, 2013) (see Figure 2.4). Within the range of 200 – 2500 nm: 6 – 7% of the spectra; distribution are in ultraviolet light; around 42% are visible light and 51% are near infra-red**.** However, various atmospheric elements, referred to the air mass (AM), absorb this emitted solar spectrum. Brooks (2014) defines AM as the amount of atmosphere that solar energy must pass through. Further investigations show that the AM depends on geographical location, time of day and year, and weather (Zdanowicz *et al.*, 2003; Kazem and Chaichan, 2016). It was reported in the literature that the extraterrestrial radiation (i.e. the solar constant 1370 W/m^2) has an air mass of zero (AM0); AM1 (one atmosphere) refers to the shortest possible path to the surface that the solar radiation can take. By industry standards, all PV modules and systems are characterised at AM1.5 (1000 W/m^2), which is 50 % longer than the shortest path length (Brooks, 2014).

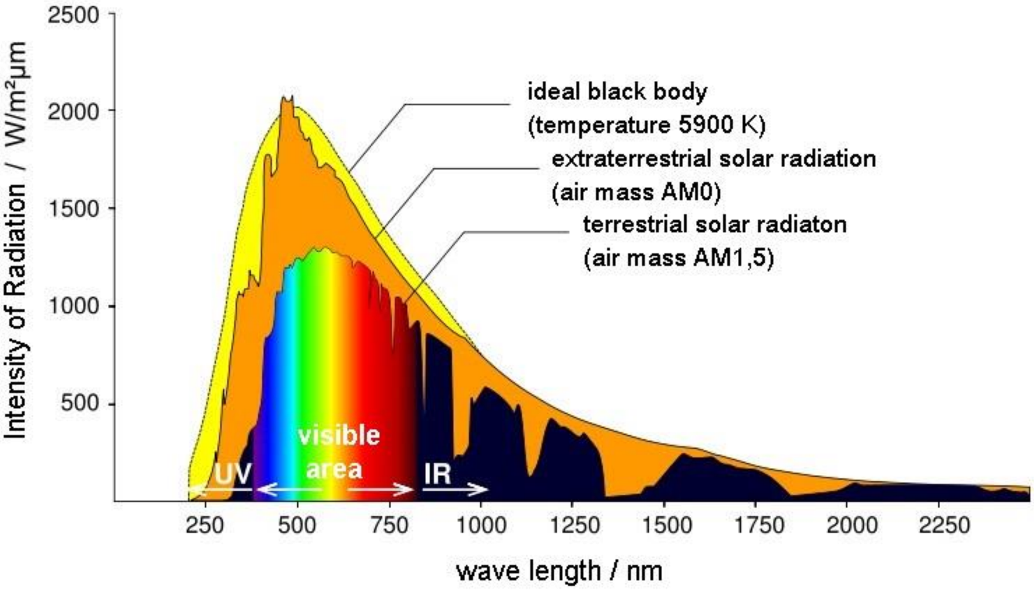

Figure 2.4: Solar spectrum of the solar radiation.

Note: Idealised solar spectrum of the solar radiation is in (yellow). The orange colour indicates the extraterrestrial solar radiation, while the multicolour and the black colour show the solar radiation modified by the atmosphere. The multicolour shows the visible part of the solar radiation and the black shows the ultraviolet and the infrared parts of the spectrum.

Source: ACCENT Global Change Magazine 2008 – Solar Energy and Earth

2.3.3.2 Air temperature

It has been reported that solar cell efficiency is typically measured under standard test conditions (STC), with PV cell irradiance of 1000 W/m^2, temperature of 25°C, and air mass of 1.5 (Schwingshackl *et al.*, 2013). However, these conditions are rarely met outdoors rather than in the laboratory. In general, a PV module converts only 6-20% of the solar irradiance into electricity, depending upon the type of solar cells used. The rest of the solar irradiance is converted into heat (Dubey et al., 2013). Since the PV cells are semi-conductors, they are also very sensitive to temperature fluctuations. Many existing studies have examined the effect of air temperature on the PV cells. The results of those studies have shown that an increase in the air temperature decreases the performance of the solar cell and consequently reduces the PV efficiency of the module (Dubey et al., 2013; Olukan and Emziane, 2014; Ibrahim and Anani, 2017). Dubey *et al*. (2013) explain the heart of the problem as follows: The parameters of the cell, like open-circuit voltage, short-circuit current, fill factor and efficiency, and maximum output power are generally affected by the solar cell's temperature. The maximum influence of the temperature on the solar cell occurs in the open-circuit voltage (Chander *et al*., 2015). A prior study found that the temperature variation of the cell parameters is nonlinear with the temperature (Griffith *et al*., 1981) because the open-circuit voltage and the fill factor decrease considerably with temperature, whereas the short-circuit current slightly increases (Skoplaki and Palyvos, 2009). For instance, in the case of crystalline silicon (used for PV cells), the voltage temperature coefficient is about -0.45%/K, while the current temperature coefficient ranges between 0.04 and 0.09%K (Chandra *et al*., 2018). Overall, any variation in the air temperature will alter the solar cell parameters, and thus affect the efficiency of the PV cells.

2.3.3.3 Wind speed

Previous studies have argued that PV cell efficiency is influenced by various meteorological variables. It is well known that, as discussed in the preceding sections, solar radiation and temperature have an impact on the efficiency of the PV cells. We know that an increase in the air temperature increases the cell temperature, which decreases the efficiency of the cell. It has been shown that, for crystalline silicon solar cells, a temperature rise of 1°C reduces the efficiency of the cells by 0.45% and even by 0.9% when the temperature rises by 10°C (Otth and Ross, 1983; Skoplaki and Palyvos, 2009). Conversely, cooler cell temperatures at STC improve the efficiency of the PV cells. A succession of studies has shown the importance of wind speed in terms of its cooling effect on PV cells. Different studies have thus included the wind speed factor in modelling solar cell temperature (Skoplaki *et al*., 2008; Kurtz et al., 2009; Schwingshackl *et al*., 2013; Kaldellis *et al*., 2014). Many different approaches have been used to show the sensitivity of PV cells to wind speed. For instance, Koehl *et al*. (2011) used two methods to highlight the importance of wind speed in cooling PV modules; one model is derived from David King's approach and the other from David Faiman. Both approaches revealed a wind cooling effect of 15-20°C for wind speeds of 10 m/s at solar irradiance of about 1000 W/m^2 (Koehl et al., 2011).

2.3.3.4 Relative humidity

Gwandu and Creasey (1995) showed that relative humidity also affects solar irradiance. This is due to the amount of water vapour in the atmosphere, which can reflect, refract, and diffract the incoming solar radiation. High amounts of relative humidity may lead to the formation of dew on the solar cell's surface. As we know, condensation causes warming, and an increase in temperature reduces the efficiency of the PV cell. Various authors have highlighted the effect of relative humidity on the PV cells. For instance, Kazem *et al*. (2012) have examined the effect of relative humidity in Oman. They used three types of PV cells (Polycrystalline, Monocrystalline and Amorphous Silicon) for their investigation. Their results show that an increase in relative humidity decreases the performance of the PV cells, and that the Monocrystalline cell performs better under low relative humidity than the Polycrystalline and Amorphous Silicon cells (Kazem et al., 2012). Another study done under the climatic conditions of Doha, the capital of Qatar, showed similar results, where the Monocrystalline cells have a higher efficiency (85%) than the Amorphous Silicon cells (70%) (Touati et al., 2013). A study by Panjwani and Narejo (2014) in Karachi, Pakistan has also focused on the effect of the relative humidity threshold on the loss of energy in the PV cells. Their study indicates that there is a loss of about 15-30% in the PV power output for relative humidity between 40-78% (Panjwani and Narejo, 2014). However, the impact of relative humidity on PV cells can be neglected under dry conditions (TamizhMani *et al*., 2003).

2.3.4 Impact of climate change on solar resource and PVP

During the last two decades, climate models have been used for climate impact studies. Several studies have investigated the potential impacts of climate change on solar radiation and the PV output and found different results over various regions of the world (e.g. Crook *et al*., 2011; Burnett *et al*., 2014; Panagea *et al*., 2014). Panagea *et al*. (2014), for example, used five Regional Climate Models (RCMs) under the IPCC A1B climate change emissions scenario to project the impact of climate change on PV output in Greece. It is projected that Greece may experience an increase of solar irradiation of 2-3 W/m^2 by 2011 - 2050 and up to 5 W/m^2 by 2061-2100. PV output is also expected to increase throughout most of the country (Panagea *et al*., 2014). China, Germany and

Spain can also expect an increase in PV power under the A1B emissions scenario during the 21st century (Crook et al., 2011). Burnett *et al*. (2014), for instance, used gridded observation data to evaluate the potential impact of climate change on solar resources in the UK. They found that it is actually feasible to use solar energy throughout the entire UK, especially in the south of England and Wales, where the daily value of solar irradiance is often above 130 W/m^2. With a high emissions scenario, it is projected that solar resources may even increase (by 3.4% in the 2050s and 4.4% in 2080s) during this century.

While some studies projected that climate change was likely to increase solar resources, others indicated that it would reduce over different regions and countries. For example, Jerez *et al*. (2015) projected a decrease over most Northern European countries. The magnitude of the decrease ranges from minus 14% to 2% with the largest decreases in Northern European countries under the RCP8.5 emissions scenario. The method employed by Jerez *et al*. (2015) to calculate the solar cell temperature differs from that used by Crook *et al*. (2011). In their study, Jerez *et al*. (2015) considered the influence of wind speed in calculating the PV cell temperature. In addition, the two studies use different emission scenarios, and Crook *et al*.'s (2015) study was based on individual models (HadGEM1 and HadCM3), while that of Jerez *et al*. (2015) was built on multi-model multi-ensemble simulations (five RCMs). Other parts of the world may also experience a decrease in PV power. Crook *et al*. (2011) revealed that PV power may decrease in the Western USA (2-3.5%) and over Saudi Arabia (5%) by the end of the 21st century. Huber *et al*. (2016) projected a general decrease on a direct normal irradiance (DNI) and a decrease also on a global horizontal decrease about 20% and 5% respectively in the period of 2035 - 2039 over the West African region. Another investigation was conducted by Bazyomo *et al*. (2016), utilising a high-resolution model (CORDEX). Their results suggest that all the RCMs project a general decrease of solar irradiation with a maximum value of the solar resource of 0.17 W/m^2/year over a longer period (2060 - 2100). They concluded that climate change will lead to a decreasing trend in PV power output in most of the West African countries where Niger denotes the most country affected with a magnitude decrease of 0.032%/year.

However, given that the focus of these future projections is over specific time periods, the policy-makers may find it difficult to apply the results to the framework of the Paris Agreement, which requires the information at specific GWLs (1.5°C and 2.0°C). Only a few studies have examined the impact of climate change at 1.5°C and 2°C GWL over West Africa. For instance, Diedhiou *et al*. (2018) found that the projected increase in the frequency and duration of heat waves over West Africa at 2.0°C GWL is much higher than at 1.5°C. Kumi and Abiodun (2018) projected a delay in the day of onset of rainfall and a shorter length rainy season over most parts of West Africa at both warming levels; however, the magnitude of the projection is higher at 2°C than at 1.5°C GWL, by more than 10 days. In contrast, Klutse *et al*. (2018) found no significant difference in the magnitude of the projected decrease in consecutive wet days at 2°C than at 1.5°C GWLs. To our knowledge, no prior studies have examined how the GWLs may affect the PV power potential over the West African region. In addition, the PV projections of Bazyomo *et al*. (2016) are based on future changes in temperature and solar radiation, neglecting to consider the influence of relative humidity and wind speed in calculating the solar cell temperature, although several studies have shown that solar cell temperature is indeed sensitive to both wind speed and relative humidity (Kazem *et al*., 2012; Jerez *et al*., 2015). Furthermore, Bazyomo *et al*.'s (2016) projections are based on simulations from a regional climate, whereas policymakers require more robust information from multi-model multi-ensemble simulations.

2.4 Modelling shortwave radiation over west Africa

Solar energy is based either on the direct normal irradiance (DNI) that is used for a solar thermal plant or on the Global Horizontal Irradiance (GHI) for use of the PV plant technology (Zempila *et al.,* 2015). It has been stated by Diagne *et al*. (2014) that incoming solar radiation is the most important meteorological variable that controls solar energy efficiency. Consequently, getting an accurate value of solar radiation helps architects and engineers to design solar power plants better. Over the last decade, there has been keen interest in using Numerical Weather Prediction (NWP) for solar energy modelling. However, in the NWP, the absorption of radiation is regarded as the main challenge when accurately calculating Rs. Water vapour and ozone are the main absorbers in the earth’s atmosphere, and respectively in the troposphere and the stratosphere (Lacis and Hansen 1974). Ozone can be accurately parameterised because the absorption takes places in the stratosphere (~90%), where there is little scattering (Lacis and Hansen, 1974). However, it is problematic to parameterise the absorption of water vapour accurately in most types of NWP (De Souza *et al*., 1997). Therefore, a better estimation of water vapour absorption in NWP would result in a better estimation of SW as well, which is the primary source of the Earth systems. To overcome this problem, some NWPs offer a set of radiation schemes within the model that can be used for sensitivity studies in order to select the best meteorological conditions (Li *et al*., 2014).

Previous studies have investigated the impact of radiation schemes on the assessment and forecasting of solar radiation. For instance, Zempila *et al*. (2015) have evaluated the

WRF radiation schemes, viz. the Dudhia, the updated Rapid Radiative Transfer Model for GCM (RRTMG), the updated Goddard and the Goddard Fluid Dynamics Laboratory (GFDL) schemes in predicting the GHI in Greece. All the schemes overestimate the GHI under the all-skies condition, and give better results under a clear sky, but the Dudhia scheme performed better than all the other schemes. The performance of the WRF radiation scheme has been also evaluated over the Xinjiang area, China, with regard to PV power application, by Chen *et al*. (2017). They reported that the Dudhia and Cam schemes give better results under clear-weather conditions than the other schemes to simulate Rs. For instance, the Dudhia scheme has showed a lower value of Rs from 0700 to 1600 Beijing Time (BJT) than the observation with a maximum error of -49.05 W/m^2 and a high value of Rs from 1600 to 2200 (BJT) than the observation with a maximum value of 50.93 W/m^2. Conversely, the Cam scheme has a greater value of Rs than the observed Rs for both period of times.

Many contributions have been made to understand how the WRF model could improve to simulate the characteristics of the West African climate systems. For example, Flaounas *et al*. (2010) used the WRF model for the regional modelling of the 2006 WAM. They tested the convection and planetary boundary layer (PBL) schemes in the model. At the end of the study, they found that the Mellor-Yamada-Janjic PBL scheme and combined with the Kain-Fritch convection scheme performs better in simulating the humidity, the temperature and the onset of rainfall over the region. A similar study also has been conducted by Klein *et al*. (2015) to simulate the characteristics of the WAM with the WRF model with a multi-physics ensemble. Their study revealed that the multi ensemble of microphysics and the PBL schemes contribute to the simulate the monsoon precipitation, but the PBL scheme influences the northward movement of the intertropical discontinuity (ITD). A recent study of Arnault *et al*. (2016) has investigated the regional precipitation recycling by two methods (the E-tagging method of Knoche and Kunstmann) implemented in the WRF model and tested over West Africa. The impacts of different WRF radiation schemes have been assessed in relation to the dynamics of the West African monsoon (WAM) and precipitation (Li *et al*., 2014). Li *et al*. (2014) reported that the Dudhia scheme improved the characteristics of the WAM with some biases compared to other schemes. However, there is a dearth of information on the impact of different WRF radiation schemes for solar energy application over the West African region.

2.5 Summary

We reviewed the importance of the solar irradiation, the air temperature, the wind speed and the relative humidity in calculating the solar cell. Then, we looked at the impact of climate change on PV energy output across the regions. After that, we reviewed also the impact of climate change on wind power potential. Finally, we reported the sensitivity of the WRF radiation schemes for solar energy application and how the WRF model has been used in the West Africa region to simulate the characteristics of the WAM. The next chapter looks at the research methodology that was used herein.

CHAPTER THREE: RESEARCH METHODOLOGY

This chapter sets out the methodology used in this research on the impact of climate change on wind power density (WPD), the PV power generation potential (PVP) and the sensitivity of different radiation schemes used in the Weather Research and Forecasting (WRF) mode. Section 1 defines the study area, being the West African region. Section 2 looks at the data that was used, namely: the station and gridded data, the satellite data and the reanalysis data. It also introduces the CORDEX dataset and the WRF model that was used in this thesis. In Section 3, the model evaluation is described, as well as the PVP, the WPD and the WRF model.

3.1 Study area

This study covers the entire West African region, but also focuses on the different climate zones, the various countries in West Africa, and the vicinities of 15 cities as shown in Figure 3.1. Following Abiodun *et al*. (2012), we divided the subcontinent into the following three zones: Guinean zone (18W:18E, 4N:8N), Savannah zone (18W:18E, 8N:12N), and Sahel zone (18W:18E, 12N:16N). The cities were selected based on their large populations and the demand for electricity (Fig 3.1). Since most of the selected cities were the capitals of the various countries that make up the West African region, there is access to roads, access to modern infrastructure, and access to transmission lines – all of which are important when assessing the wind power. Moreover, in order for a wind farm to be economically feasible, it should be located at sites where there is access to roads and transmission lines (Pandian and Iyappan, 2012; Moiloa, 2009). At the country scale, we also selected fourteen countries that make up the member states of

ECOWAS, which all have agendas to increase their electricity production by means of PV solar technology (Table 3.1).

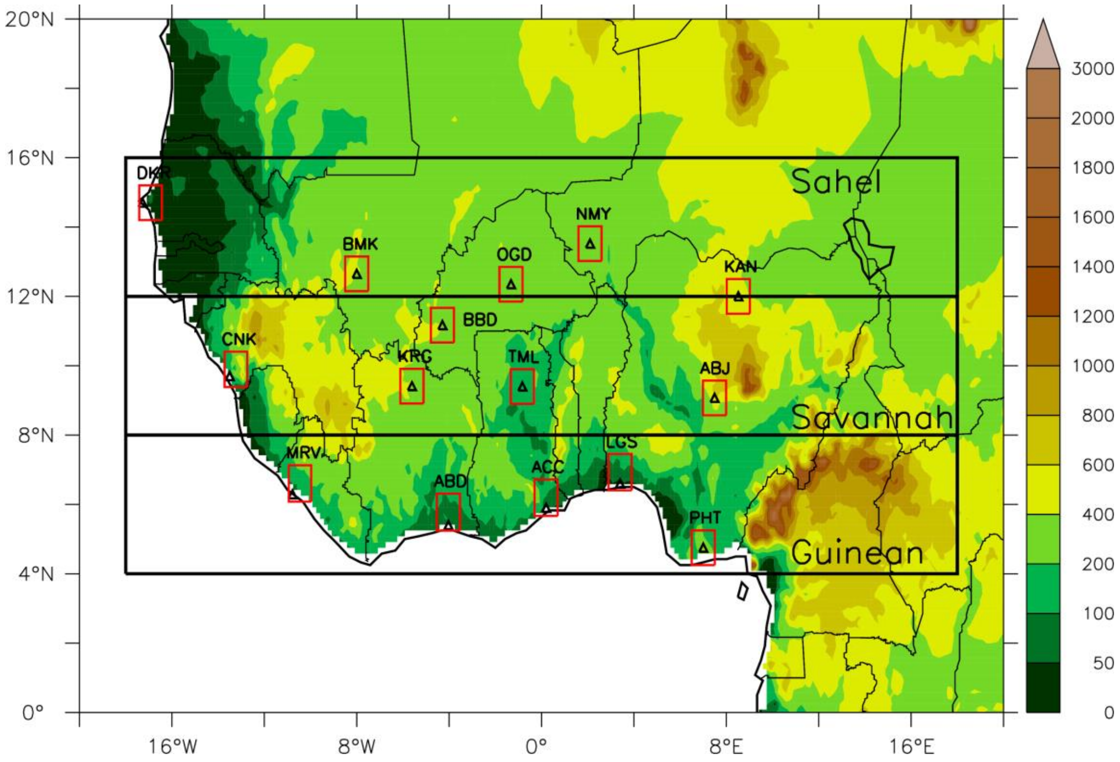

Figure 3.1: The study domain showing the topography of West Africa (in metres).

Note: The region's climatic zones (the black rectangle indicates the Guinea, Savannah, and Sahel zones) and the selected 15 cities (indicated by triangles). The red boxes around the cities show the area (1° x 1°) that has been designated as the vicinity of the city. The names of the cities are listed in Table 3.1.

Table 3.1: Some information about the selected cities for the study.

Code	Cities	Country	Population
ABD	Abidjan	Côte d'Ivoire	4,707,404
ACC	Accra*	Ghana	4,917,262
BMK	Bamako	Mali	4,347,997
BBD	Bobo-Dioulasso*	Burkina Faso	806,939
CNK	Conakry	Guinee	2,317,376
DKR	Dakar	Senegal	3,529,300
KAN	Kano	Nigeria	4,956,615
LGS	Lagos	Nigeria	22,829,561
ABJ	Abuja	Nigeria	1,568,853
MRV	Monrovia	Liberia	1,716,637
NMY	Niamey	Niger	1,175,446
OGD	Ouagadougou*	Burkina Faso	2,868,034
PHT	Port Harcourt	Nigeria	2,306,662
KRG	Korhogo	Côte d'Ivoire	286,071
TML	Tamale*	Ghana	427,054

Note: The geographical locations of the cities is indicated in Figure 3.1. The population data are from https://www.populationdata.net/palmares/villes/afrique/

3.2 Data

For this study, observation datasets and model simulations datasets were considered. For the observation datasets: station data, satellite data, gridded data and reanalysis data have been used. The observation data were used to evaluate the capability of the model simulations to reproduce the climate features accurately. To project the impact of climate change on solar PV and wind energy over West Africa, the Coordinated Regional Climate Downscaling Experiment (CORDEX) datasets were used. Conversely, to simulate the Rs over the subcontinent, the WRF model was the preferred model.

3.2.1 Station and gridded data

The station observation dataset consists of surface wind speed data from station data at 10 m above the ground level (AGL). Due to data restrictions and the policies of the various meteorological services, we were only able to obtain data from four stations: Bobo-Dioulasso (1986 - 2016) and Ouagadougou (1986 - 2016) in Burkina Faso, and Accra (1986 - 2000) and Tamale (1986 - 2000) in Ghana. The four stations obtained represent the Guinea zone (Accra), Savannah (Bobo-Dioulasso and Tamale and Sahel (Ouagadougou) zones. The station data were used to evaluate how well the climate simulation reproduces the daily distribution of surface wind speed over the four cities.

3.2.2 Satellite data

The CM SAF (Satellite Application Facility on Climate Monitoring) second edition of the Surface Solar Radiation Data Set – Heliosat Edition 2 (SARAH-2; hereafter SARAH) (Pfeifroth *et al.*, 2018). SARAH is a product derived from satellite observations of the visible channels of the MVIRI (Meteosat Visible and InfraRed Imager) and the SEVIRI (Spinning Enhanced Visible and Infrared Imager) instruments onboard the geostationary Meteosat satellites, which cover Africa, Europe and the Atlantic Ocean. The second edition SARAH is an improvement of the first edition (SARAH-1); the stability has been improved during the transition from the MVIRI to the SEVIRI instrument in 2006. The new SARAH also takes into account slant view geometries and topographically corrected integrated water vapour data (Pfeifroth *et al.*, 2018). It covers the region of ±65 degrees longitude and ±65 degrees latitude with a spatial resolution of 0.05° by 0.05°. The temporal resolution of SARAH can be retrieved at daily, monthly means, hourly data scales. SARAH offers the following parameters: Effective Cloud Albedo (CAL), Surface Incoming Shortwave radiation (SIS; hereafter, Rs), Surface Direct Irradiance (SDI), Spectrally Resolved Irradiance (SRI) and Sunshine Duration (SDU). The SDI includes two direct radiation products, the Surface Incoming Direct radiation (SID) and the Direct Normalised Irradiance (DNI), which is the basis for the retrieval of SDU (Kothe *et al.*, 2017). It covers 33 years; from 1983 to 2015. The quality of the SARAH data has been demonstrated through many studies regarding looking at the Baseline Surface Radiation Network (Stöckli, 2013; Wild *et al.*, 2015). We downloaded hourly data of Rs from the CM SAF website (https://wui.cmsaf.eu/).

3.2.3 Reanalysis data

The reanalysis dataset consists of two reanalysis products from the European Centre for Medium-Range Weather Forecasts (ECMWF): the ERA-Interim (hereafter, ERAINT) (Dee *et al.*, 2011) and the ERA-Twenty-Century (hereafter, ERA20C) (Hersbach *et al.*, 2015). The third reanalysis dataset comes from the Climate Forecast System Reanalysis (CFSR) of the National Centers for Environmental Prediction (NCEP). The purpose of reanalysis data is to assess the closest state of real atmosphere and land surface characteristics by assimilating large numbers of observations, such as satellite, radiosonde, buoy, aircraft and ship reports, which cover complete global and temporal data series (Gao, 2013).

3.2.3.1 ERA-Interim (ERAINT)

The ERAINT dataset is a global atmospheric reanalysis dataset. The atmospheric model is coupled to an ocean-wave model resolving 30 wave frequencies and 24 wave directions at the nodes of its reduced 1° x 1° latitude/longitude grid (Berrisford *et al.*, 2009). ERAINT uses 4D-variational analysis on a spectral grid with triangular truncation of 255 waves (corresponding to approximately 80 km) and a hybrid vertical coordinate system with 60 levels with the top level at 0.1 hPa (Mooney *et al.*, 2011). In addition, the ERAINT uses the variational bias correction for satellite data, a revised humidity analysis, and other improvements in data handling (Berrisford *et al.*, 2009). The coverage period extends from 1979 till the present. The ERAINT used in this study has a 0.75° x 0.75° horizontal grid size. From the ECMWF website, we retrieved daily surface zonal and meridional wind (u and v respectively), surface pressure (Ps), surface temperature (T), zonal wind stress (τu), meridional wind stress (τv), dewpoint (Td) and specific humidity (hss) data. The surface wind speed has been computed based on the zonal and meridional wind speed with $Ws = \sqrt{(u^2 + v^2)}$.

3.2.3.2 ERA-Twenty-Century (ERA20C)

The ERA20C is also a global atmospheric reanalysis dataset. However, the observation data used by the ERA20C reanalysis differ from the data used by ERAINT. The ERA20C uses observation data provided by the International Surface Pressure Databank (ISPD) version 3.2.6 and the International Comprehensive Ocean Atmosphere Data Set (ICOADS) version 2.5.1, which includes additional other geophysical parameters above oceans, such as atmospheric and oceanic temperatures, and atmospheric near-surface winds (Poli *et al*., 2013). The ERA20C configuration uses 10 members in total: 9 perturbed members and 1 unperturbed member or control. It has 91 vertical model levels between the surface and 0.01 hPa or about 80 km altitude, and uses 4D-Var analysis like ERAINT (Poli *et al*., 2013). The 4D-Var analysis window is 24-hours-long, instead of 12 hours as in ERAINT (Dee *et al*., 2011). Unlike ERAINT, the ERA20C has a spectral triangular truncation of T159m, which is roughly 125 km and covers a period of 111 years (1900 - 2010). A similar bias correction method (Integrated Forecast System) is applied for the ERA20C, but at the surface pressure observations (Poli *et al*., 2013). In addition, the ERA20C offers wind speed at 100 m above the ground level (AGL). We therefore retrieved wind speed data at 100m from the ECMWF platform (https://www.ecmwf.int/). The ECMWF platform proposes a set of grid sizes that the users can select according to their needs. The ERA20C dataset wind speed data retrieved has a horizontal grid size of 0.125° x 0.125° and a period from 1980 to 2009.

3.2.3.3 Climate forecast system reanalysis (CFSR)

The CFSR is one of the third generation reanalysis products and was the first quasi-global, high-resolution and fully coupled atmosphere-ocean-land model used at NCEP for seasonal prediction (Saha *et al*., 2014). The CFSR was generated from four different models from different institutions. The atmospheric and the land surface initial conditions were provided by the NCEP Department of Energy (DOE) Global Reanalysis 2 (R2) (Kanamitsu *et al*., 2002), while the global ocean data assimilation system (GODAS) operational at NCEP derives from the ocean initial model (Behringer, 2007), which goes along with the Modular Ocean Model, version 3 (MOM3), from the Geophysical Fluid Dynamics Laboratory. Finally, the NCEP's Global Forecast System

(GFS) contributed to the atmospheric model. The CFSR atmospheric model also incorporates observed variations in carbon dioxide (CO_2), aerosols and other trace gases and solar variations. Additionally, the global atmosphere resolution of the CFSR is about 38 km with 64 levels. The temporal resolution of the CFSR is 6-hourly data (at 0000, 0600, 1200, and 1800 UTC) and the products are available at 0.3, 0.5, 1.0, 1.9, and 2.5-degree horizontal resolutions.

3.2.4 CORDEX dataset

The climate model simulations used for climate change projection in the present study come from the Coordinated Regional Climate Downscaling Experiment (CORDEX). CORDEX provides a framework for investigating climate change impact scenarios at a regional scale (Nikulin et al., 2012; Figure 3.2). CORDEX covers five major domains: the entire African, Australian, North American, South American, and European continents. The present study uses the CORDEX-Africa dataset for the climate projection studies over West Africa. The CORDEX-Africa dataset consists of 25 RCM simulations downscaled by 13 General Climate Models (GCMs), which originated from the Climate Model Intercomparison Project phase 5 (CMIP5) (Taylor *et al.*, 2012). The CORDEX simulations cover a large period of data and are thus divided into two parts. The hindcast period (1950 - 2005), also referred to as the control simulations, is forced by observed natural and anthropogenic atmospheric composition, such as CO_2 and non-CO_2 GHGs, land cover and aerosols (Moss et al. 2010). The future periods (2006 - 2100) are forced by the Representative Concentration Pathway (RCP) emissions from the IPCC's climate change scenarios (IPCC, 2007b). For the future period, we can evaluate three RCPs, namely, RCP2.6, RCP4.5, and RCP8.5, where each number denotes the radiative forcing reached at the end of this century compared to the pre-industrial period

(1850 - 1900). From the CORDEX-Africa dataset, hydrology, climate, and oceanography parameters are all accessible (Mba et al., 2018). The spatial resolution of the CORDEX datasets is roughly 50 km (0.44° x 0.44°).

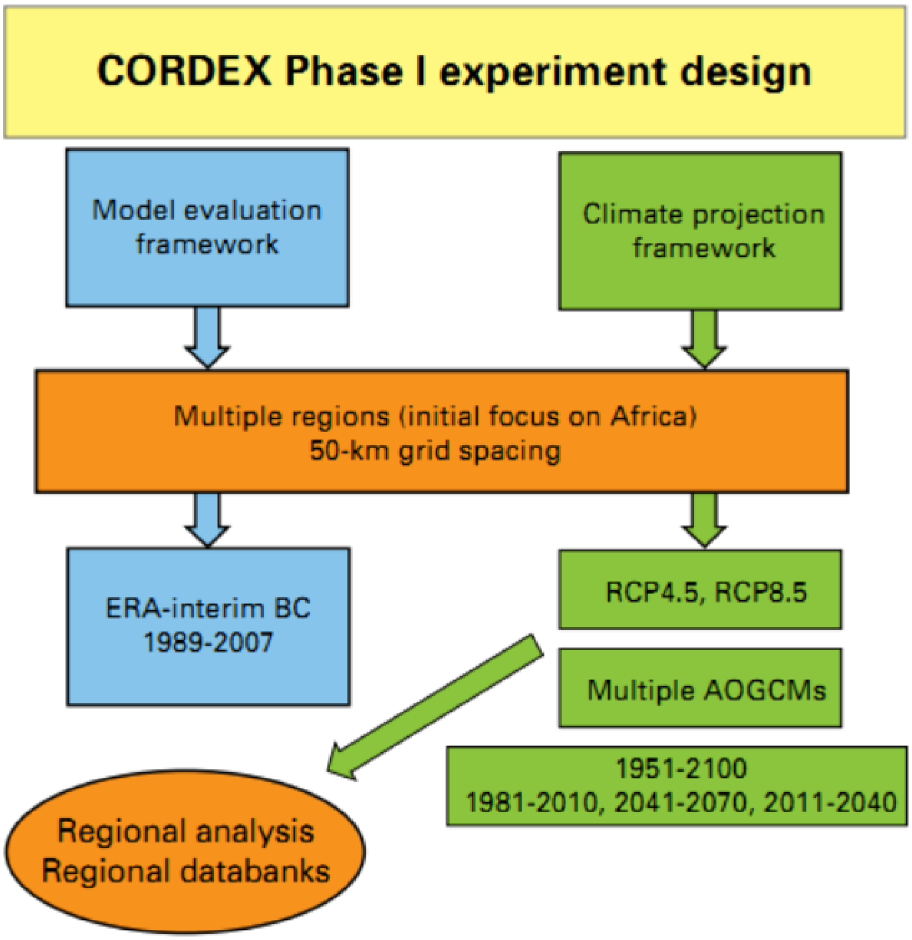

Figure 3.2: Schematic depiction of the first phase CORDEX experiment set-up (Giorgi et al., 2009)

For this study, an ensemble of fourteen simulations to determine the impact of climate change on PVP has been used; in addition, an ensemble of eleven simulations has been used for WPD projections over West Africa to conduct this study. The names of the RCMs and the driving GCMs used in this study are shown in Table 3.2 and Table 3.3 respectively. From the CORDEX datasets, surface-downwelling radiation (Rs), air temperature (Ts), wind speed (Ws) and specific humidity (hss), zonal wind stress (τu), meridional wind stress (τv) and surface temperature were downloaded.

Table 3.2: List of the RCMs used in this study and their configuration. Taken from (Nikulin et al., 2012; Strandberg *et al*., 2015)

	DMI HIRHAM5	**MPI REMO**	**KNMI RACMO2.2b**	**CLMcom CCLM4.8**	**SMHI RCA4**	**CNRM ARPEGE5.1**
Institute	Danmarks Meteorologiske Institut, Denmark	Max Planck Institute, Germany	Koninklijk Nederlands Meteorologisch Instituut, Netherlands	Climate Limited-Area Modelling Community (www.clm-community.eu)	Sveriges Meteorologiska och Hydrologiska Institut, Sweden	Centre National de Recherches Météorologiques, France
Short name	HIRHAM	REMO	RACMO	CCLM	RCA4	ALADIN
Projection resolution	Rotated pole 0.44°	Rotated pole 0.44°	Rotated pole 0.44°	Rotated pole 0.44°	Rotated pole 0.44°	Polar, stretching factor 2 (TL179)
Vertical coordinate/levels	Hybrid/31	Hybrid/27	Hybrid/40	Terrain following/35	Hybrid/40	Hybrid/31
Advection	Semi-Lagrangian	Semi-Lagrangian	Semi-Lagrangian	Fifth-order upwind; (Baldauf, 2008)	Semi-Lagrangian	Semi-Lagrangian
Time step (s)	600	240	720	240	1200	1200
Convection scheme	(Tiedtke, 1989)	(Tiedtke, 1989)	(Tiedtke, 1989)	(Tiedtke, 1989)	(Bechtold *et al*., 2001; Jiao and Jones, 2008)	(Bougeault, 1985)
Radiation scheme	(Fouquart and Bonnel, 1980; Mlawer et al., 1997)	(Morcrette, 1990; Giorgetta and Wild, 1995)	(Fouquart and Bonnel, 1980)	(Ritter and Geleyn, 1992)	(Savijärvi, 1990; Sass et al., 1994)	(Morcrette, 1990)
Turbulence vertical diffusion	(Louis, 1979)	(Louis, 1979)	Eddy-diffusivity (first-order K) mass flux approach	(Herzog et al., 2002 ; Buzzi et al., 2011)	(Lenderink and Holtslag, 2004)	(Mellor and Yamada, 1982)
Cloud microphysics scheme	(Tompkins, 2002; Tiedtke, 1989)	(Lohmann and Roeckner, 1996)	(Tiedtke, 1993)	(Doms et al., 2011; Baldauf and Schulz, 2004)	(Tiedtke, 1996)	(Ricard and Royer, 1993)
Land surface scheme	(Schulz et al., 1998; Hagemann, 2002)	(Hagemann, 2002) (Rechid et al., 2009)	TESSEL; (ECMWF, 2007)	TERRA-ML; (Doms et al., 2011)	(Samuelsson *et al*., 2010)	ISBA; (Douville *et al*., 2000)

Table 3.3: List of CMPI5 data considered in the study

Driving GCMs	RCMs downscaling	Atmospheric resolution of the GCMs		Simulations used	
		Horizontal	Vertical	wind energy	PV power generation potential
CCCma	RCA4	128 x 64	35	x	x
CSIRO		192 x 96	18	x	x
IPSL		144 x 143	39	x	x
MIROC		256 x 128	56	x	x
CNRM	RCA4	256 x 128	31	x	x
	CCLM				x
	ALADIN				x
MPI-LR	RCA4	192 x 96	47	x	x
	REMO			x	
	CCLM				x
NCC	RCA4	144 x 96	26	x	x
	HIRHAM			x	
ICHEC	CCLM	320 x 160	62		x
	RACMO			x	x
HadGEM	RCA4	192 x 144	38	x	x
	CCLM				x

Note: For each GCM the following features are described: the RCMs used to downscale, the atmospheric resolution and the simulations used for the impact of climate change on wind energy and the PV power potential.

3.2.4.1 Representative Concentration Pathways (RCPs)

A climate change projection is based on various socio-economic and emission scenarios. These scenarios include socio-economic change, technological change, land use, energy, and emissions of GHGs and air pollutants (Van Vuuren *et al*., 2011). Over many decades, two emission scenarios have been used to support potential policy responses to the impacts of climate change. The first includes the IS92 scenarios (Leggett *et al*., 1992), while the second consists of the scenarios from the Special Report on Emission Scenarios (SRES) (Nakicenovic *et al*., 2000). For the cost and the benefits of climate goals and in order to explore climate change adaptation from previous scenarios, it is necessary to improve it (Moss et al., 2010). Under the IPCC, a new scenario has emerged, called the Representative Concentration Pathways (RCPs). These RCPs form a set of GHG concentration and emission pathways designed to support research-based climate change projections (Riahi et al., 2011). The new scenario establishes a radiative forcing (at the end of this century) and varies from low as 2.5 W/m^2 to between 8 and 9 W/m^2 and higher (Moss et al., 2010). For this study, we use the RCP8.5, because it offers more realistic patterns (using the assumption of ‘business as usual’) in terms of GHG emissions. Figure 3.3 shows the framework on which the RCP8.5 has been built in order to make it consistent and plausible.

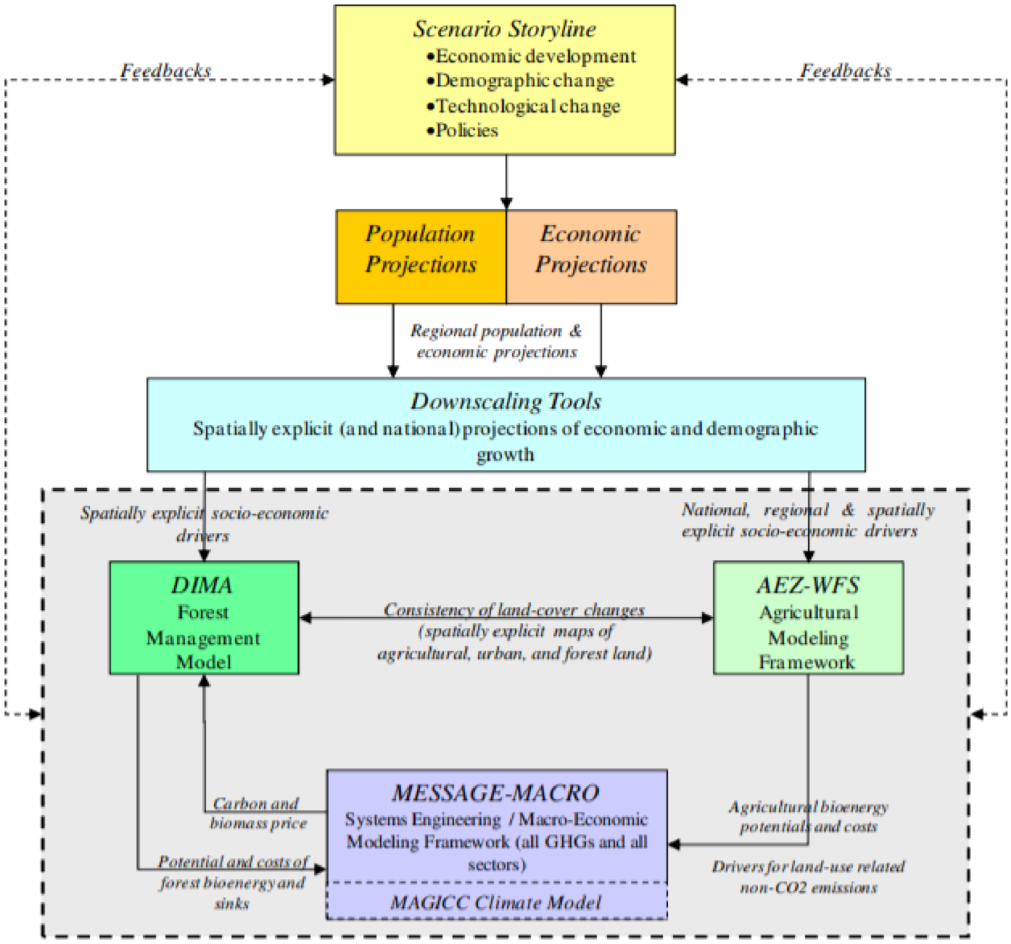

Figure 3.3: International Institute for Applied Systems Analysis (IIASA) modeling framework (Riahi et al., 2011)

3.2.4.2 Global warming level (GWL) periods

Nikulin *et al*. (2018) has defined the period of global warming levels (hereafter, GWLs) as the centre year of a long enough period when global mean temperature (GMT) reaches predefined anomalies (1.5, 2, 2.5, 3°C etc.) relative to pre-industrial levels. Many ways have been proposed to compute these GWLs, but all of them rely on the pre-industrial baseline by using an averaged window period of 15, 20, or 30 years (Schleussner *et al*., 2016). Moreover, the period of the GWL also depends on the climate scenario used (RCP2.6, RCP4.5 and RCP8.5). Therefore, the period of the desired GWL is extracted from the baseline when the GMT is reached. Here, in this study, we adopt the methodology used by Déqué *et al*. (2017). They used 1881 - 1910 to define the pre-industrial period and 30 years as the moving average of the GMT above 1.5, 2, 2.5, 3°C and then calculated the 30 years GWL for individual GCM simulations under the RCP8.5. The reference period is defined as 1971 – 2000. In the study, the same period of individual GCM simulation has been used to extract the RCM downscaling. For the climate change projections, we used four GWLs (1.5°C, 2.0°C, 2.5°C and 3.0°C; hereafter, GWLs: GWL1.5, GWL2.0, GWL2.5, and GWL3.0) above the pre-industrial level. The period of each GWL for each GCMs is depicted in Figure 3.4.

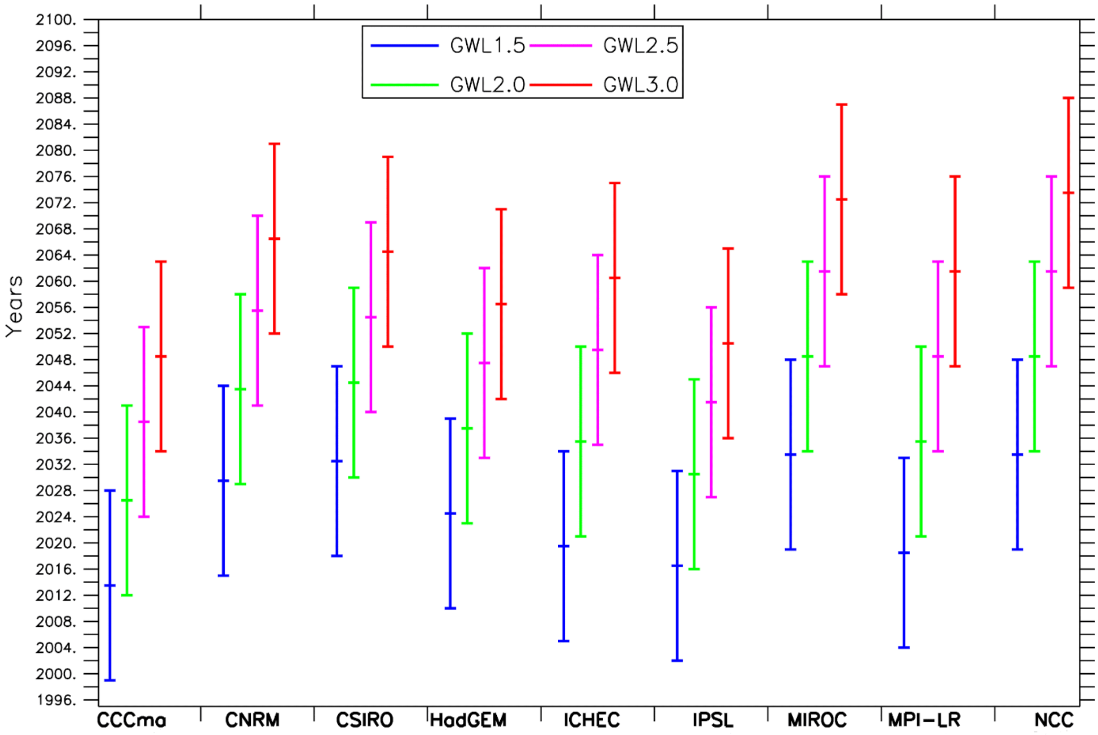

Figure 3.4: The extracted 30-year global warming period.

Note: The 30-year global warming period is based on the method of Deque *et al*. (2017) under the RCP 8.5 climate scenario. Each line denotes the start year (the bottom), the middle year (the median of the line) and the end year (the top) of the warming level.

3.2.5 Weather Research and Forecasting (WRF) model

Over the last decade, the Weather Research and Forecasting (WRF) model has become the most used atmospheric model, which is evident from the number of users and peer-reviewed articles (Powers *et al.*, 2017). The WRF model therefore has been used to simulate the impact of radiation schemes on the shortwave radiation flux over West Africa in assessing solar energy. The WRF is a mesoscale numerical weather prediction (NWP) and atmospheric simulation system designed for both research and operational applications (Skamarock *et al.*, 2005). WRF is a supported community model and its development is led by the National Center for Atmospheric Research (NCAR), NOAA/ESRL (Earth System Research Laboratory) and NOAA/NCEP/EMC (Environmental Modeling Center) with partnerships at the Air Force Weather Agency (AFWA), the Federal Aviation Administration (FAA), DOE/PNNL (Pacific Northwest National Laboratory) and collaborations with universities and other government agencies in the US and overseas (Dudhia, 2010). Moreover, the WRF model offers users different dynamical cores than can be used for different studies. The Advanced Research WRF (ARW) and Non-hydrostatic Mesoscale Model (NMM) are the two dynamical cores of the WRF. In this study, we used the ARW core. The ARW dynamical core has an equation set that is fully compressible, Eulerian and non-hydrostatic with a possible hydrostatic run. It is a conservative scalar flux for prognostic variables with a complete Coriolis and curvature terms. The model uses a mass-based terrain, following coordinates with a vertical grid-spacing, which can vary with height. The horizontal grid is the Arakawa-C grid, and the timestep option scheme in the model employs the second and the third order Runge-Kutta scheme. The spatial discretisation of the model uses the 2nd- to 6th-order advection. The WRF model further includes a full physics option for radiation, land-surface, and Planetary Boundary Layer (PBL), microphysics and cumulus parameterisation. The model supports one-way, two-way, and moving nest options. The WRF model also allows both idealised and real-data simulations with various lateral boundary condition options (Bianco, 2008).

3.2.5.1 WRF configuration

The WRF model version 3.8 has been used to simulate the shortwave SW radiation flux over West Africa. Six-hourly data of pressure, surface variables and sea surface temperature (SST) from the NCEP-NCAR reanalysis dataset (Kalnay *et al.*, 1996) have been obtained to ascertain the initial and lateral boundary conditions of the WRF model. The model domain is shown in Figure 3.5, where the domain varies between -8° to 30° latitude and -25° to 25° longitude. The spatial resolution has been set to 25 km with a timestep of 100 and the horizontal and the vertical grid space are fixed to 219 and 169 respectively. This domain setup is enough to capture all necessary features (especially the WAM) needed for the West African climate. The study domain extends from -20° to 20° longitude and 0° to 25° latitude, focusing on the West African zones, which were defined in Section 3.1. The model used 38 levels of terrain-following eta layers from the Earth’s surface to 50 hPa. For the vertical interpolation, the linear in pressure interpolation has been preferred to the log pressure interpolation method.

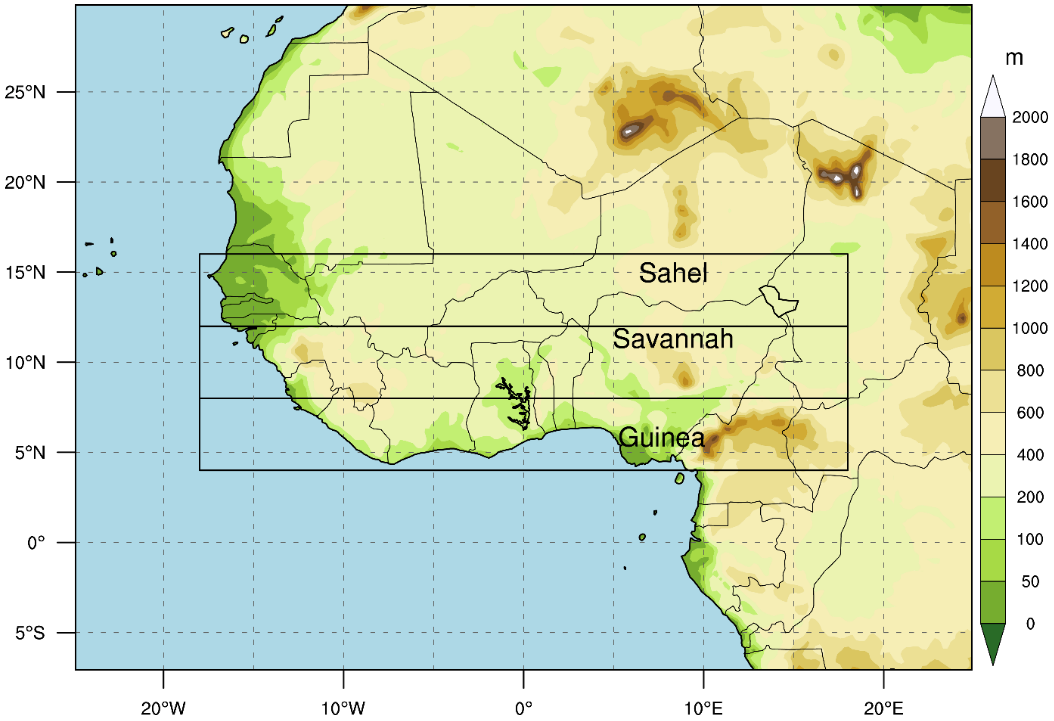

Figure 3.5: WRF domain showing the topography of the region. The delimited lines shows the different sub regions (Guinea, Savannah and Sahel).

All the simulations have been performed with a resolution from the following: The United States Geological Survey (USGS), the 10m topography from the GEODATA TOPO 10M, the green vegetation index field interpolated from the Fraction of Photosynthetically Active Radiation (FPAR) generated with the Moderate Resolution Imaging Spectroradiometer (MODIS), and the land use index and the land use fraction fields interpolated from the 21-class MODIS. All the data has been interpolated to 30-arc-second data. The physical parameterisation schemes used in all the experiments include the WRF single-moment (WSM) 6-class graupel scheme (Hong et al., 2004), the Mellor-Yamada-Janjic boundary layer scheme (Janjić, 1994), the Kain-Fritsch cumulus scheme (Kain, 2004), the Monin-Obukhov surface layer scheme (Monin and Obukhov, 1954), followed by the layer Thermal Diffusion Scheme (Dudhia, 1996). The initial field and boundary conditions were taken from the CFSR data.

For this study 17 simulations have been carried out over the studied domain. Firstly, the impact of the Rs has been tested by using different parameterisation radiation schemes in the WRF model. Table 3.4 summarises the WRF model shortwave radiation schemes used with different longwave radiation parameterisations. The second set of the experiment is based on improving the Dudhia Rs parameterisation. In order to do so, ten simulations were executed. Finally, two long-term run simulations of the default Dudhia shortwave radiation scheme and the improved Dudhia (DudhiaM) scheme have been performed. The first and the second set of the simulations were done for the period of 01 December 2009 - 2010 with the whole December 2009 discarded for model spin-up. The long-term runs were simulated for the period of 1980 - 2010 and 1 year discarded for the model spin-up as well. The simulations start at 0000 UTC and end at 2100 UTC.

All the simulation results are given on an hourly basis. The results are presented in the results and discussions section.

Table 3.4: Different WRF shortwave and longwave radiation schemes used in this study

Longwave radiation	Shortwave radiation	References
RRTM scheme	Dudhia scheme	(Dudhia 1989; Mlawer *et al*. 1997)
Cam scheme	Cam scheme	(Collins *et al*. 2004)
Goddard scheme	Goddard scheme	(Chou and Suarez 1994; Chou *et al*. 2001)
New Goddard scheme	Goddard scheme	(Chou and Suarez 1999; Chou *et al*. 2001)
rrtmg	rrtmg	(Iacono *et al*. 2008)

3.3 Methods of the study

The sub-section elaborates the evaluation of the models – CORDEX and WRF, discussing the PV power generation potential (PVP), the wind power density (WPD) and looking at the original and the modified Dudhia WRF model.

3.3.1 Model evaluation

3.3.1.1 CORDEX simulations

The CORDEX simulations have been evaluated with the multi-model ensemble (Rmean) because it gives better results in terms of long-term climate change projection than the individual member (Houghton et al., 2001). Nevertheless, all the simulations with observations are evaluated to determine the ability of the models to simulate the present climate (Randall et al., 2007). For the analysis in this study, all the models and observations were remapped to 0.44° x 0.44° grid points. All the results are presented based on the annual mean and the monthly climatology. However, the annual mean and the monthly climatology are computed from the annual mean and the monthly climatology of each variable of each model. To evaluate the climate model simulations of the wind energy, 30 years of data (1980 - 2009) were used, for which both reanalysis datasets overlap (ERA20C and ERAINT). With regard to the evaluation of the PV power potential, the selected period ranges from 1985 to 2014 due to the temporal coverage of SARAH. In addition, we used the spatial correlation value to see how the Rmean is able to reproduce the pattern of the observation. The boxplot has also been used to compare the Rmean and the observed value. Table 3.5 summarises the variable used for the wind energy and for the PV power generation potential. For the rest of the study, all reanalyses data, satellite and gridded data are referred to as observations.

Table 3.5 List of the type of data, their sources and the variables used for wind energy and PV power generation potential

Type	source	Variable	Variable used	
			WPD	PVP
Observation	Station data	Surface wind speed	x	
Reanalysis	ERAINT	zonal wind	x	x
		meridional wind	x	x
		specific humidity		x
		dewpoint		x
		surface temperature	x	
		meridional wind stress	x	
		zonal wind stress	x	
		surface pressure	x	x
	ERA20C	wind speed (100m)	x	
Satellite	SARAH	incoming shortwave solar radiation		x
Gridded	CRU	Air temperature		x

3.3.1.2 WRF model

Statistical analyses were performed to evaluate the output of the WRF model for each simulation over the different zones. Over decades, the root mean square error (RMSE) and the mean absolute error (MAE) are widely used as a standard statistical metric to evaluate the model performance in the meteorology field (Chai and Draxler, 2014). They are defined as:

$$RMSE = \sqrt{\frac{\sum_{i=1}^{n}(y_i - \hat{y}_i)^2}{n}} \tag{3.1}$$

$$MAE = \sum_{i=1}^{n}|y_i - \hat{y}_i| \tag{3.2}$$

where y_i is the model value while $\hat{y}_i$ is the observation value.

The Taylor diagram is used to evaluate the performance of the simulations vis-à-vis the observations. The Taylor diagram offers graphical information showing how closely a pattern matches the observations (Taylor, 2005). Moreover, the bias (difference) and the spatial and temporal correlations between the models and the observations have been assessed.

3.3.2 Wind energy

3.3.2.1 Wind speed distribution

Weibull distribution function, the most used probability density function (PDF) for wind speed distribution (Burton *et al*. 2011; Ouammi *et al*., 2010) was used to characterize wind over the cities. The Weibull PDF is expressed as:

$$f(v) = \left(\frac{k}{c}\right)\left(\frac{v}{c}\right)^{k-1} exp\left[\left(\frac{-v}{c}\right)^{k}\right] \tag{3.3}$$

Where $f(v)$ is the probability of the measured wind speed$v$; k is the Weibull shape parameter (dimensionless), and c is the Weibull scale parameter [m/s]. k and c are defined as:

$$k = \left(\frac{\sigma}{v_m}\right)^{-1.086} \qquad 0 < k \leq 10$$

(3.4)

and

$$c = \frac{v_m}{\Gamma\left(1+\frac{1}{k}\right)} \tag{3.5}$$

Where v_m is the mean wind speed; σ is the standard deviation and Γ is the gamma function. We assessed daily surface wind speed of the driving GCM members; the RCM members, the two reanalyses, and observations for the present-day climate. We also assessed the future climate of the PDF under both climate change scenarios and the global warming levels. The ensemble mean of the GCMs and RCMs for the wind speed distribution is defined as the subset of each individual member.

3.3.2.2 Wind power density (WPD)

WPD was used to assess wind energy resource over the study area. WPD indicates how much energy is available at the site for conversion by a wind turbine (Ghosh and Prelas, 2011). Since wind power in a wind flow is directly proportional to the cube of the wind speed (Patel, 2005), here we defined the wind power density (hereafter, WPD; unit: W/m^2) as:

$$P_w = \frac{1}{2}\rho\bar{V}^3 \tag{3.6}$$

Where ρ is the air density and $\bar{V}$ is the annual mean wind speed at 100 m AGL. The WPD was calculated at each grid point over our study area using the two reanalyses (ERAINT and ERA20C) and 11 simulation datasets for historical climate and the GWL climates under RCP8.5 scenarios. However, while ERA20C has wind speed data at 100 m AGL, ERAINT and the RCM simulations only have wind speed data at the surface (i.e. 10 m AGL). Hence, to obtain the 100 m wind speed for the WPD calculations, we extrapolated the surface wind speed to 100 m AGL using the wind logarithmic profile described by Stull (2012):

$$V_z = \frac{u_*}{k}(ln\, Z/Z_0) \tag{3.7}$$

Where k is Karman constant (k = 0.4); Z_0 is the roughness length; V_z is the wind speed at the height Z. The roughness length Z_0 was obtained by substituting the friction velocity and the wind speed at 10 m AGL in Equation 3.7. Furthermore, based on the roughness length found over calm water, we applied for each grid point a lower limit to roughness length, such as $Z_0 \geq 0.0002$ m (Stull, 2012). It should be noted that the same method has been used by Davy *et al.* (2017) who qualified it as a realistic method for wind speed extrapolation using data from the model with a time-variant roughness length; u_* is the friction velocity. It is expressed as (Schlichting and Gersten, 2000):

$$u_* = \left(\frac{\tau}{\rho}\right)^{\frac{1}{2}} \tag{3.8}$$

Where $\tau = \sqrt{\tau_u^2 + \tau_v^2}$ and $\rho = p_s/RT_s$ with $R = 287.06 Jkg^{-1}K^{-1}$

Nonetheless, the method used to extrapolate the surface wind speed to the 100 m AGL may underestimate the wind speed in the stable condition and overestimate in the unstable condition.

We also computed the kinetic energy (hereafter KE) dissipation into the boundary layer over the West Africa region. It is defined as the energy that the wind turbine in a wind farm can extract from the mean flow and convert it into electricity (Possner and Caldeira, 2017). We used the surface wind stress (τ) and the surface wind speed (V) to compute the KE and it can be expressed as (Miller *et al.*, 2011):

$$\mathrm{KE} = \tau * \mathrm{V} \tag{3.9}$$

3.3.3 PV power generation potential (PVP)

The PV power output is defined as the amount of energy received from the sun's rays hitting the Earth's surface and being converted into electricity through a PV module. The PV power output depends on the PV power generation potential (PVP) and the installed capacity. As characterised by Jerez *et al.* (2015) in their methodology, the PVP is dimensionless, and it describes the performance of the PV cells regarding their nominal power capacity according to the actual ambient conditions. The PV power production results from the PVP multiplied by the nominal installed watts of PV power capacity. Here, we thus used the PVP to assess and to project the solar energy over West Africa. The PVP depends on the solar resource available at the location, as well as air temperature, wind speed, cloud cover, aerosols, the spectral distribution of incident radiation, the angle of incidence of radiation, and the operational efficiencies of system components (Njoku, 2013). For this study, however, we used only the solar resource, the temperature, the wind speed and the relative humidity to quantify the PVP over the studied domain. It can be expressed as (Mavromatakis *et al.*, 2010):

$$PVP(t) = P_r(t).\frac{Rs(t)}{Rs_{STC}} \tag{3.10}$$

where Rs is the surface-downwelling shortwave radiation at the location site, Rs_{STC} is the solar irradiance of 1000W/m^2. $P_r(t)$ is the performance ratio and accounts for changes in the PV cells efficiency due to changes in their temperature (Jerez *et al.*, 2015) and defined as:

$$P_r(t) = 1 + \gamma.[T_{cell}(t) - T_{STC}] \tag{3.11}$$

where T_{cell} is the PV cell temperature and T_{STC} is the ambient air temperature at STC i.e. 25°C. γ is a constant and depends on the PV cells. In this study, we use a monocrystalline silicon solar panel for the simulations because it is the most used PV solar technology in West Africa and γ is taken as -0.005 °C^{-1} (Jerez *et al.*, 2015). For the purposes of this study, we are assuming that the technology will remain the same in the future. Tcell is modelled as a function of Rs, Ws, Ts, and Rh (TamizhMani *et al.*, 2003):

$$T_{cell}(t) = c + c_1.Rs(t) + c_2.Ts(t) + c_3.Ws(t) + c_4.Rh(t) \quad (3.12)$$

with $c = 1.57°C; c_1 = 0.0289°C/W/m^2; c_2 = 0.961; c_3 = -1.457°C/m/s;$ and $c_4 = 0.109°C/Rh\%$

where $c, c1, c2, c3$ and $c4$ are system-specific regression coefficients determined by TamizhMani *et al*. (2003).

We chose this model because it includes the influence of wind speed and relative humidity in calculating the impacts of temperature on PV cells. Other models based their calculations of solar cell temperature on solar irradiance and ambient temperature alone (Crook *et al*., 2011), while some studies (Kazem *et al*., 2012; Bhattacharya *et al*., 2014) have shown that the solar cell temperature is sensitive to ambient wind speed and relative humidity as well. An increase in relative humidity can reduce the performance of PVP, because it may lead to the formation of dew on the solar cell surface. Physically, the moisture can damage the connection bounds of the cells when it permeates the polymer layer down to the cell (Hamdi *et al*., 2018). Hence, choosing this model helps us to obtain a more reliable cell temperature and compare the contribution of the two additional variables to the cell temperature. Moreover, the model has been developed and evaluated using field measurements of the module's (i.e. the cell's) temperature, ambient temperature, wind speed, wind direction and relative humidity from the weather station. TamizhMani *et al*. (2003) showed that the correlation between the model results and the observations is more than 0.9. Jerez *et al*. (2015) have also used the model to project impacts of climate change on PV power generation over Europe.

For the analysis of this study, all models and observations were remapped to 0.44° x 0.44° grid points and presented on the annual and monthly average from the daily data downloaded. It should be noted that from the daily data, we computed the monthly and annual average of each variable before computing the PVP. All the simulations were compared to the observation before making the climate change projection.

3.3.3.1 Induced changes in PVP

To compute the contribution of each variable to the projected changes in PVP, we substituted Equations (3.11) and (3.12) into Equation (3.10) and can be express as:

$$\begin{aligned} PVP(t) = \beta_1 . Rs(t) + \beta_2 . Rs(t)^2 + \beta_3 . Rs(t) . Ts(t) + \\ \beta_4 . Rs(t) . Ws(t) + \beta_5 . Rs(t) . Rh(t) \end{aligned} \tag{3.13}$$

where $\beta 1 = 1.11715.10^{-3}(W/m^2)^{-1}; \beta 2 = -1.45.10^{-7}10^{-3}(W/m^2)^{-2};$

$$\beta 3 = -4.805.10^{-6}10^{-3}(W/m^2.°C)^{-1}; \beta 4 = 7.285.10^{-6}(W/m^2.m/s)^{-1};\wedge$$

$$\beta 5 = -5.45.10^{-7}(W/m^2.RH)^{-1}$$

From Equation (3.13), the change in PVP can be expressed as:

$$\begin{aligned} \Delta PVP = \Delta Rs . (\beta_1 + \beta_2 . \Delta Rs + 2\beta_2 . Rs + \beta_3 . Ts + \beta_4 . Ws + \beta_5 . Rh) + \\ \beta_3 . Rs . \Delta Ts + \beta_4 . Rs . \Delta Ws + \beta_5 Rs . \Delta Rh + \\ \beta_3 . \Delta Rs . \Delta Ts + \beta_4 . \Delta RH . \Delta Ws + \beta_5 . \Delta Rs . \Delta Rh \end{aligned} \tag{3.14}$$

Equation (3.14) can be rewritten as:

$$\varDelta PVP = \varDelta Rs.PVP + \varDelta Ts.PVP + \varDelta Ws.PVP + \varDelta Rh.PVP + \varDelta Rs.\varDelta Ts.PVP + \varDelta Rs.\varDelta Ws.PVP + \varDelta Rs.\varDelta Rh.PVP \quad (3.15)$$

where : $\varDelta Rs.PVP = \varDelta Rs.(\beta 1 + \beta 2.\varDelta Rs + 2\beta 2.Rs + \beta 3.Ts + \beta 4.Ws + \beta 5.Rh)$;

$\varDelta Ts.PVP = \beta 3.Rs.\varDelta Ts$;

$\varDelta Ws.PVP = \beta 4.Rs.\varDelta Ws$;

$\varDelta Rh.PVP = \beta 5.Rs.\varDelta Rh$;

$\varDelta Rs.\varDelta Ts.PVP = \beta 3.\varDelta Rs.\varDelta Ts$;

$\varDelta Rs.\varDelta Ws.PVP = \beta 4.\varDelta Rs.\varDelta W$; *and*

$\varDelta Rs.\varDelta Rh.PVP = \beta 5.\varDelta Rs.\varDelta Rh$

The total change in PVP ($\varDelta PVP$) due to the contribution of change in temperature ($\varDelta Ts.PVP$) is obtained by:

$$\varDelta PVP = \varDelta Ts.PVP \quad (3.16)$$

Similar analysis can be used to isolate the other terms from Equation (3.15). Table 3.6 summarised all the parameters used, with their respective meaning and unit.

Table 3.6: List of parameters with their meanings and units used in this study.

Parameter	Meaning	Unit
Rs	solar irradiation	W/m^2
Ts	Air temperature	$°C$
Ws	Surface wind speed	m/s
Rh	Relative humidity	RH
PVP	PV power potential	dimensionless
ΔRs	Change in solar irradiation	W/m^2
ΔTs	Change in air temperature	$°C$
ΔWs	Change in surface wind speed	m/s
ΔRh	Change in relative humidity	$RH\%$
ΔPVP	Change in PV power potential	dimensionless
$\Delta Rs.PVP$	The total ΔPVP due to the contribution of ΔRs	dimensionless
$\Delta Ts.PVP$	The total ΔPVP due to the contribution of ΔTs	dimensionless
$\Delta Ws.PVP$	The total ΔPVP due to the contribution of ΔWs	dimensionless
$\Delta Rh.PVP$	The total ΔPVP due to the contribution of ΔRh	dimensionless

3.3.4 WRF model

3.3.4.1 Original Dudhia shortwave radiation parameterisation

The Dudhia SW radiation parameterisation (Dudhia, 1989) is adopted from the Pennsylvania State University (PSU)/NCAR mesoscale model version 5 (MM5). Many factors influence the downward shortwave radiation; for instance, the albedo and absorption of clouds, and the solar zenith angle that increases path length and reduces scattering and water vapour absorption in clear air. These factors can be shaped as:

$$S_d(Z) = \mu S_0 - \int_z^{top} (dS_{cs} + dS_{cs} + dS_{ca} + dS_s + dS_a)$$

(3.17)

Where μ is the cosine of the solar zenith angle and S_0 is the solar constant. Due to the assumed stratiform nature of the clouds, the cloud fraction is either 0 or 1 in the grid box. Moreover, the vertically integrated liquid water path (w) derived from Stephens (1978) has been used to model the cloud back-scattering or albedo and cloud absorption. The model uses bilinear interpolation from tabulated functions of μ, and $\ln(w/u)$. Nevertheless, SW radiation reflected upward by clouds and the surface is ignored. However, the clear-air water vapour absorption is calculated as a function of the water vapour path allowing for the solar zenith angle. In the Dudhia parameterisation, the water vapour absorption is taken from Lacis and Hansen (1974). It can be expressed as:

$$A(y) = \frac{2.9y}{(1 + 141.5y^{0.635}) + 5.925y} \qquad (3.18)$$

Where $A(y)$ is the total water vapour absorption and y is the water amount (centimetres of precipitable water vapour).

3.3.4.2 Modified Dudhia shortwave radiation parameterisation

We have modified the water vapour absorption model in the Dudhia parameterisation in the WRF model (Equation (18)) by considering the atmospheric profile of the water amount. Lacis and Hansen (1974) suggested an approximation correction for the pressure and temperature dependence of the absorption in a non-homogenous path by using an effective water vapour amount:

$$y^{eff} = y\left(\frac{P}{P_0}\right)^n \left(\frac{T_0}{T}\right)^{\frac{1}{2}} \tag{3.19}$$

where $T_0 = 273K$ and $P_0 = 1013mb$; P and T are the pressure and temperature respectively, depending on the atmospheric levels. According to Lacis and Hansen (1974), “there is little theoretical justification for using Equation (19) for the entire spectrum of water vapour bands, but it is probably better than applying no pressure and temperature correction at all”. Typically, the value of n varies between 0.5 and 1 for the Earth’s atmosphere. The value of n equal to 1 has been applied in other to determine the effective water vapour amount (Lacis and Hansen, 1974; Davies, 1982).Conversely, another version of correction involves using a pressure-weighted path based upon the scaling function (Briegleb, 1992). A new empirical equation has been suggested by Chou and Lee (1996) by using the scaling function. It can be expressed as follows (Chou and Lee, 1996):

$$y^{eff} = \left(\frac{P}{P_0}\right)^n exp\big(0.00135 * (T - T_0)\big) \tag{3.20}$$

where $T_0 = 240K$ and $P_0 = 300mb$. The value of n is determined empirically and it is less than 1. A value of n close to 0 as seen as weak absorption while $n = 0.8$ represents a strong absorption (Chou and Arking, 1981). The value of P_0 (reference pressure) differs from the sea level pressure (1013 hPa) because of the basic features of the water vapour vertical distribution and the relative importance of line centres and line wings to the absorption at a given level (Plana-Fattori *et al*., 1997). Here, the water amount of the WRF Dudhia scheme in the physics folder (module_ra_sw.F) is corrected by changing the y in Equation (3.18) by y^{eff} in Equation (3.20). We therefore performed a sensitivity test by changing the value of n between 0 and 1 by a step of 0.1 to find the best absorption amount by keeping $T_0 = 240K$ and $P_0 = 300mb$. After a series of simulation, it was found that the value of n equal to 1 has a strong absorption.

3.4 Summary

In this section, the methodology to model the solar cell temperature and the calculation of the PVP have been presented. In addition, the total change in PVP due to the contribution of change in temperature, solar irradiation, wind speed and relative humidity have been also investigated. Moreover, the methodology to extrapolate the surface wind speed to the height of 100 m AGL and the WPD have been well explained. Lastly, the details of the algorithm used to improve the Dudhia scheme in the WRF model to assess the Rs over West Africa have been exposed. The next chapter discusses the results that have obtained on the evaluation of PVP, WPD and the WRF model and the projection of the impact of climate change on PVP and WPD.

CHAPTER FOUR: RESULTS AND DISCUSSIONS

This chapter presents and discusses the results obtained in this study about wind power density (WPD), PV power generation potential (PVP) and the sensitivity of the WRF model. The objective one exhibits the evaluation of the surface wind speed and WPD and the projection changes. Objectives two looks at the PVP by first evaluating the model, and then considering projected changes in PVP in respect of the various climate variables over the West African region, before presenting the contributions of Rs, Ts, Ws and Rh to such changes in PVP. Objective three focuses on the WRF model, by first evaluating a one-year simulation of the WRF model. Secondly, we present the results obtained from conducting a sensitivity test on the variation in the n values in simulating Rs of the DudhiaM over West Africa, and lastly, we discuss the results of a long-term simulation of the WRF model.

4.1 Wind energy

We present the results of the evaluation of the surface wind speed and the WPD. The results of the projection in the impact of climate change on PVP is also presented in this sub-section.

4.1.1 Model evaluation in historical climate

Although several studies have demonstrated the capability of CORDEX RCMs in simulating various climatic variables over West Africa (Gbobaniyi *et al.*, 2014; Mariotti *et al.*, 2014; Klutse *et al.*, 2016) no study has shown how well the models reproduce wind power over the region. Hence, before discussing the model projections on wind power potential, we evaluate the RCMs by comparing the simulated 10 m wind speed and 100 m wind power potential with the reanalysis results. A comparison of the simulation with observation is a better option, but no observation wind datasets were available for the study. So, we used only four stations that were available for the study to evaluate the capability of the reanalysis, RCMs, and the forcing GCMs in reproducing the observed PDF for the daily surface wind speed over the stations.

4.1.1.1 Probability distribution of surface wind speed

Figure 4.1 exhibits the probability distribution of daily surface wind speed for each station of each GCM and RCM members and their individual ensemble mean. Clearly, the performance of the RCM in reproducing the PDF of the daily wind speed varies over the four stations. The RCMs perform best over Bobo-Dioulasso and Ouagadougou, where they all capture the shape of observed PDF, which is symmetrical around the mode (about 3 m/s). However, the tails of the all the simulated PDFs are shorter than the observed, meaning that the RCMs underestimate the magnitude of extreme wind speed (< 2 m/s or > 4 m/s). The worst performance of the RCMs occurs over Tamale, where all the simulated PDF are located right of the observed PDF, indicating the models overestimate the frequency of high wind (> 2 m/s) over the city. Hence, the RCM downscaling improves on the GCM simulations of Bobo-Dioulasso, Ouagadougou, and Accra, but not over Tamale. In addition, the table 4.1 shows high variation in the observed data than the RCMs. For instance, over each station, the standard deviation is greater than the ones of the RCMs with a difference of more than 0.5 m/s. Also, the average surface wind of most of the RCMs underestimates the value over Accra and Bobo-Dioulasso with less than 0.8 m/s and overestimates those of Ouagadougou and Tamale with more than 0.5 m/s. From Table 4.1, it is clear that the error between the observed and RCMs is important in Tamale than the other stations. This could be due to either to the quality of the observed or the RCMs configuration.

This suggests that the error may alter the potential yield of the WPD over the region. Nevertheless, there is a better agreement among RCM simulated PDFs than among the GCM simulated PDFs.

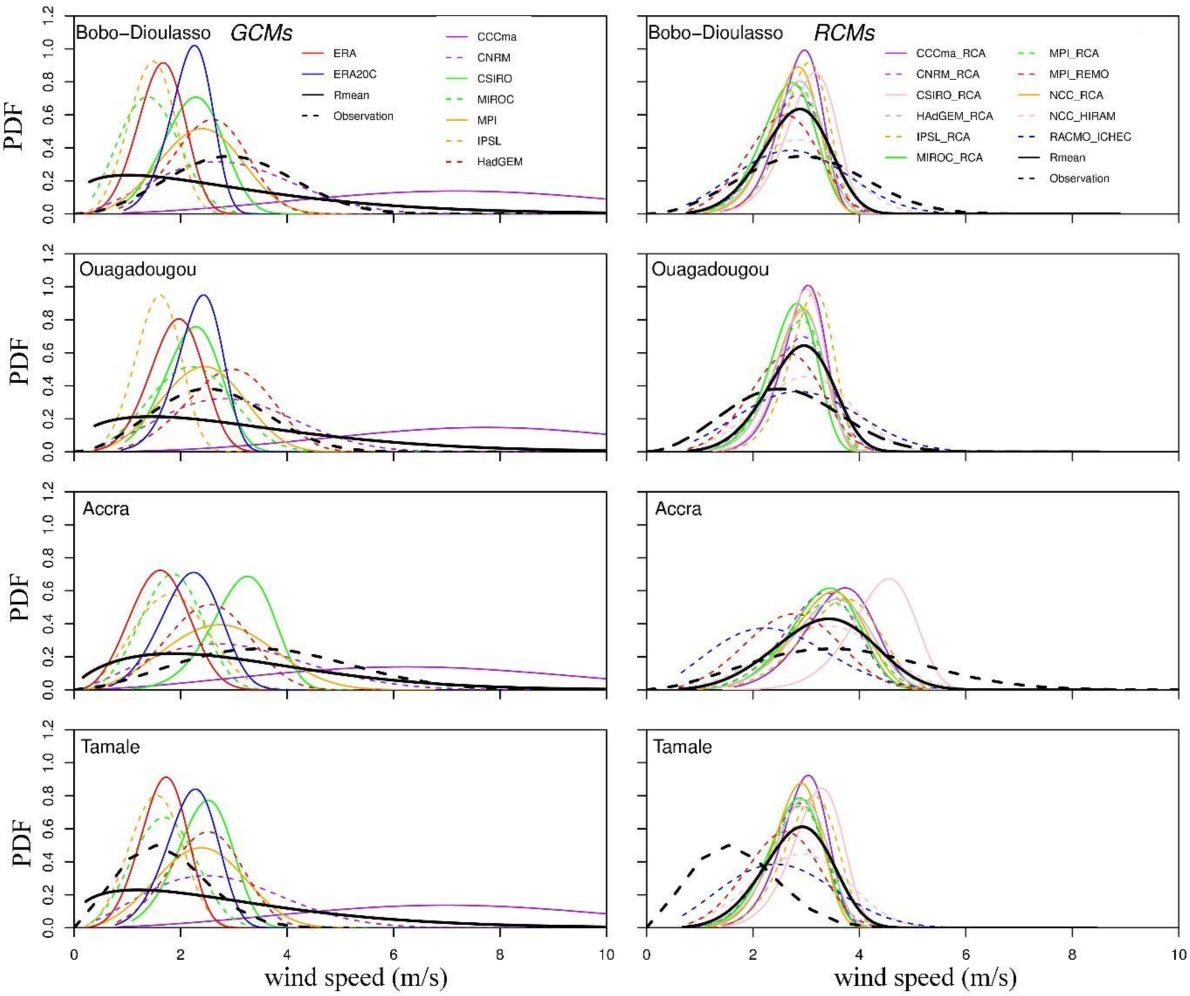

Figure 4.1: Probability distribution of daily surface wind speed for each station of each GCM and RCM members and their individual ensemble mean.

Table 4.1: Statistical analysis of the observed surface wind speed and the RCMs.

	Accra		Bobo-Dioulasso		Ouagadougou		Tamale	
	mean	**bias**	**mean**	**bias**	**mean**	**bias**	**mean**	**bias**
Observation	3.71±1.51	NA	2.99±1.10	NA	2.60±1	NA	1.73±0.74	NA
CCCma_RCA	3.57±0.65	-0.14	2.84±0.42	-0.15	2.91±0.41	0.31	2.91±0.44	1.2
CNRM_RCA	3.22±0.67	-0.49	2.72±0.54	-0.27	2.82±0.57	0.22	2.75±0.53	1.0
MIROC_RCA	3.30±0.64	-0.41	2.62±0.50	-0.37	2.70±0.45	0.10	2.75±0.51	1.0
HadGEM_RCA	3.41±0.73	-0.30	2.75±0.51	-0.24	2.81±0.48	0.21	2.82±0.52	1.1
MPI_RCA	3.31±0.74	-0.40	2.71±0.52	-0.28	2.80±0.50	0.20	2.77±0.54	1.0
NCC_RCA	3.37±0.67	-0.34	2.73±0.46	-0.26	2.81±0.47	0.21	2.78±0.47	1.1
IPSL_RCA	3.59±0.72	-0.12	2.93±0.45	-0.06	3.04±0.43	0.44	3.02±0.51	1.3
CSIRO_RCA	4.37±0.62	0.66	3.03±0.48	0.04	2.88±0.42	0.28	3.16±0.49	1.4
NCC_HIRHAM	3.34±0.99	-0.37	2.81±0.86	-0.18	2.94±0.85	0.34	2.87±0.86	1.1
RACMO_ICHEC	2.42±1.03	-1.29	2.76±0.99	-0.23	2.91±1.04	0.31	2.55±1.00	0.8
MPI_REMO	2.73±0.84	-0.98	2.53±0.65	-0.46	2.59±0.65	-0.01	2.53±0.67	0.8

Note: Summary of the average surface wind speed, standard deviation and the bias over the different station from the RCMs and the observed value. NA means not applicable.

4.1.1.2 Spatial distribution of annual wind speed over West Africa

Figure 4.2 depicts the spatial distribution of surface wind speed over West Africa by the mean of the two reanalyses (ERAINT and ERA20C; panel a), CORDEX ensemble mean (Rmean; panel b) and forcing GCM ensemble (1971-2000; Panel c). The contours in Panels (b) and (c) shows the biases in the RCM and GCM ensembles (with respect to the reanalysis), while the r in bracket denotes the spatial correlation between simulation and the reanalyses result. Panels (d) shows the spread of the RCM and GCM simulations (boxplot), the reanalyses, over the indicated areas. Panels (e) exhibits the spread of RCM, the reanalyses and available station data over the selected cities. Each boxplot indicates the minimum, 1st quartile, median, 3rd quartile, and maximum of RCM and GCM ensemble.

It is obvious that there is a good agreement between the model ensemble means (GCM: Gmean; RCM: Rmean) and the reanalyses on the spatial distribution of 10 m wind speed. The correlation between the simulation and reanalysis results is high (r = 0.95 for Gmean and r = 0.91 for Rmean. In agreement with the reanalysis, both models simulate strongest winds north of 14°N (i.e. over Sahel) and weakest winds south of 12^{o}N (i.e. over Guinea). The weaker wind speed over Guinea may be due to the stronger frictional drag on the monsoon wind over the Guinean zone. The simulations reproduce a tongue of wind speed (about 5 m/s) with a local acceleration over the ocean near the Guinea coast (between Cote D'Ivoire and Nigeria), though the magnitude of the jet is stronger in the Rmean ensemble than in the Gmean and reanalysis. However, there are some discrepancies between the Rmean and other datasets. While the magnitudes of the wind speed are similar in the Gmean and reanalysis, they are higher in Rmean. In Rmean, the wind speeds are up to 5 m/s over Guinea and 6 m/s over central Sahel; but in GCM (or reanalysis), they are about 2 m/s over Guinea and 4 m/s over central Sahel. The higher resolution of Rmean simulations make them resolve meso- or local-scale circulations better than Gmean and reanalysis. Nevertheless, the level of disagreement is minimal over the Atlantic Ocean (i.e. off the coast of Dakar) where the synoptic-scale forcing is stronger.

All the datasets indicate that, among the selected cities, Dakar has the strongest wind speed (Figure 4.2e), possibly because of the intrusion of a mid-latitude system with strong winds over the city. The best agreement between Rmean and observation (at the four stations) occurs over Accra, where the observation falls within the model spread, although more than 75% of the simulations overestimate the observation. The relative poor performance of Rmean over the other three stations (where all the simulations overestimate the observation) may be due to the low quality of the observation data. It may also be due to biases in the RCM simulations.

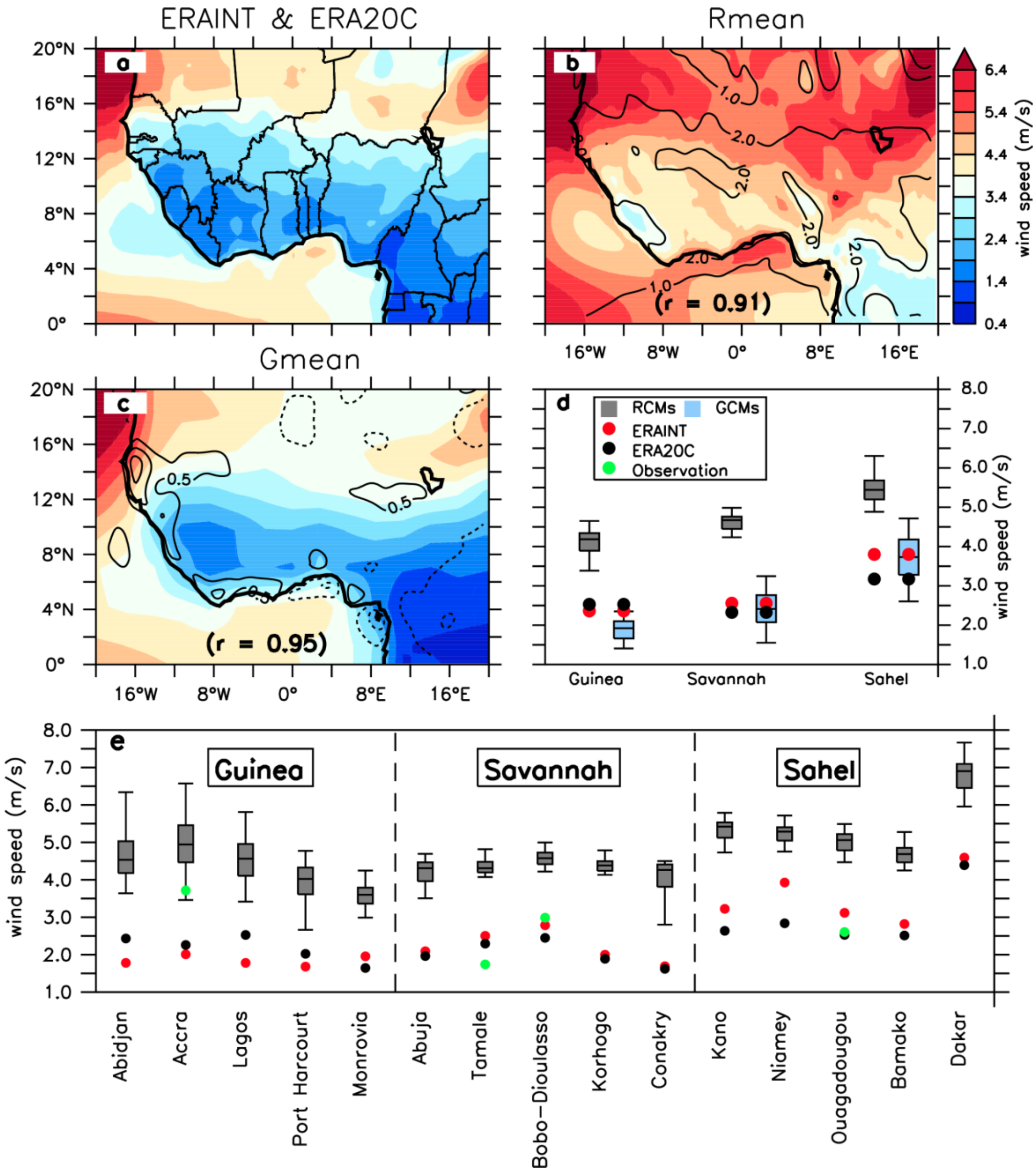

Figure 4.2: The spatial distribution of surface wind speed over West Africa as depicted by the mean of the two reanalyses (ERAINT and ERA20C), the RCM ensemble mean (Rmean) and the GCM ensemble mean (Gmean).

4.1.1.3 Wind power density in historical climate

Figure 4.3 presents the spatial distribution of wind power density over West Africa. Panel (a) show the mean of ERAINT and ERA20C; panel a and CORDEX RCM ensemble (1971-2000; panel b). Panels (d) shows the biases in the ensemble mean results (with respect to the reanalyses), while the r in bracket denotes the spatial correlation between simulation and the reanalysis result. Panels (c) and (e) show the spread of the RCM simulations (boxplot), and the reanalyses over the indicated areas.

The simulations agree with reanalysis that the spatial distribution of WPD at 100 m are similar to that of surface wind (Figure 4.3). The model ensemble reproduces the same features as in reanalysis data (Figure 4.3a and 4.3b), except that the simulated values are higher than the reanalyses (Figure 4.3d). The discrepancy may be because higher resolution of the model makes them resolve more local-scale features with stronger circulations than what is obtainable with the reanalysis. However, the simulation shows that the average WPD over West Africa is about 73.36 W/m^2, ranging from 50.94 W/m^2 over Guinea, to 61.10 W/m^2 over the Savannah, and 104 W/m^2 over the Sahel zone. The local averaged values over some of the cities are much higher (Fig 4.3e). Dakar features the highest value (186.4 W/m^2), followed by Kano (about 85.25 W/m^2), Niamey (81.77 W/m^2), and Accra (77.41 W/m^2). In general, these values suggest that the wind power over West Africa is weak, especially when compared with other regions of the world where wind energy is being harnessed for electricity (e.g. in Morocco WPD ranges from 100 to 1000 W/m^2) (Nfaoui *et al*. 1998). BWEA (2005) shows that most wind turbines start to generate electricity at WPD of about 16.54 to 39.2 W/m^2 hence, the annual WPD of 39.2 W/m^2 is usually considered as a threshold for wind farms (IRENA, 2012). Going by this threshold, the GCMs and reanalysis results indicate only four cities (Kano, Niamey, Ouagadougou, and Dakar; none in Guinea and Savannah) are suitable for power generation, but the RCMs ensemble mean suggests that 13 (about 87%) of the cities (including the Sahelian cities) have a potential wind power generation in the historical climate. However, given that the RCMs have a tendency to overestimate the annual wind speed, they might have overestimated the WPD over these cities.

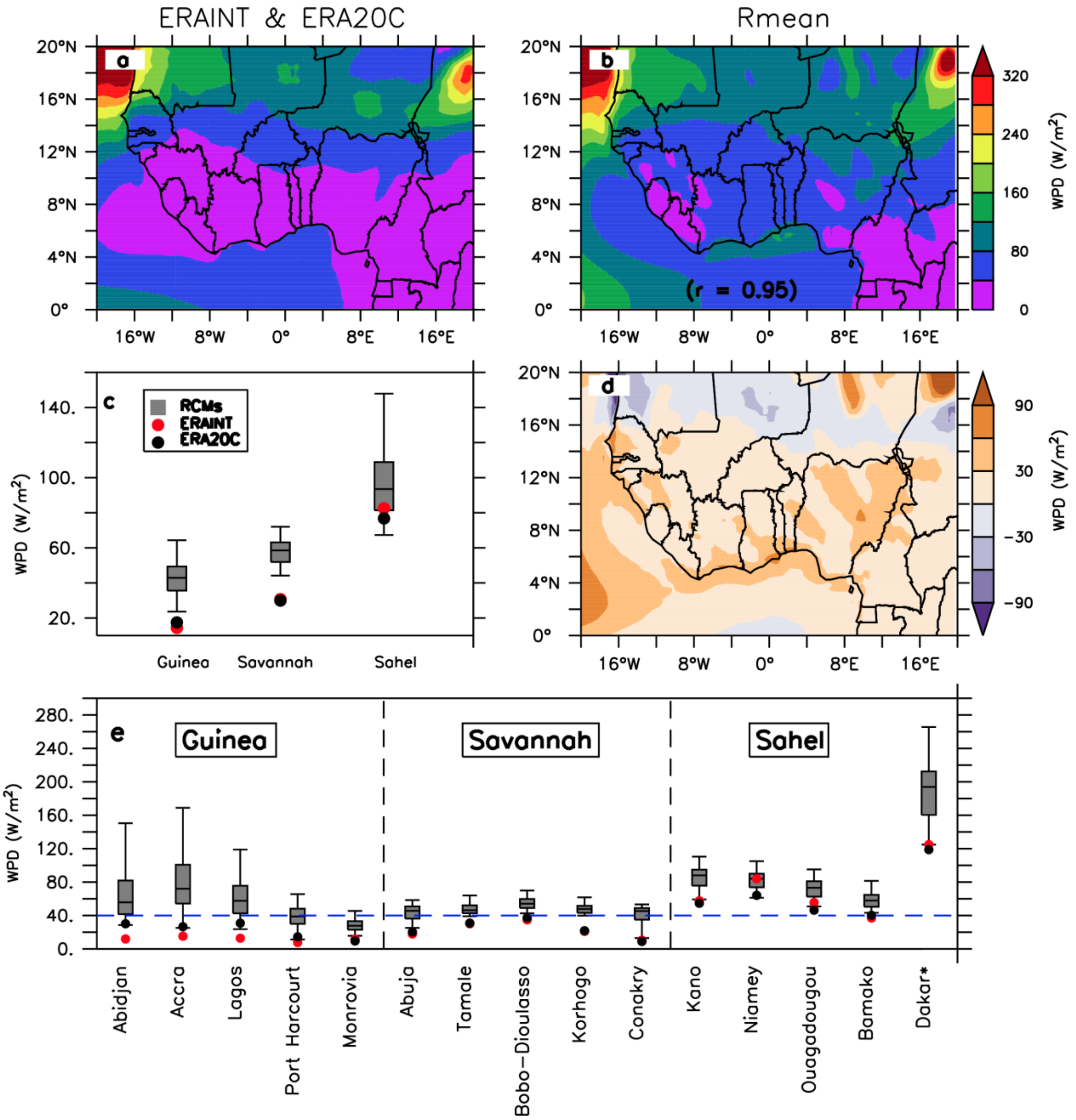

Figure 4.3: The spatial distribution of wind power density over West Africa as depicted by the mean of the two reanalyses (ERAINT and ERA20C), the RCM ensemble mean (Rmean) and the GCM ensemble mean (Gmean).

.

4.1.1.4 Kinetic energy (KE) dissipation into the boundary layer in historical climate

Figure 4.4 shows that the Rmean reproduces the (KE) dissipation into the boundary layer over West Africa as in the reanalyses. Panel (a) show the mean of ERAINT and ERA20C; panel a and CORDEX RCM ensemble (1971-2000; panel b). Panels (d) shows the biases in the ensemble mean results (with respect to the reanalyses), while the r in bracket denotes the spatial correlation between simulation and the reanalysis result. Panels (c) and (e) show the spread of the RCM simulations (boxplot), and the reanalyses over the indicated areas.

The Rmean capture the south-north gradient of the reanalyses. High KE is located over the Sahel region while low over the Guinea zone. There is also a good pattern between both datasets for the KE (r = 0.78). The Rmean pick up the maximum value which is located in the North-West over the domain. However, the Rmean indicate some biases (Figure 4.4d). Over the sub-region, the RCMs failed to capture the mean of both reanalyses. All the RCMs overestimate the magnitude of the KE. The maximum bias can go beyond 0.4 W/m^2 while the minimum bias can reach 0.08 W/m^2. These biases may come from the RCMs configurations or the reanalyses themselves. Moreover, these biases are consistent over the cities wherein low biases are located over the Guinea and Savannah zone and high biases over the Sahel zone (Figure 4.4e). The RCMs also show some uncertainties in computing the KE of the wind energy especially over Abidjan, Accra, Lagos and Dakar. Nonetheless, the RCMs denote high potential of the KE over the Sahel area with an average of 0.7 W/m^2 in Dakar.

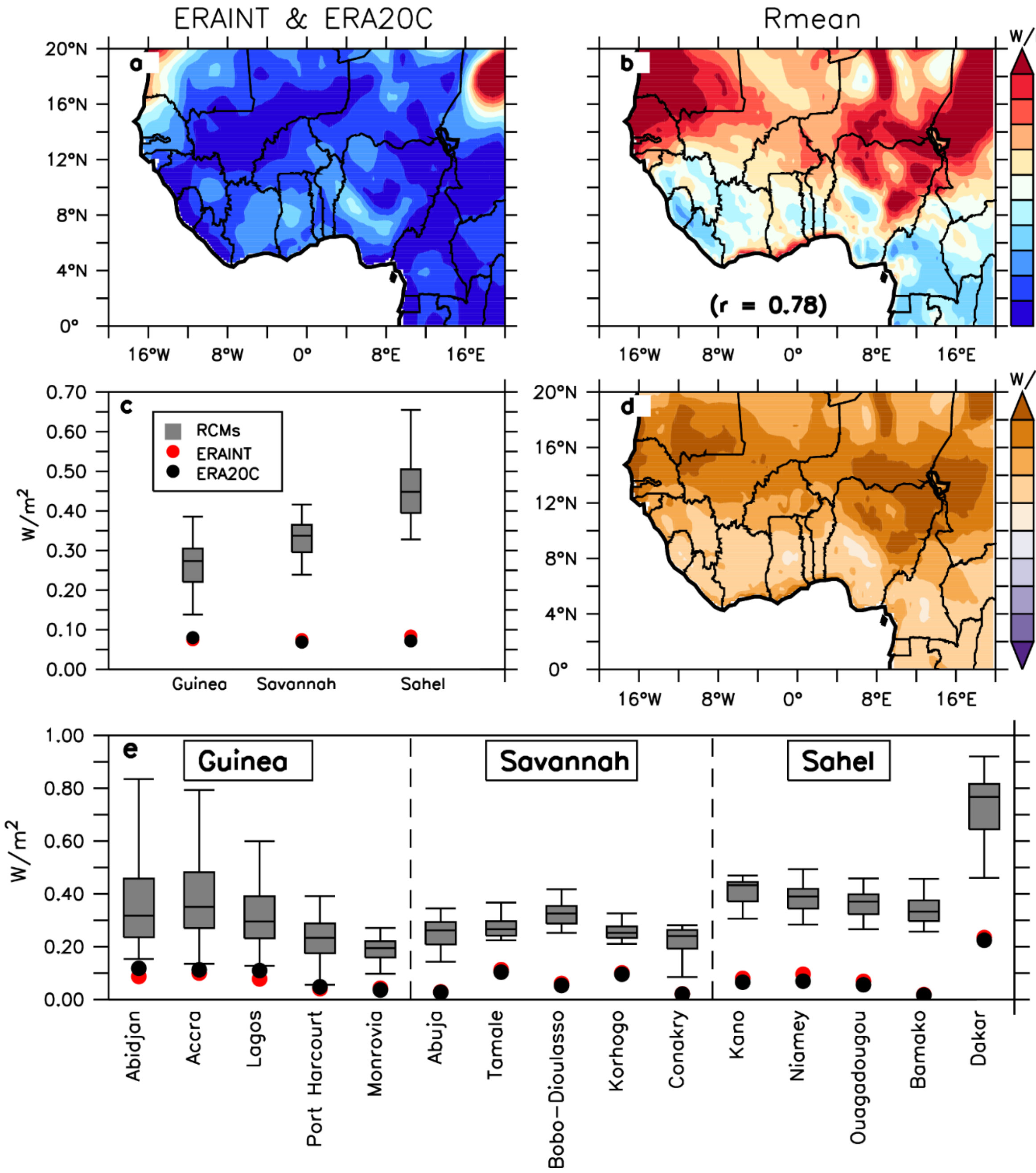

Figure 4.4: Same as Figure 4.3, but for kinetic energy (KE) dissipation into the boundary layer.

4.1.2 Climate change projection

4.1.2.1 Wind power density (WPD)

Figure 4.5 characterizes the projected changes in wind power density (WPD) change over West Africa under RCP 8.5 scenario. Panel (a), (b), (c), and (d) denote the spatial distribution of annual mean WPD over the regions under the 1.5°C, 2°C, 2.5°C and 3°C global warming level. The difference between the changes under the GWLs (GWLs minus GWL1.5) is indicated with contours in panel (b), (c), and (d). The dot shows the significant level at $p<0.01$ for 60% of the RCMs. Panel (c) shows the boxplot of the annual wind WPD change over the climatic zones, while Panel (d) shows a similar result over the cities.

At global warming level 1.5°C (GWL1.5), the RCM ensemble projects an increase in WPD over land, but a decrease over the ocean (Figure 4.5a-d). The maximum increase in WPD is projected over the eastern and western part of the Sahel zone (>10 W/m^2) and along the coast (> 6 W/m^2). These are areas of maximum WPD in the historical climate (Figure 4.3). However, the magnitude of the increase in WPD over these areas grows with the warming level, such that an additional increase of about 2.0 W/m^2 is projected at GWL2.0 and about 4.0 W/m^2 at GWL3.0. This suggests that the global warming strengthens the low-level monsoon flow in West Africa.

To investigate the link between the global warming and the West African monsoon flow, Figure (4.6) presents the spatial distribution of the corresponding changes in temperature, sea level pressure, and wind speed over the subcontinent. Figure (4.6a) shows that the magnitude of the warming varies over West Africa, featuring the highest warming over the Sahel and the lowest over the Guinea coast. This pattern is consistent with previous studies (i.e. Sylla *et al*., 2010a; Abiodun *et al*., 2012) which attributed the less warming over the Guinea coast to be due to the influence of relatively cool moist air from the ocean and increased cloud cover over the coastal region. However, Figure (4.6a-e) indicates that the temperature gradient over the region (i.e. between the Guinean and Sahel zones) increases with the GWL. And, in response, the monsoon pressure gradient increases, and the monsoon flow becomes stronger (Fig 4.6i-l), deflecting more to the east under the influence of the Coriolis force. Several studies have also projected an increase in wind speed and density over various parts of the world following global warming. For example, Johnson and Erhardt (2016) projected an increase of 2% in WPD over some regions in the United States (i.e. Kansas, Oklahoma, and northern Texas), while the magnitude of the change in surface wind speed varies from -0.5 to 0.1 m/s which is quite similar to our results (-0.2 - 0.2 m/s). Pryor *et al*. (2006) projected a change (about -15% to 15%) in the 90th percentile wind speed over northern Europe.

The level of agreement among the simulations on the WPD projection over the zones and the cities also varies with the global warming levels (Figure 4.5 a-d). For instance, at GWL1.5, there is a large uncertainty (-7 to 28 W/m^2) on the sign of the WPD changes over the three zones (Guinea, Savannah, and Sahel), but as the warming level increase, more simulations agree on the increased WPD over the Guinea and Sahel zones, such that, at GWL3.0 more than 75% of the RCMs featuring the increase and the mean of each RCM indicates more than 8 W/m^2 increase. The worse agreement among the projections is over the Savannah zone (-7 to 14 W/m^2). At a more local scale, the best agreement among simulations occurs over the Guinean cities (i.e. Abidjan, Accra, Lagos, Port Harcourt, and Monrovia), one Savannah city (i.e. Conakry), and one Sahelian city (i.e. Dakar), where more than 75% of the simulations indicate an increase WPD, especially at GWL2.0 and above. This suggests that global warming could improve the viability of WPD for wind energy over these cities in the future. However, the risk associated with uncertainties is lowe over the Guinean and Savannah cities. For instance, none of the Guinean cities is viable for wind energy generation in the present-day climate and the projected increase of PWD at any of the global warming levels is too small to make the cities viable for wind energy generation. The same is true for the Savannah cities. The risk is lower for the Sahel cities, where most cities (except Bamako) are already viable for wind energy generation in the present-day climate and the magnitude of the projected changes are too small to make any substantial change. Nevertheless, Dakar is the most viable city for wind energy generation in West Africa.

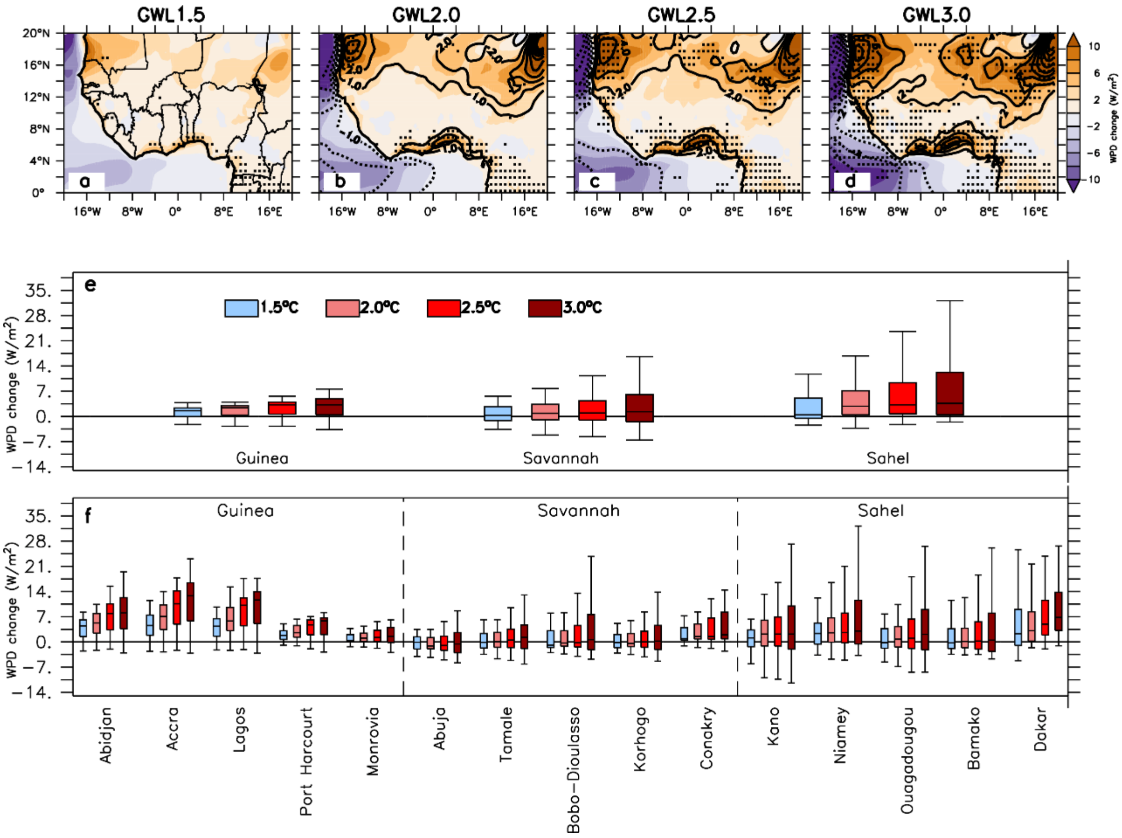

Figure 4.5:Projected changes in wind power density (WPD) change over West Africa under RCP8.5 at 1.5°C, 2°C, 2.5°C and 3°C global warming levels (GWL1.5, GWL2.0, GWL2.5 and GWL3.0 respectively).

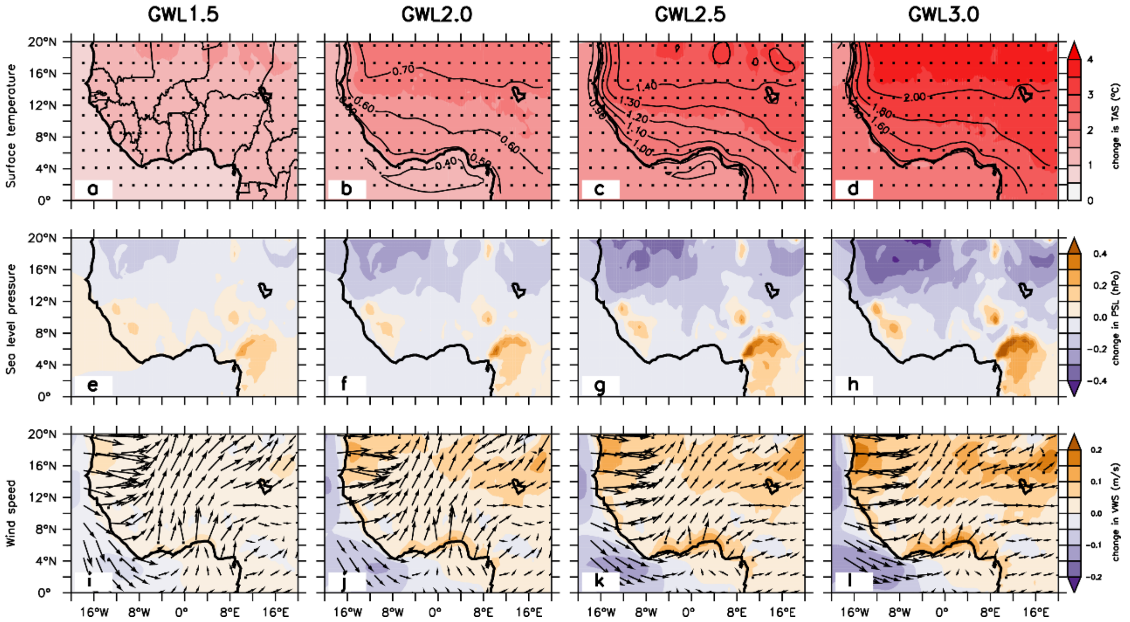

Figure 4.6: Projected change of surface temperature, sea level pressure and the surface wind speed and direction over West Africa under RCP8.5 at 1.5°C, 2°C, 2.5°C and 3°C global warming levels (GWL1.5, GWL2.0, GWL2.5 and GWL3.0 respectively).

4.1.2.2 Kinetic energy (KE) dissipation into the boundary layer

Similar to the WPD, the Rmean projects an increase in the kinetic energy (KE) dissipation into the boundary layer under the various GWLs over the West Africa region (Figure 4.7a-d). The increase of KE goes up with the increase of the GWLs over the subcontinent. The high average KE is located along the coastal areas under the GWLs and statistically significant and also over the Sahel zone for all the warming levels but statistical significant the GWL2.5 and GWL3.0. For instance, over Guinea, the average KE under GWL1.5 (7.12 10^{-3} W/m^2), GWL2.0 (10.22 10^{-3} W/m^2), GWL2.5 (13.92 10^{-3} W/m^2) and GWL3.0 (16.13 10^{-3} W/m^2) is lower than that of GWL1.5 (11.01 10^{-3} W/m^2), GWL2.0 (17.64 10^{-3} W/m^2), GWL2.5 (23.79 10^{-3} W/m^2) and GWL3.0 (29.78 10^{-3} W/m^2) over the Sahel area. Like Guinea and the Sahel zones, the Savannah also exhibit an increase of KE as the warming level increase but less than both zones. The results imply that the increase in global warming may increase the dissipation of turbulent kinetic energy over the region. Furthermore, the Sahel zone is expected to have a high increase in KE due to the strong surface wind speed compared to the other zones. In addition, over the cities like the WPD, 75% of the RCMs agree on the increase in KE and the magnitude also increases with the warming level over the Guinea cities. However, there is a discrepancy in the RCMs wherein 50% of the RCMs show an increase whereas 50% exhibit a decrease over the Savannah cities except for Conakry. Over the Sahel cities, there are uncertainties in the projection of KE except in Dakar where 75% of the RCMs project and increase. Overall the Rmean suggest climate change may enhance the turbulent kinetic of wind energy over West Africa.

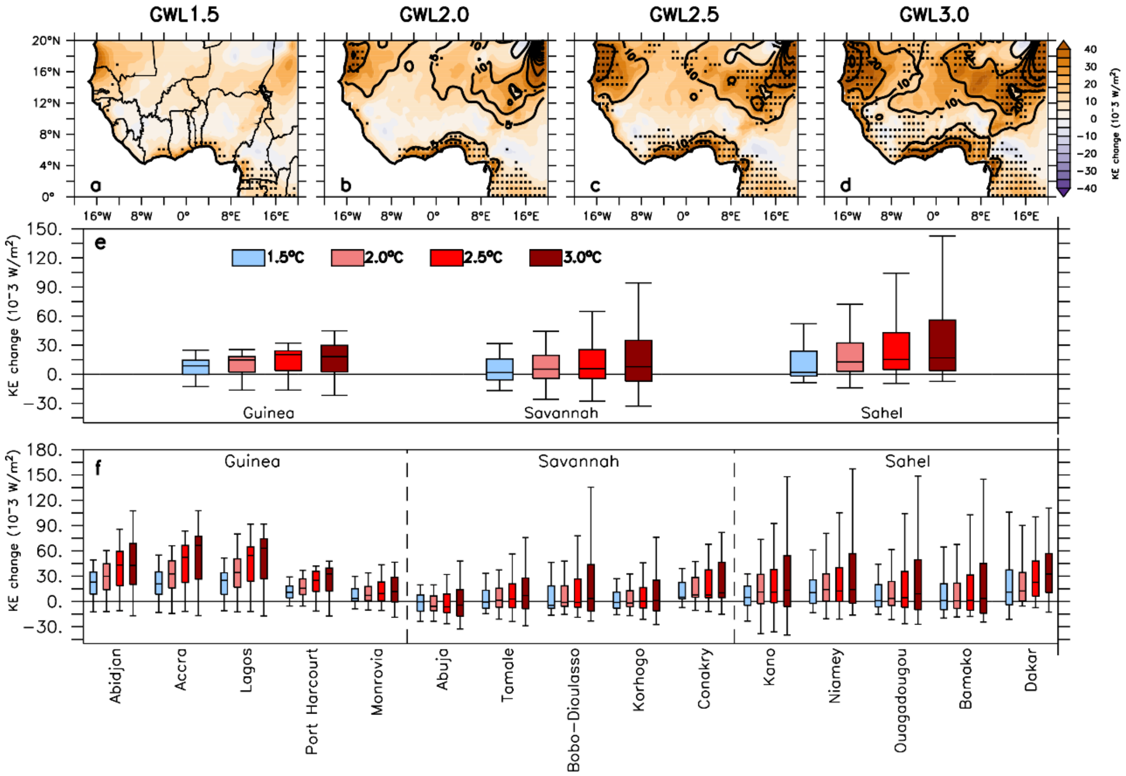

Figure 4.7: Same as Figure 4.5, but for kinetic energy (KE) dissipation into the boundary layer.

4.2 PV power generation potential (PVP)

We assess the evaluation of the PVP and related meteorological variables to the observations. After that, the results of the impact of climate change on PVP and wind speed, solar irradiation, air temperature and relative humidity are shown.

4.2.1 Model evaluation

Figure 4.8 illustrates the spatial distribution of different variables over West Africa: Solar irradiation (Rs), surface temperature (Ts), surface wind speed (Ws) and relative humidity (Rh) as observed (left column) and simulated (Rmean; right column) over West Africa. The correlations (r) between the observed and simulated fields are indicated in the brackets, while the simulation biases are depicted with contours. All the correlations are statistically significant at 95% confidence interval.

The RCMs simulation ensemble mean (Rmean) reproduces well the spatial distribution of solar irradiation (Rs), surface temperature (Ts), wind speed (Ws), and relative humidity (Rh) over West Africa (Figure 4.8). For each variable, the correlation between the simulated and the observed value is high (significant at 95% of confidence level), ranging from 0.90 in Ts to 0.99 in Rh. Furthermore, the simulations capture the latitudinal variations of the variables. In agreement with the observations, the RCMs simulate the minimum Rs, Ts and Ws over the Guinea coast and the maximum values over the Sahel zone. While the minimum Rs (about 160 W/m^2) over the Guinean zone can be attributed to cloudiness from deep convection and land-sea breezes that may intercept the incoming solar radiation (Knippertz *et al.*, 2011), the maximum Rs (about 300 W/m^2) over the Sahel zone may be due to cloudless conditions over that zone for most of the year (Parker et al., 2017). Nevertheless, the lower Ts over the Guinean zone (compared to that over the Sahel zone) may be due to the lower Rs and more vegetation cover (i.e. more evapotranspiration induced cooling) over the zone. The weaker Ws over the Guinean zone (compared to that over the Sahel zone) may be due to the stronger frictional drag on the monsoon flow over the zone. The simulations and observations agree that, in contrast to Rs, Ts and Ws, a maximum Rh (> 66%) is indicated in the Guinean zone and a minimum Rh (< 34%) in the Sahel zone. The maximum Rh over the Guinean zone occurs because the moisture laden monsoon air is advected into the sub-continent through the Guinean zone, and the monsoon flow loses some of its moisture (through rainfall) before reaching the Sahel zone.

Despite the good performance of the RCMs in producing results compatible with the observations, there are some notable biases in the simulation (Figure 4.8). For instance, the Rmean underestimates the Rs over most parts of West Africa by up to 20 W/m^2 along the Guinean coast and in the eastern Sahel zone, while overestimating it over the western Sahel by up to 10 W/m^2 (Figure 4.8b). This bias suggests that the RCMs overestimate the cloudiness over the Guinean coast and underestimate it over the western Sahel. However, the largest negative biases in the Rs are located over the mountainous areas (like the Jos Plateau in Nigeria and the Fouta Djallon mountain in Guinea), suggesting that the RCMs may be too active in simulating orographic cloud (Aguilar *et al*., 2010), or in triggering deep convection over the mountains. Several studies have shown that the cloud representation still poses a major challenge for climate models (Solomon, 2007; Palmer, 2016; Tang et al., 2018). The discrepancies between the simulated and observed Rs may also be due to shortcomings in the satellite observations over a cloudy area. While the RCMs overestimate Ws over the Guinean and Savannah zones and underestimate it over the Sahel zone (Figure 4.8f), they underestimate Ts and Rh over the entire West African region. The largest Ts bias is located in the Sahel zone and the lowest in the Guinean and Savannah zones. The reverse is the case for the Rh bias. Nonetheless, the generally good agreement between the simulated and the observed patterns suggests that the model accurately captures the relevant West African climate dynamics needed for the present study.

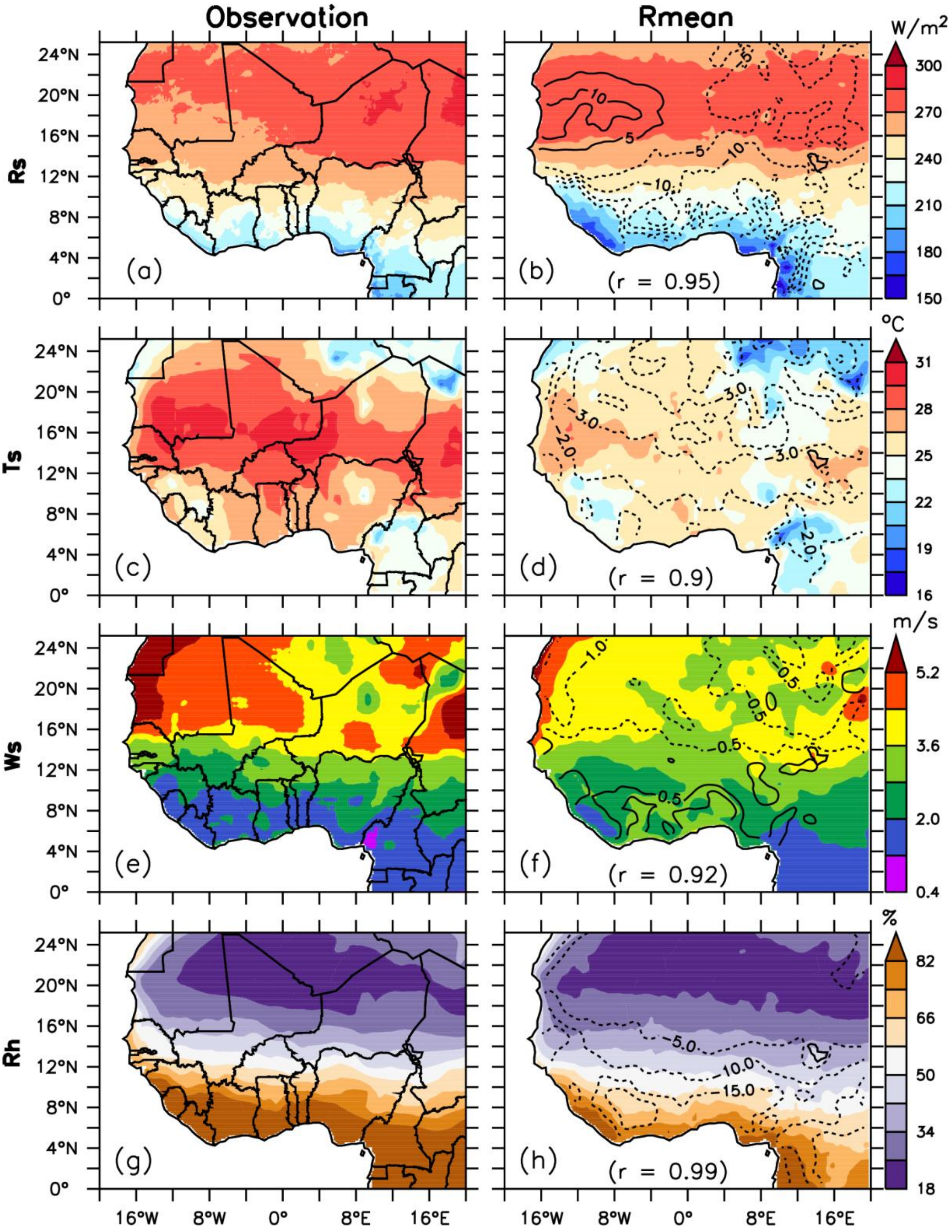

Figure 4.8: The spatial distribution of different variables over West Africa; solar irradiation (Rs), air temperature (Ts), surface wind speed (Ws) and relative humidity (Rh) between the observation and simulated (Rmean) data.

Figure 4.9 portrays the observed and simulated annual cycle of different variables (solar irradiation, Rs; air temperature, Ts; surface wind speed; Ws and relative humidity, Rs) over the three West African zones (Guinean, Savannah and Sahel). The simulation spread is in grey, while the simulation mean (Rmean) and observed values are in black and red lines, respectively. The correlation (r) between the observation and Rmean is indicated in the bracket. The asterisk (*) indicates the correlations that are statistically significant (at 95% confidence level).

As we can see, the RCMs (Rmean) replicate the observed annual cycle of the variables (Rs, Ts, Ws, and Rh) over each climate zone. The correlation between the simulated and the observed cycle is strong ($r > 0.7$) and significant (at 95% confidence level) for all the variables. The RCMs capture the maxima and minima of the Rs, Ts, Ws and Rh over each zone, although with different magnitudes. Over the Guinean zone, in agreement with the observations, the Rmean simulates the Rs and Ts maxima with the Rh minimum in the dry season from December to February, before the arrival of the moist monsoon flow (Sylla *et al.*, 2015); it also shows Rs and Ts maxima with an Rh maximum in the peak wet season (August, during the monsoon flow). However, the Rmean underestimates the observed Rs minimum (by more than 50 W/m^2) and underestimates Rh throughout the year (by about 20%), except in the Sahel zone; it also overestimates the wind speed in all months of the year (by about 1 m/s) over the Sahel zone and by less than 0.5 m/s over the Guinean and Savannah zones. The annual cycles of these variables over the Savannah and Sahel zones are similar to those over the Guinean zone, except that both the observations and the Rmean indicate that Rs and Ts maxima with Rh minima over the Savannah zone occur a month later than their counterparts over the Guinean zone, and that those over the Sahel zone also occur a month later than their counterparts over the Savannah zone. This is consistent with the northward movement of the pre-monsoon conditions over West Africa (Cornforth, 2012). The magnitudes of the Rmean biases over the Savannah-Sahel zones are also comparable to those over the Guinean coast. These results agree with those obtained in previous studies (e.g. Dimas et al., 2011; Abdullahi *et al*., 2017), which showed that high temperature goes with high solar radiation, while high relative humidity reduces solar radiation.

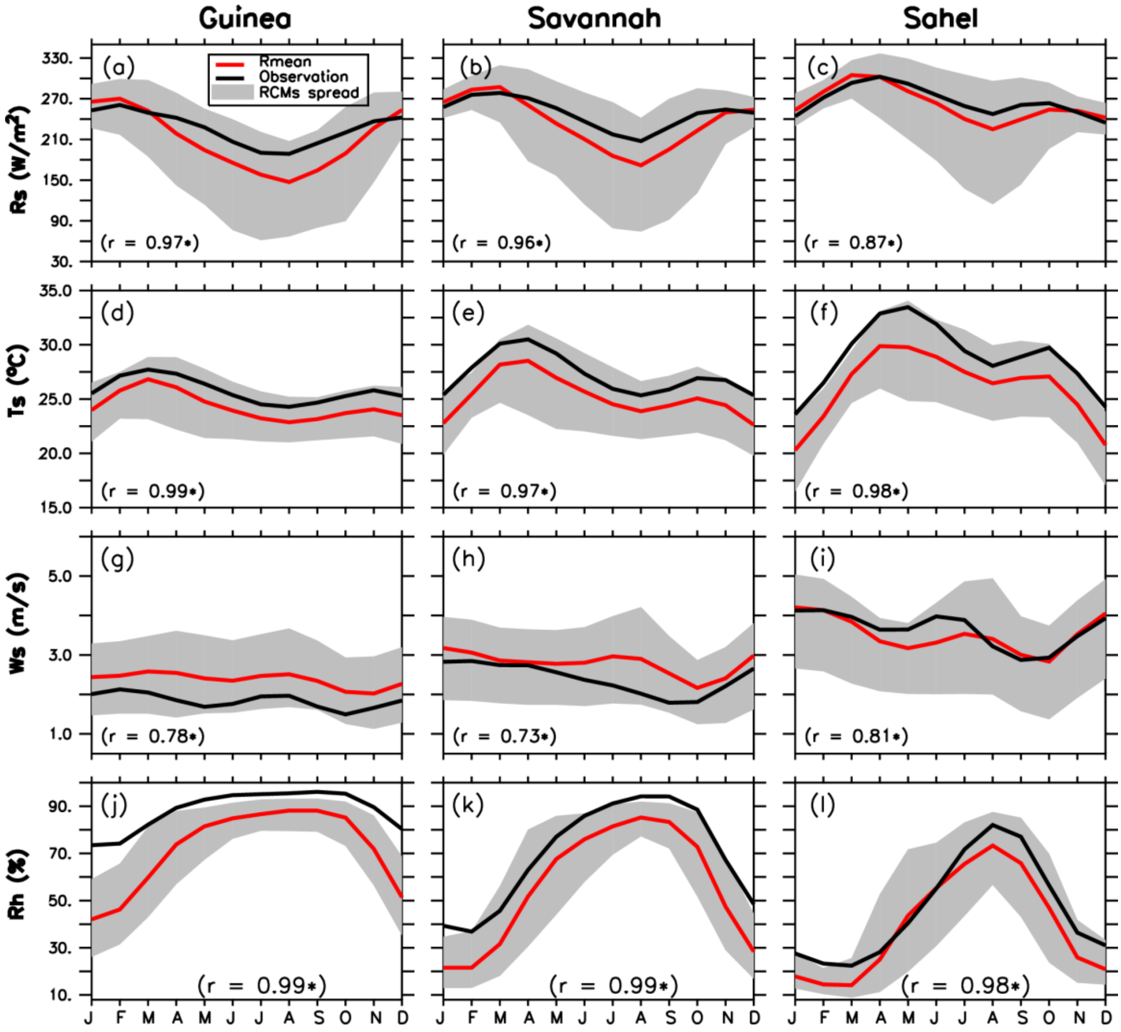

Figure 4.9: The observed and simulated (Rmean) annual cycle of different variables (solar irradiation, Rs; air temperature, Ts; surface wind speed; Ws and relative humidity, Rh) over the different zones.

Figure 4.10 displays the climatology of PV power potential during the reference period (1971-2000) as observed and simulated (Rmean). The contours in panel (a) show the use of Rs and Ts only in the PV calculation, while the contours in panel (b) show the simulation bias. Panels (c -d- e) show the spread of the simulated PV power potential over the three zones (Guinea, Savannah, and Sahel) while panel (f) shows the same over the countries. Each boxplot indicates the minimum, 1st quartile, median, 3rd quartile, and maximum of RCMs.

Clearly, the Rmean also replicates the spatial distribution of PVP over West Africa, with a high correlation value (0.97) (see Figure 4.10a and Figure 4.10b). In agreement with the observations, the Rmean locates the highest PVP over the Sahel zone (19.53 - 28.75%) and the lowest over the Guinean zone (13.05 - 24.75%). The pattern mostly follows the spatial distribution of Rs, and to an extent, that of Ts. The major shortcoming in the spatial distribution of the simulated PVP is the positive bias (about 1%) over the western Sahel zone and the negative bias over the western Guinean zone (about 0.5%). Over all three zones (Guinean, Savannah, and Sahel), the observed annual cycle of PVP mimics that of Rs, showing the highest PVP (24.89%, 27.15%, 29.28%, respectively) in February when the clear skies lead to maximum Rs and the lowest values of PVP, in August when the presence of clouds reduces the Rs to the minimum. The Rmean realistically reproduces this annual cycle, but with a larger amplitude than the observations; moreover, while it overestimates the maximum values, it underestimates the minimum values. These biases are consistent with those obtained from the simulated Rs. Nevertheless, the simulated annual mean of PVP over the country is in good agreement with the observations.

Over all the West African countries, the observed values fall within the interquartile of the model spread (Figure 4.10f). The simulations and the observations agree that the highest PVP efficiency is in Niamey (25.98%), while the lowest value is in The Gambia (14.85%). The good agreement between the simulations and the observations in relation to the spatio-temporal variation of Rs, Ts, Ws and PVP suggests that the simulations correctly capture the necessary atmospheric processes (e.g. monsoon systems) that control PVP variation over West Africa. The strong correlation between Rs and PVP found in this study is consistent with previous studies, which also found an increase in solar flux and an increase in the PV power output (Ghitas, 2012; Ettah *et al*., 2011). In addition, the results indicate that the inclusion of Ws and Rh generally decreases the PVP over West Africa, with the maximum decrease over the Guinean coast. This decrease is generally small over the sub-continent, but it can be up 1.1% (i.e. 6.6% of the results without including Ws and Rh) over the Guinean zone, where the wind speed is low and relative humidity is high.

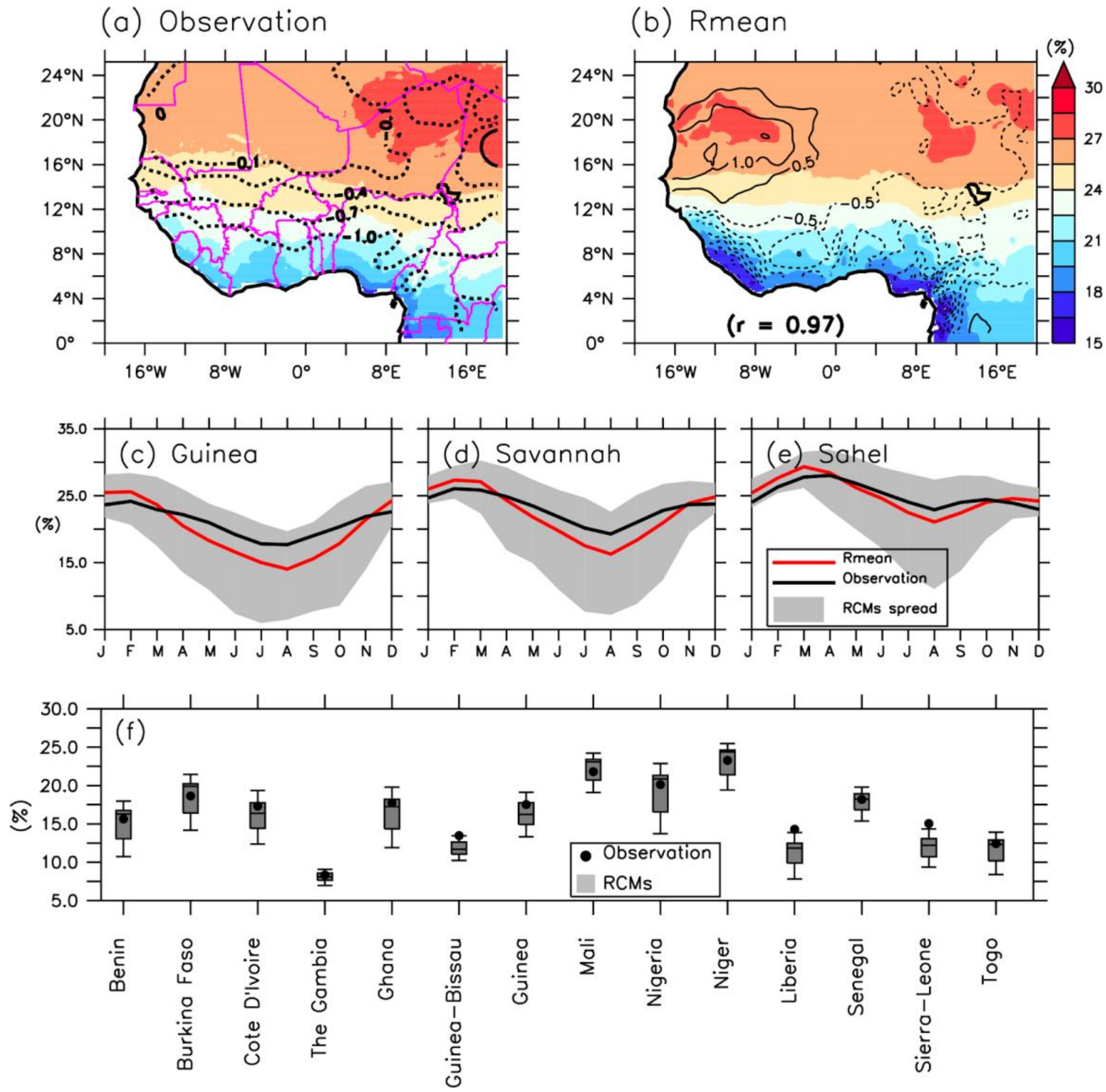

Figure 4.10: The climatology of PV power potential during the reference period (1971-2000) as observed and simulated (Rmean).

4.2.2 Climate change projection

4.2.2.1 PVP and climate variables

Figure 4.11 depicts the projection of the ensemble mean (Rmean) of the annual mean of PV power generation potential (PVP), solar irradiation (Rs), surface temperature (Ts), wind speed (Ws), and relative humidity (Rh) over West Africa under the four global warming levels (GWL1.5, GWL2.0, GWL2.5, and GWL3.0) over West Africa. The area where the changes are statistically significant (at 95% confidence level) are indicated with dots. The contour lines indicate the difference between GWL1.5 and each corresponding GWL. The correlation between the PVP pattern and other variables is shown in brackets.

From the Figure 4.11, the simulation ensemble projects a decrease in the PVP over West Africa, except along the coastal and mountainous areas where it projects an increase. These changes are statistically significant at 95% over the whole region under the GWLs. However, the magnitude of the change varies over the region and increases non-linearly with increasing GWLs (Figure 4.11a-d). At GWL1.5, the decrease is about 0.72% north of 16^{o}N and less than 0.72% south of the latitude. In general, the PVP decreases by 0.5% between GWL1.5 and GWL2.0 but by 0.4% between GWL2.0 and GWL2.5 (Figure 4.11). So, at GWL2.5, a decrease of about -1.5% is projected north of 16^{o}N and about 1.35% is projected south of the latitude. The result is consistent with previous studies that have shown that climate change may reduce the PV power output over West Africa. For example, Huber *et al*. (2016) projected a general decrease in PVP over West Africa. They used an ECHAM4 (GCM) coupled with aerosol-climate model for the future period of 2035-2039 compared to the past period (1995-1999). Using eight regional climate models (CORDEX), Bazyomo *et al*. (2016) also projected a decrease of PVP over the West African countries. However, the magnitude of the decrease of

PVP found in this paper differs with that of Bazyomo *et al*. (2016). This may due either to the method used to compute the solar cell temperature or the future period used in their study (2006-2045), while our paper focuses on the projection at specific warming level as suggested the Paris agreement. In addition, the difference may come the fact that we used the multi ensemble mean while they study focused on individual models

The projected changes in PVP (hereafter, ΔPVP) can be explained by the corresponding changes in the four climate variables (hereafter, ΔRs, ΔTs, ΔWs and ΔRh; Figure 4.11). Among the four, ΔRs has the highest spatial correlation ($r > 0.93$) with ΔPVP (Figure 4.11 e-h). As with ΔPVP, ΔRs generally decreases (up to 3 W/m^2) over West Africa with a little increase along the coastal zones and mountainous areas at all the GWLs; the maximum decrease is located in the Sahel zone, and the minimum decrease is in the Savannah zone. Counterintuitively, the global warming may reduce the solar irradiance over West Africa. This reduction (known as solar dimming) is due to the feedback of the global warming change Rs through increasing cloud cover and aerosols. For instance, some studies have projected an increase in precipitation and cloud cover over the Guinean zone (Sylla *et al*., 2010) and a higher concentration of aerosols over the Sahel zone (Touré *et al*., 2012) under the warmer climate. Both changes will reduce Rs. This result is consistent with previous regional studies that have attributed a long-term decrease in solar energy in the past climate to atmospheric aerosol from anthropogenic activities (Stanhill and Cohen, 2001; Wild *et al*., 2005; Pinker *et al*., 2005). The present study thus shows that global warming may indeed reduce PVP over West Africa through solar dimming.

The spatial distribution of ΔTs also has a high but negative spatial correlation ($|r| \geq 0.82$) with ΔPVP, although the magnitude of the correlation reduces with increasing GWLs (Figure 4.11i-l). As anticipated, an increase in Ts over West Africa is projected with increasing GWLs, but the regional warming rate is higher than the global rate, especially above 12°N, where warming is more than 1.2°C per 1°C GWL; the rate is even more over the eastern Sahel zone (> 1.3°C per 1°C GWL). This pattern is consistent with previous studies (e.g. Sylla *et al.*, 2016; Abiodun *et al.*, 2012), which attributed the lowest warming rate along the coast to the cooling effect of the monsoon air from the ocean. The cooling effect, which decreases inland, may be weak or absent over the Sahel zone. However, the strong negative spatial correlation between the changes in Ts and PVP indicate that an increase in Ts contributes to the projected decrease in PVP. This is consistent with previous studies, which report that an increase in temperature leads to a decrease in PVP (Fesharaki *et al.*, 2011; Jerez *et al.*, 2015; Wild *et al.*, 2015). Hence, in addition to the influence of solar dimming, the maximum increase in Ts over the Sahel zone could also induce the maximum decrease in PVP over the zone.

In contrast to ΔRs and ΔTs, ΔWs and ΔRh are poorly correlated with ΔPVP (Figure 4.11). The correlation between ΔWs and ΔPVP ranges from -0.18 (at GWL1.5) to 0.47 (at GWL2.5), while the correlation between ΔRh and ΔPVP ranges from -0.02 (at GWL2.0) to 0.21 (at GWL3.0). However, ΔWs and ΔRh are only significant (at 95% confidence level) at GWL2.0 and GWL3.0, where an increase in Ws (maximum: 0.2 m/s) and a decrease in Rh (maximum: 2%) were projected over the Sahel zone. The increase in Ws can be attributed to the projected stronger temperature gradient over West Africa (Abiodun *et al.*, 2012), while the decrease in Rh can be due to the high saturated mixing ratio in the projected warmer climate (Abiodun *et al.*, 2012). However, the direction of changes in Ws and Rh are not consistent with that of PVP, in that the projected increase in Ws and decrease in Rh over the Sahel zone would increase the PVP. This suggests that the influence of change in Rs and Ts would dominate the projected change in PVP.

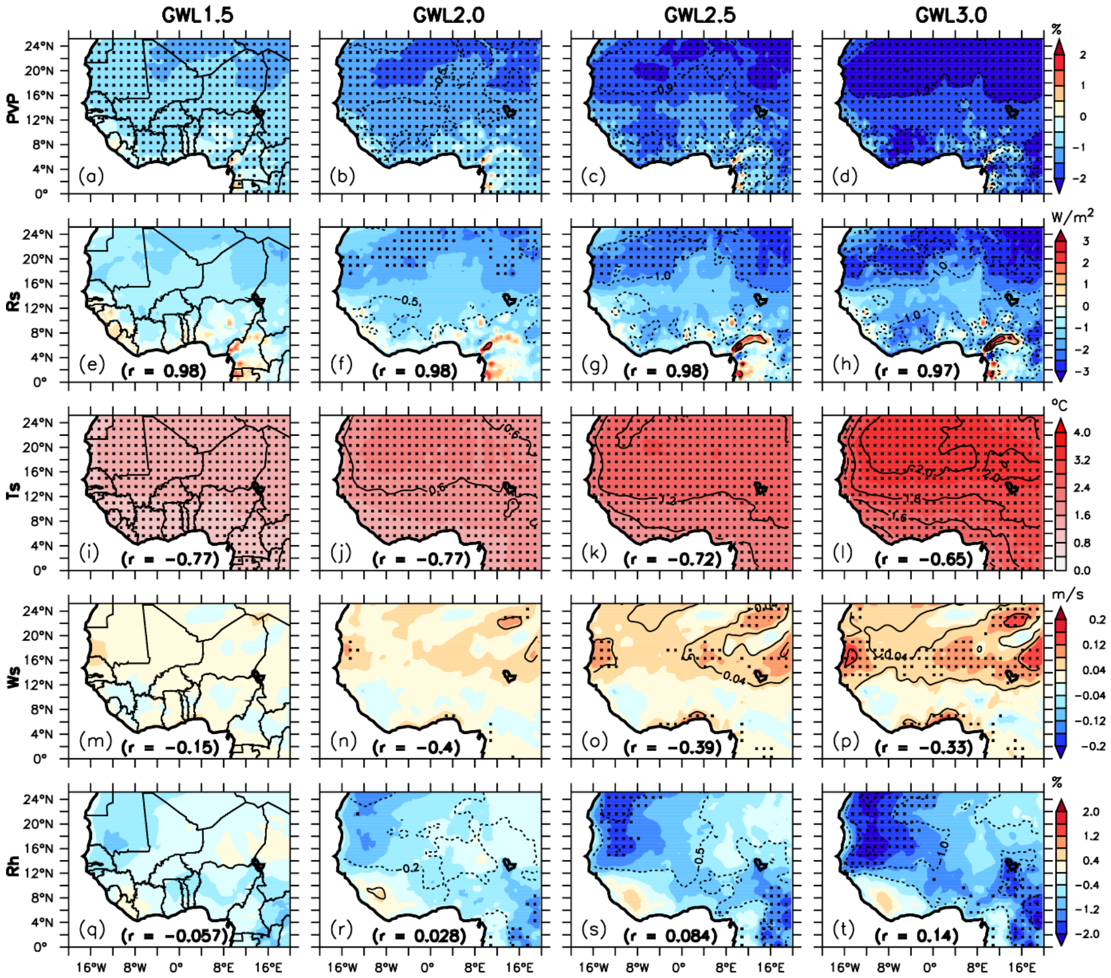

Figure 4.11: Projection of the ensemble mean of the annual mean of PV power generation potential (PVP), solar irradiation (Rs), surface temperature (Ts), wind speed (Ws), and relative humidity (Rh) over West Africa under the four global warming levels (GWL1.5, GWL2.0, GWL2.5, and GWL3.0).

Figure 4.12 evinces the projected changes of the model ensemble mean in the annual cycle over different West African zones. These projections are based on the four GWLs (GWL1.5, GWL2.0, GWL2.5, and GWL3.0). Panel (a-c) shows the changes in respect of the PV power generation potential (PVP); (d-f) solar radiation (Rs); (g-i) air temperature (Ts); (i-k) surface wind speed (Ws) and (i-n) relative humidity (Rh).

Figure 4.12 reveals that the projected decrease in PVP (i.e. negative ΔPVP) over West Africa does not occur throughout the year. A positive ΔPVP is projected in April to May over the Guinea zone, in May and July over the Savannah and the Sahel zone (Figure 4.12a-c). However, while the negative ΔPVP can be as much as -2.8% (in November–January; Figure 4.12c), the maximum positive ΔPVP is about 2.41% over the Sahel and the Savannah zones (in July; Figure 4.12c). The monthly variation of ΔPVP is similar to the ΔRs, ΔWs and ΔRh than with ΔTs (Figure 4.12). This implies that the impacts of global warming on PV over each zone are minimal in the months when the monsoon system arrives over the three zones. Figure 4.12 shows that these periods are associated with positive ΔRs and ΔWs and negative ΔRh. The positive ΔWs is consistent with the projected increase in the monsoon flows, following the stronger temperature gradient over West Africa (Abiodun *et al.*, 2012). The negative ΔRh suggests drier conditions and less cloudiness because the warmer atmosphere would require more moisture to reach saturation and produce cloud. Moreover, the positive ΔRs is consistent with less cloudiness, as a decrease in cloudiness will allow more insolation to reach the surface. All these changes would tend to induce a positive ΔPVP during this period. Hence, the arrival of the monsoon system plays a crucial role in modulating the impact of global warming on the seasonal variation distribution of ΔPVP.

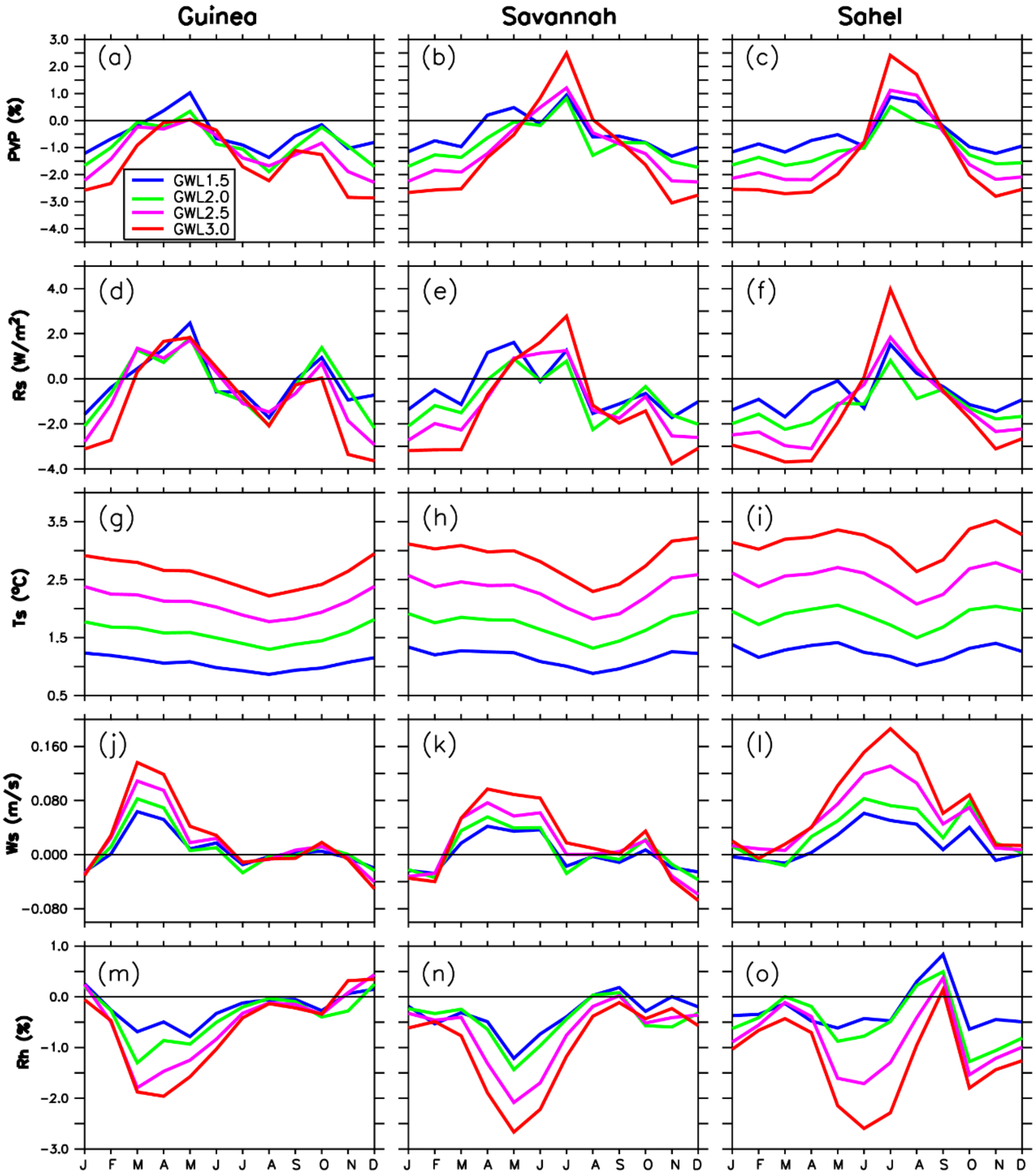

Figure 4.12: Projected changes of the model ensemble mean in the annual cycle distribution of PV power generation potential (PVP), solar irradiation (Rs), surface temperature (Ts), wind speed (Ws), and relative humidity (Rh) over different West African zones under the four global warming levels (GWL1.5, GWL2.0, GWL2.5, and GWL3.0).

4.2.2.2 PVP over West African countries

Figure 4.13 exhibits the projection of the ensemble mean of the annual mean PV power generation potential (PVP) over the West African countries under the four global warming levels (GWL1.5, GWL2.0, GWL2.5, and GWL3.0). Each boxplot indicates the minimum, 1st quartile, median, 3rd quartile, and maximum of the RCMs.

Obviously, the simulation ensemble projects a decrease in PVP over all the selected West African countries. However, the level of agreement among the simulations on the projection (which is a measure of the robustness of the projections) varies over the countries. For example, at GWL1.5, while less than 75% of the simulations agree on the decrease in Sierra-Leone and Liberia, more than 75% of the simulations agree on it over other countries. This discrepancy among the simulations in respect of the projection may be attributed to the differences in the simulation configuration (Jerez *et al.*, 2018; Giorgi, 2010), but it could also be attributed to the magnitude of the signal-to-noise ratio in the climate variables. Nonetheless, the robustness of the projection over all the countries does increase with increasing GWLs, such that, at GWL3.0, more than 75% agree on the decrease over all the countries. The magnitude of the projected decrease also varies over the countries. Among the countries, Niger is projected to experience the largest decrease (about -2.13% at GWL1.5 and about -3.59% at GWL3.0). This is coherent with the study of Bazyomo *et al.* (2016), which indicated Niger would have the highest decrease in PVP in West Africa by 2045. However, the magnitude of this decrease differs from the results of Bazyomo *et al.* (2016), who found a maximum decrease of the mean trend of about 0.032%/year or 1.28% for the period of 2006 – 2045. However, the magnitude of the decrease of PVP differs with the results of Bazyomo *et al.* (2016) where the maximum decrease of the mean trend is about 0.032% /year or 1.28% for the period of 2006-2045. In general, the results of Bazyomo *et al.* (2016) in the PVP projection are lower than our results. Our study reveals that including Ws and Rh in calculating the PVP influence the magnitude. Even though the total change in PVP (ΔPVP) due to the contribution of change in Ws and Rh is negligible, the results show that the two variables contribute to affect the PV generation potential over West Africa.

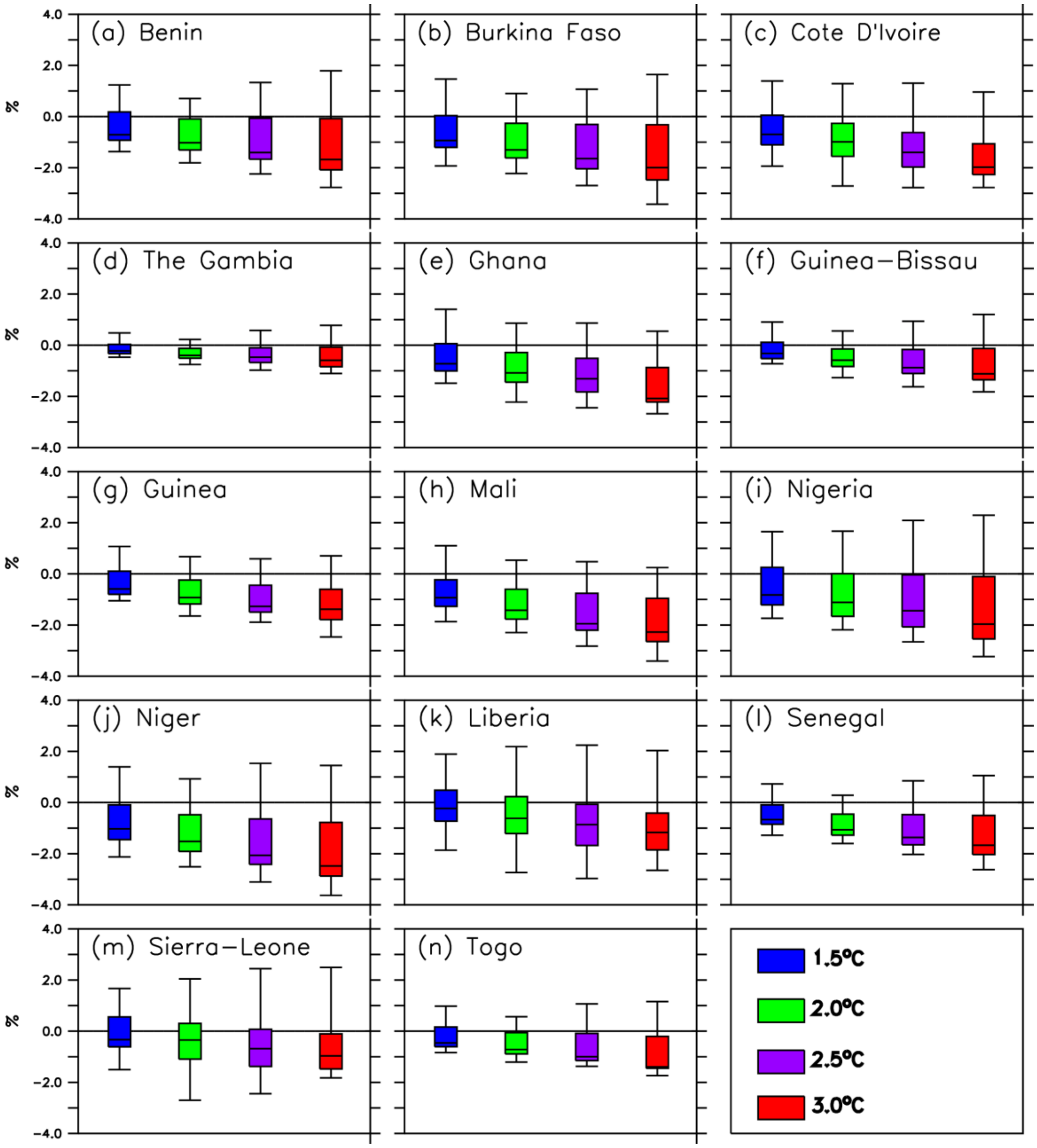

Figure 4.13: Projection of the ensemble mean of the annual mean PV power generation potential (PVP) over the West African countries under the four global warming levels (GWL1.5, GWL2.0, GWL2.5, and GWL3.0).

The magnitude of the decrease in PVP projected over the West African countries is much lower than the one projected in Europe and similar to some region in the world. For instance, using EURO-CORDEX simulations, Jerez *et al* (2015) projected -14% decrease over some Northern European countries. In addition, with the HadGEM1, California (~ -2%), Nevada (~ -3.5%), Algeria (~ -1%), Saudi Arabia (~ -5%) and Australia (~ -0.5%) may experience a decrease in PVP. In the other hand, some countries like China, Spain, and Germany may know an increase in the PVP (Crook *et al*., 2011). This suggests that the impact of climate change on PVP varies according to the regions with different magnitudes. Even if our results show a similar magnitude in the change of the PVP compared to other regions, the results of this study should be taken with care due to the model errors and uncertainties in the projection. However, with the ongoing project over the region (see table 1) at the large scale for electricity production, decision-makers should take into account the future decrease of the PVP in their agenda.

4.2.2.3 Total change in PVP due to the contribution of Rs, Ts, Ws and Rh

Figure 4.14 and 4.15 present the projection of ensemble mean of the total change in PVP due to the contribution of each variable. The spatial distribution of the total change in PVP (ΔPVP) due to the contribution of changes in temperature ($\Delta\mathrm{Ts.PVP}$) exhibits the largest influence over West Africa (Figure 4.14e-h). This contribution increases as the warming level increases. Moreover, at all GWLs, the highest magnitude of the contribution is in the Sahel zone, whereas the lowest magnitude in the Guinean zone. For instance, over the Sahel the GWL1.5 (-0.632%), GWL2.0 (-0.93%), GWL2.5(-1.26%) and GWL3.0 (-1.58%) is higher than the GWL15 (-0.53%), GWL2.0 (-0.79%), GWL2.5 (-1.06%) and GWL3.0 (-1.32%) over the Guinea zone. This study reveals that as the global warming level increases, the increase in local temperature over the region contributes to decrease the PVP. The results of this study are in lines with previous study showing that the increase in temperature drops the efficiency of the solar cells; hence the PVP (Radziemska 2003; Fesharaki *et al*., 2011). This explains why some studies advocate reducing the vulnerability of the PV cells' performance to the ambient temperature (Patt *et al*., 2013; Jerez *et al*., 2015). The general decrease in Rs also contributes to the total change in PVP over the region. The ΔPVP due to the contribution of change in solar irradiation ($\Delta \mathrm{Rs.PVP}$) exhibits a positive value along the coastal area and in the mountainous zones, and a negative value elsewhere (Figure 4.14a-d). Furthermore, the contribution of $\Delta \mathrm{Rs.PVP}$ increases with increasing warming levels. For example, over the Sahel zone, the $\Delta \mathrm{Rs.PVP}$ contributes about -0.24% under GWL1.5 while -0.54% under GWL3.0. Conversely, the contribution of $\Delta \mathrm{Ws.PVP}$ (Figure 4.14i-l) and $\Delta \mathrm{Rh.PVP}$ (Figure 4.14m-p) has an insignificant effect on the total change in the PVP under the various warming levels. This could be explained either by the small contribution of Ws and Rh used in Equation (3.12) or to the small changes of the projection in respect of both variables. Overall, this suggests that the total change in PVP may come from the change in Rs and Ts but mostly from the change of Ts.

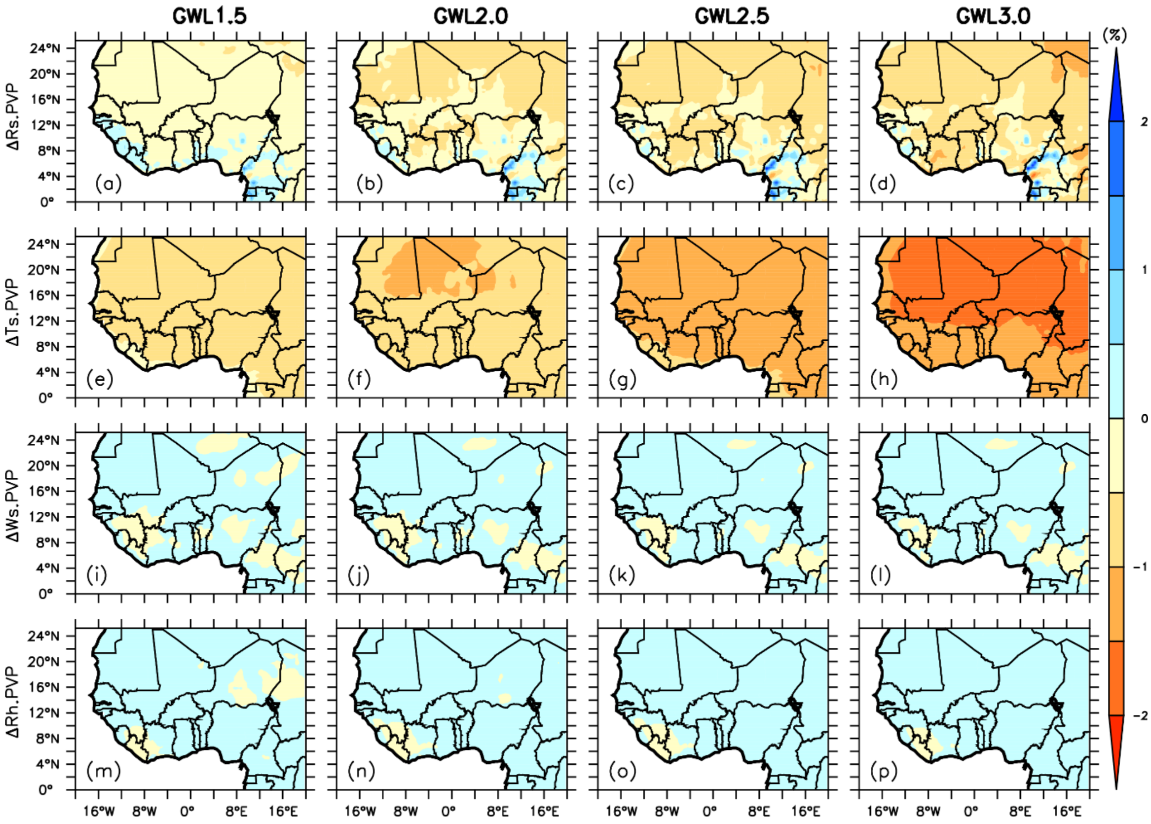

Figure 4.14: Projection of ensemble mean of the total change in PVP due to the contribution of each variable; solar irradiation ($\Delta Rs.PVP$); air temperature ($\Delta Ts.PVP$); surface wind speed ($\Delta Ws.PVP$); relative humidity ($\Delta Rh.PVP$ over the West Africa under the four GWLs (GWL1.5, GWL2.0, GWL2.5, and GWL3.0).

Among the seven components of ΔPVP in Equation (15), $\Delta Rs.PVP$ and $\Delta \mathrm{Ts.PVP}$ make the largest contributions to ΔPVP (Figure 4.15). The contributions of other components $(\Delta \mathrm{Ws.PVP}, \Delta \mathrm{Rh.PVP})$ are negligible. This is why their plots are overlaid and close to zero. However, the characteristics of $\Delta Rs.PVP$ and $\Delta \mathrm{Ts.PVP}$ differ. For instance, in the annual cycles, $\Delta \mathrm{Rs.PVP}$ features positive values in some seasons and negative values in others, while $\Delta \mathrm{Ts.PVP}$ features negative values throughout the year. Thus, the contributions of $\Delta \mathrm{Ts.PVP}$ and $\Delta \mathrm{Rs.PVP}$ to ΔPVP are additive in some seasons, but opposite in other seasons. In addition, while the magnitude of $\Delta \mathrm{Rs.PVP}$ is virtually invariant at increasing GWLs, that of $\Delta \mathrm{Ts.PVP}$ increases with increasing GWLs. At GWL1.5, the negative contribution of $\Delta \mathrm{Ts.PVP}$ to ΔPVP is lower than the positive contribution from $\Delta \mathrm{Rs.PVP}$ in some seasons, making ΔPVP positive. But, at GWL3.0, the negative contribution overwhelms the positive contribution of $\Delta \mathrm{Rs.PVP}$ throughout the year.

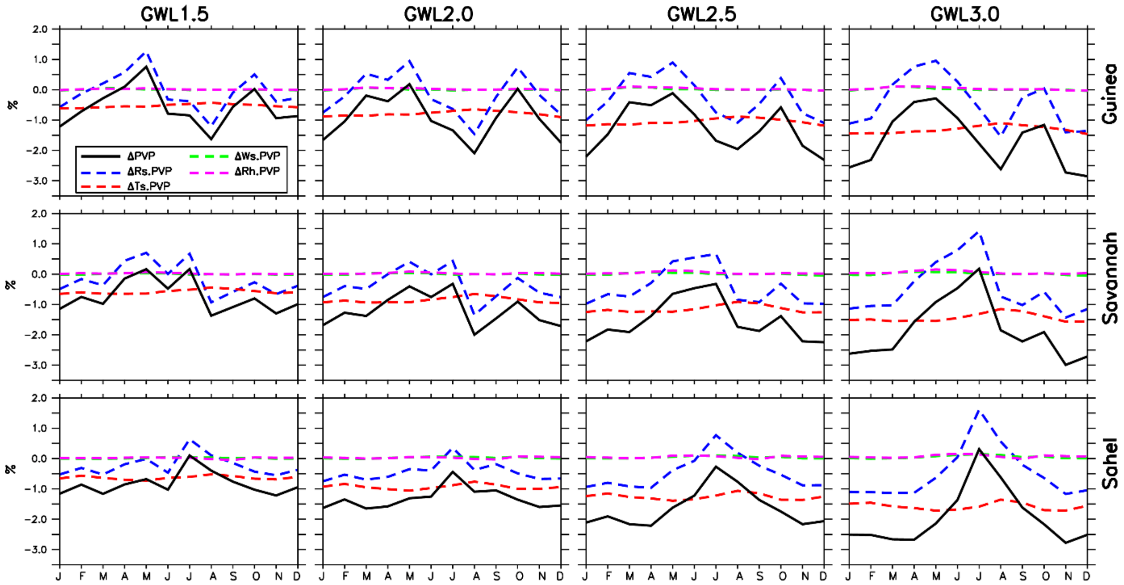

Figure 4.15: Projected annual cycle of the contribution of each term to the projected change PV power generation potential over different West African zones and under various global warming levels.

4.3 WRF model

Firstly, in this sub-section, we evaluate the Rs of WRF model output of the one-year simulation vis-à-vis observations over the West Africa and its three zones. Then, the results of the sensitivity of the water vapour absorption in the Dudhia scheme in WRF model is presented. Finally, the results of the long-term simulation of the improved Dudhia scheme and the default Dudhia scheme in WRF model are exposed.

4.3.1 Evaluation of one-year simulation of WRF model

4.3.1.1 Spatial distribution of the downward shortwave radiation (Rs)

Figure 4.16 displays the spatial distribution of the downward shortwave radiation (Rs) over West Africa using different WRF shortwave radiation schemes and the WRF Dudhia modified shortwave radiation scheme (DudhiaM). The contour lines depict the difference between the observed Rs and the different simulations. The value in bracket specifies the spatial correlation between the observation and the different schemes.

Most of the schemes correctly reproduce the spatial distribution of the observed Rs over West Africa (Figure 4.16). In agreement with the observations, the schemes exhibit low values of Rs over the Guinean zone and high values over the Sahel zone as a result of cloudless conditions throughout the year (Parker *et al.*, 2017). In other words, they capture the annual northward movement of the Rs over West Africa. Moreover, the correlation between the observations and the schemes ranges from 0.71 to 0.88. However, the modification of the Dudhia scheme (hereinafter referred to as DudhiaM) is closer to the observation than the Dudhia scheme and the other schemes used in this study in simulating the Rs over the region. For instance, the DudhiaM has the highest spatial distribution in mimicking the Rs over the subcontinent. Over the region, the observed value of the Rs is roughly 244.9 W/m^2, while the simulated Rs of the DudhiaM shows a value of about 249.8 W/m^2. In comparison with the other schemes, namely, Dudhia (269.4 W/m^2), Cam (268.1 W/m^2), rrtmg (288.1 W/m^2), Goddard (303.5 W/m^2) and GoddardM (295.5 W/m^2), the DudhiaM has the closest magnitude of the observed Rs over West Africa. At the zonal scale, over the Guinean zone (222.7 W/m^2 with the observations), the magnitude of the DudhiaM (234.7 W/m^2) is lower than those of Dudhia (254.6 W/m^2), Cam (234.8 W/m^2), rrtmg (277.3 W/m^2), Goddard (289.1 W/m^2) and GoddardM (280.1 W/m^2). This suggests that the DudhiaM simulates the Rs the Dudhia and other schemes under cloudy conditions. Also, a similar finding occurs under cloudless conditions (over the Sahel zone). The results demonstrate that the improvement of the water absorption in the Dudhia scheme enhances the accuracy of the simulation of Rs over the West African region. This result ties in well with previous studies suggesting that the model of Lacis and Hansen (1974) (used in the Dudhia parameterisation of the WRF model) overestimates the available Rs (Ramaswamy and Freidenreich, 1991; Briegleb, 1992; Chou and Lee, 1996).

Despite the good performance of the simulations based on the WRF model schemes and the DudhiaM in respect of Rs, there are notable biases. All the WRF schemes overestimate the magnitude of Rs over the region. These biases vary over the three zones. High positive biases are located in the coastal area at the magnitude of 30 to 60 W/m^2 and lower positive biases (10 -30 W/m^2) over the Sahel zone. However, the biases differ from one scheme to another. For example, the highest bias is found in both Goddard schemes (the modified and the non-modified), where the magnitude reaches 60 W/m^2, whereas the Dudhia and the Cam scheme simulate a value of 30 W/m^2 over the Guinean zone. In the same area, the bias can reach 40 W/m^2 with the use of the rrtmg scheme. This implies that climate models are still struggling to simulate correctly the

Rs in cloudy areas, which has been proved in prior studies (Stephens and Tsay 1990; O’Hirok and Gautier 2003). Over the Sahel zone, the maximum bias is lower in the Dudhia scheme (20 W/m^2) than in the Cam (30 W/m^2), rrtmg (40 W/m^2), Goddard (50 W/m^2) and GoddardM (40 W/m^2) schemes. The differences between the schemes can result from the different configurations used in each scheme, such as aerosols, water vapour absorption, ozone atmospheric gases and so on. Nevertheless, the Dudhia scheme exhibits good results in terms of simulating Rs over West Africa. However, the DudhiaM further reduces the biases over the West African region and its zones. The DudhiaM overestimates the Rs over the Guinean zone (10 W/m^2), while it underestimates the Rs over the Sahel zone (-5 W/m^2). Nonetheless, it leads to good results, even if the improvement does underestimate the Rs over the Sahel zone and overestimate it over the Guinean zone.

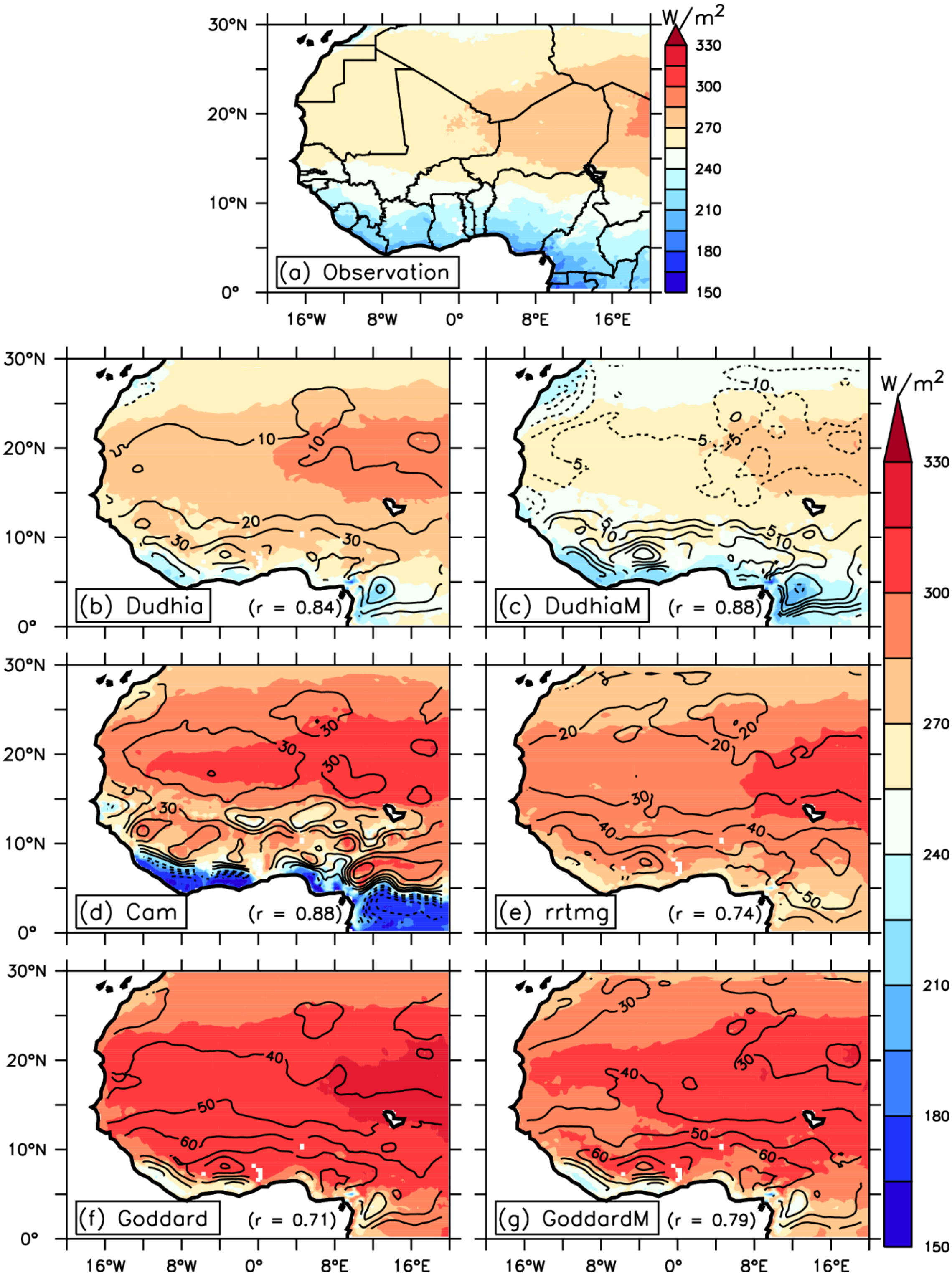

Figure 4.16: Spatial distribution of the downward shortwave radiation (Rs) over West Africa using different WRF shortwave radiation schemes and the WRF Dudhia modified shortwave radiation scheme (DudhiaM).

4.3.1.2 Temporal distribution of the downward shortwave radiation (Rs)

Figure 4.17 shows the temporal distribution of the diurnal and annual cycle and the Tailor Diagram of the downward shortwave radiation (Rs) of different WRF shortwave radiation schemes and the modified one (DudhiaM). Panels (a-d) show the observed diurnal cycle of the downward shortwave radiation (Rs) compared to the different WRF shortwave radiation schemes and the WRF Dudhia modified shortwave radiation scheme (DudhiaM) over West Africa and in its different zones. Same for (e-h), but for the annual cycle of Rs. Same also for (i-l), but for the Taylor diagram of the hourly simulation data.

The model simulations follow the pattern of the annual mean diurnal cycle of the observed Rs over West Africa and its different zones (Figure 4.17a-d). In line with the observations, in general, the model simulations correctly capture the sunrise (600 UTC) and the sunset (1800 UTC) over the different zones. The simulations also capture the rapid increase of the Rs in the early morning (800 UTC), the maximum around noon (1200 UTC) and the decrease in the Rs in the late afternoon (1700 UTC). However, most of the simulations failed to capture the magnitude of the diurnal cycle of the Rs over West Africa. The magnitude of the Rs before 900 UTC and after 1600 UTC is mostly close to the observed value for most of the simulations. The DudhiaM gives much better results after 900 UTC than the other simulations over the different zones. This may due to the high absorption of water vapour in the DudhiaM scheme because of the presence of the morning stratus cloud in the region, especially over the Guinean zone (Knippertz *et al*., 2011). In addition, the DudhiaM scheme catches the apex of the Rs over the subcontinent. For instance, over the Sahel zone, the observed value reaches around 874.5 W/m^2, whereas the magnitude of DudhiaM is about 875.9 W/m^2, which is lower than Dudhia (935.9 W/m^2), Cam (928.7 W/m^2), rrtmg (955.1 W/m^2), Goddard

(999.3 W/m^2) and GoddardM (980.7 W/m^2). From the results, it is clear that the improved Dudhia scheme (DudhiaM) gives better results for the diurnal cycle of the Rs over West Africa than the WRF radiation schemes (Dudhia, Cam, rrtmg, Goddard and GoddardM) used in this study.

The WRF radiation scheme and the DudhiaM correctly replicate the annual cycle of the Rs over West Africa (Figure 4.17e-h). Most of them moreover capture the monthly variation of the Rs over the region and its different zones. In agreement with the observations, the simulations catch the monthly peak (March and April) and the nadir (August) of Rs over the region. Also, the magnitude of the simulation in the monthly variation of the Rs increases with an increase in the latitude. That is, high values are in the Sahel zone and low values on the Guinean coast. Even though there exists a good pattern in simulating the annual cycle of the Rs, there are some poor tendencies in the simulations. Most of the simulations overestimate the magnitude of the Rs throughout the year. However, the magnitude of the Rs of the DudhiaM scheme is closer to the observed Rs than is the case with the WRF radiation scheme over the region. Over the Sahel zone, from March to July, the DudhiaM and the observations were matched. Nonetheless, from March to October, the DudhiaM overestimates the Rs, while it underestimates it in the other months over West Africa and its climatic zones. These biases are lower than is the case with the WRF radiation schemes, however. Our results thus demonstrated that the DudhiaM reduces the biases in simulating the annual cycle of the Rs over the West African region.

Figure 4.17i-l depicts the normalised standard deviation and the correlation coefficient between the observations and each of the simulations for the hourly data (over one year of simulated data). The result shows how well the simulations capture the temporal variability and standard deviation of the Rs over the region. The correlation between each simulation and the observations is more than 0.95 over the region and the different climatic zones. Conversely, the normalised standard deviation is less than 1.3. However, the normalised standard deviation of the DudhiaM in close to 1 over the region, especially over the Sahel zone. This indicates the almost perfect simulation of the DudhiaM over the Sahel zone. Over the Guinean zone, the value is lower than the Cam scheme, but it has a lower correlation coefficient value than the DudhiaM scheme.

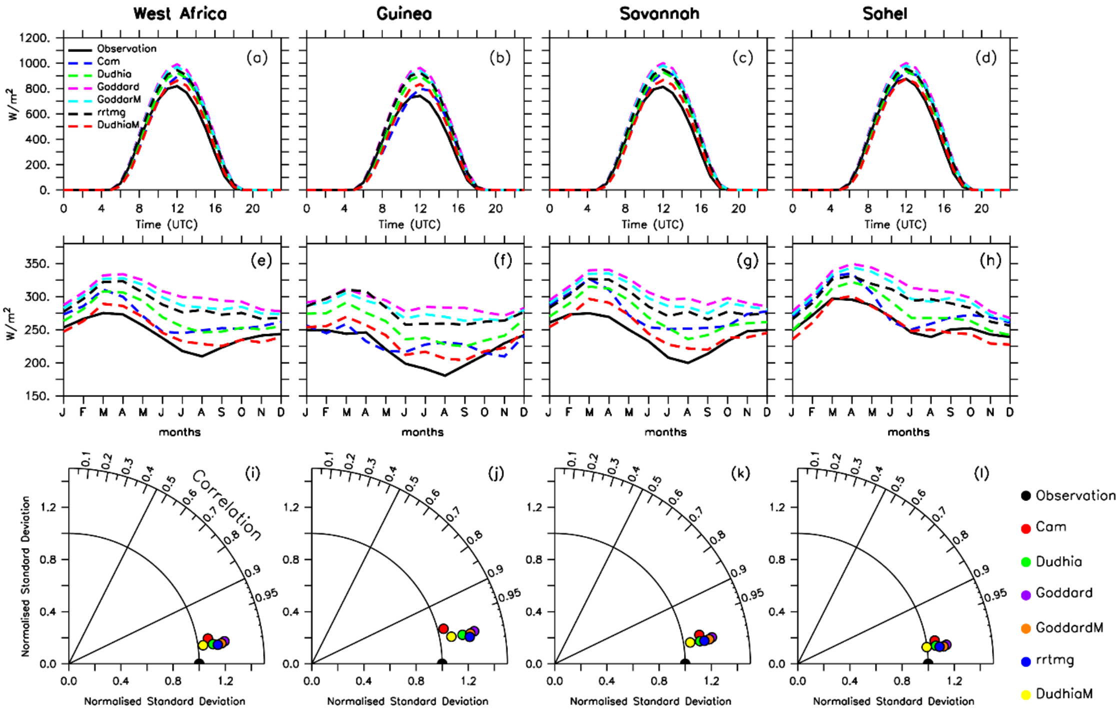

Figure 4.17: Temporal distribution of the diurnal and annual cycle and the Tailor Diagram of the downward shortwave radiation (Rs) of different WRF shortwave radiation schemes and the modified one (DudhiaM).

4.3.1.3 Statistical analysis

Figure 4.18 indicates the Statistical analyses on the downward shortwave radiation (Rs) over West Africa and the three zones (Guinea, Savannah and Sahel). We Compare the root mean square error (RMSE), mean absolute error (MAE) and the bias between the WRF shortwave radiation schemes and the WRF Dudhia modified shortwave radiation scheme (DudhiaM). On other hands, Figure 4.19 presents the linear regression between WRF shortwave radiation schemes and DudhiaM and the observed shortwave radiation (Rs) over West Africa and the three zones.

The DudhiaM outperforms better than the different schemes in simulating the Rs over West Africa (Figure 4.18). Most of the WRF radiation schemes exhibit high values over the three zones in the statistical analysis. For instance, the Goddard scheme shows high RMSE of about 99 W/m^2, 119 W/m^2, 109.4 W/m^{2}and 82 W/m^2 respectively over the entire region, the Guinean, the Savannah and the Sahel zones, whereas the Dudhia scheme shows a lower RMSE over the entire West African region (61 W/m^2), as well as the Guinean (83 W/m^2), the Savannah (70 W/m^2) and the Sahel zones (52 W/m^2). Similar results are indicated with the MAE and the bias between the WRF radiation schemes and the observed schemes; the Dudhia scheme has the lowest value of all the other WRF schemes. Note that, the value of the RMSE, the MAE and the bias decrease as the altitude increases for all the schemes. These results corroborate the earlier discussion on the challenges facing climate modellers when parameterising cloud conditions. In addition, Figure 4.19 denotes a good relationship between the Dudhia scheme and the observations, with $R^2 = 0.98$ over the entire region. However, even better results are achieved when using our modified scheme (DudhiaM). For instance, the RMSEs of the DudhiaM over West Africa (45 W/m^2) and over the Guinean (63.23 W/m^2), the Savannah (52.65 W/m^2) and the Sahel zones (42.57 W/m^2) outmatch those found in the Dudhia scheme. Similarly, while the MAE of the DudhiaM over the entire region is about 24 W/m^2, the Dudhia scheme has a value of 28.85 W/m^2. Furthermore, the bias recorded with the DudhiaM has a magnitude of -3.6 W/m^2, while that of the Dudhia is 15.91 W/m^2. The results of the statistical analysis are clear support that the DudhiaM improves the simulation of the Rs over the West African region, by showing a good relationship with the observations (Figure 4.19).

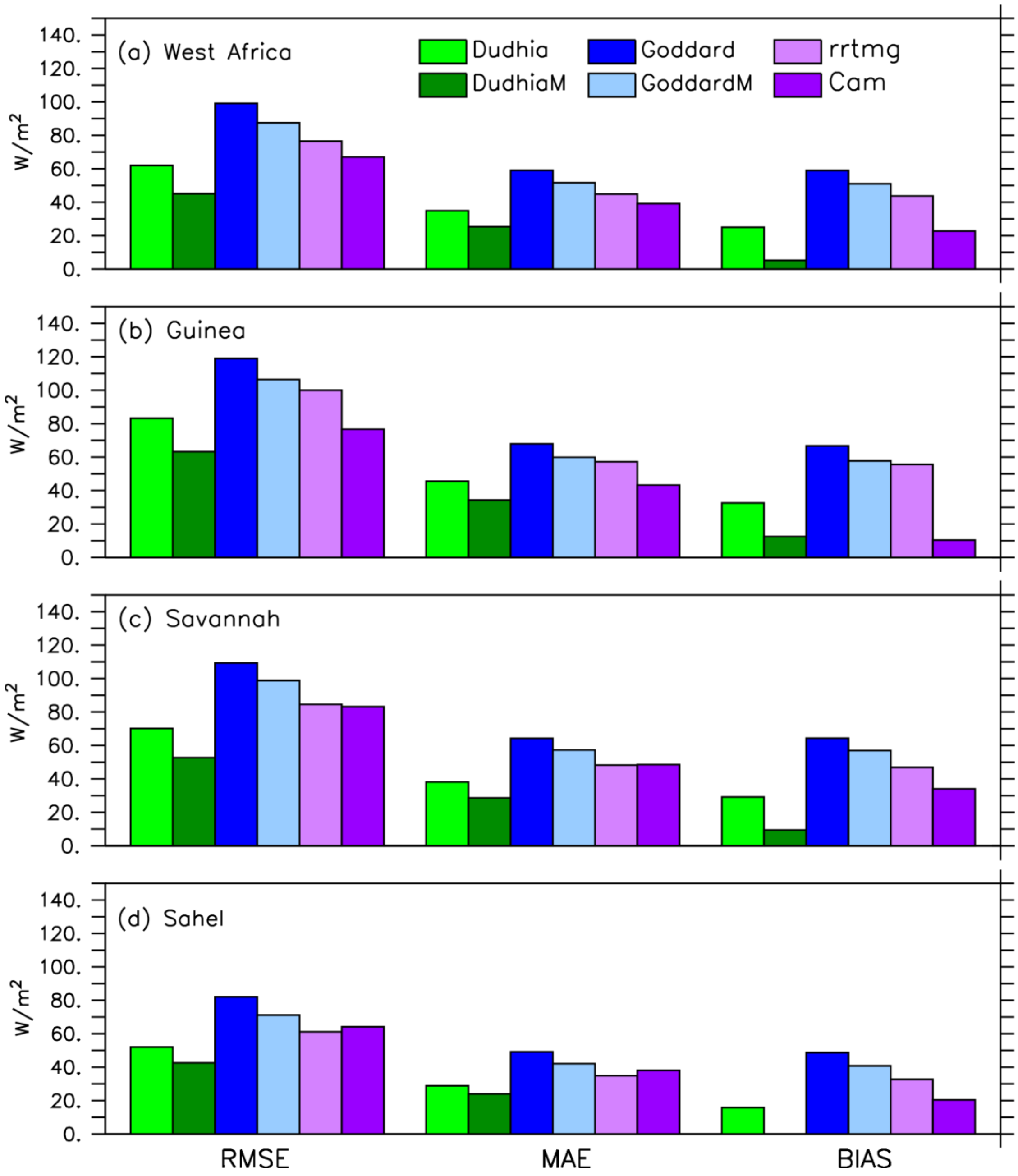

Figure 4.18: Statistical analyses on the downward shortwave radiation (Rs) over West Africa and the three zones of different WRF shortwave radiation schemes and the modified one (DudhiaM).

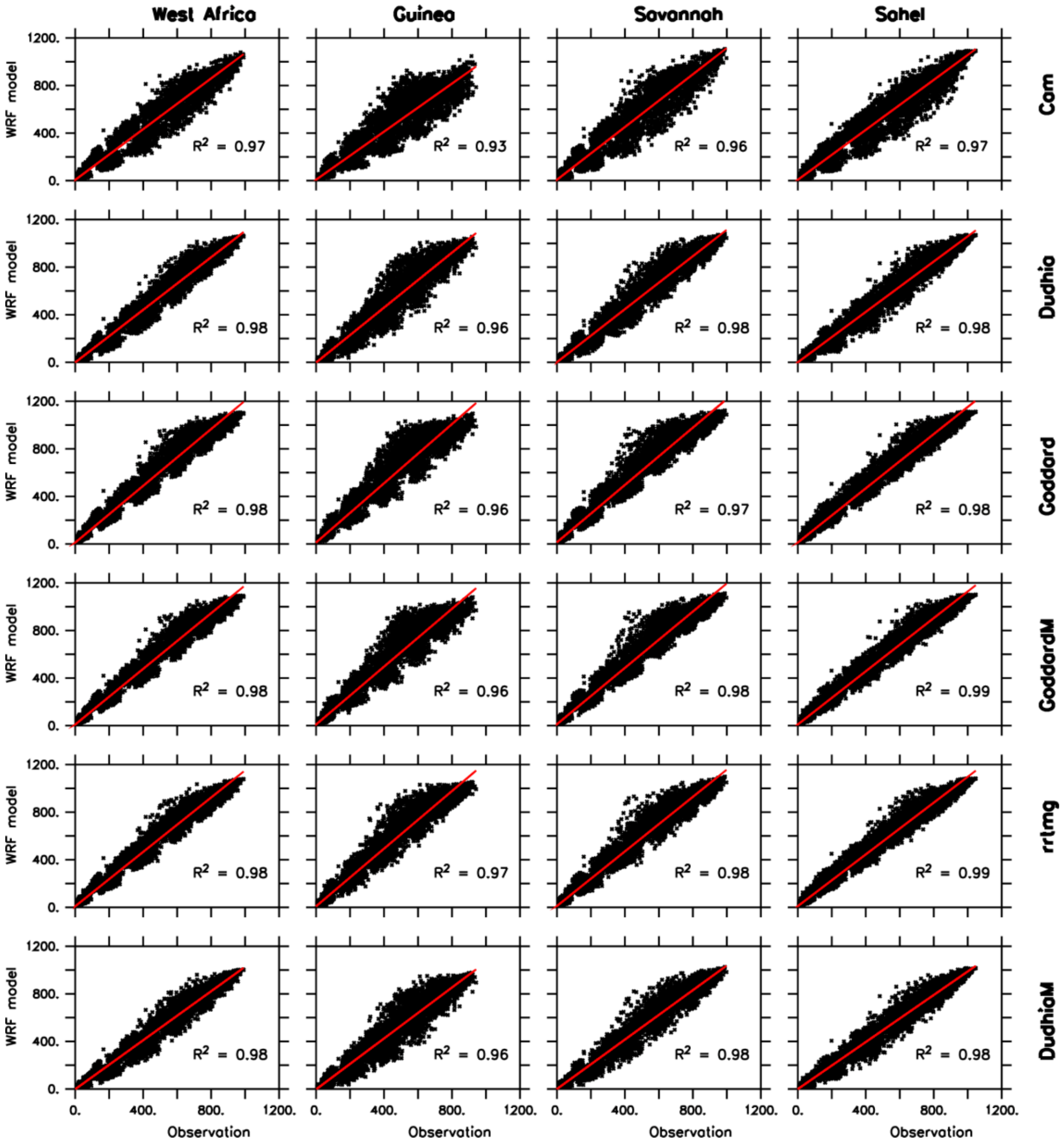

Figure 4.19: Linear regression between the observation and different WRF shortwave radiation schemes and the modified one (DudhiaM) over West Africa and the three zones.

.

4.3.1.4 Sensitivity test of the variation in the n values in simulating Rs of the DudhiaM

a. Spatial distribution of the downward shortwave radiation

Figure 20 illustrates the spatial distribution of the downward shortwave radiation (Rs) over West Africa of the variation of different empirical (n) values simulations. The contour lines depict the difference between the observed Rs and the different simulations of the n values. The value in brackets specifies the spatial correlation between the observation and the different schemes.

All simulations of the n values of the DudhiaM replicate well the spatial distribution of the observed Rs over West Africa (Figure 4.20). In agreement with the observations, the simulations capture the latitudinal variation of the Rs over the region. Moreover, their spatial correlation ranges from 0.85 to 0.88. However, there is a discrepancy among the simulations in respect of the spatial correlation. For n ranges from 0 to 0.1, the spatial correlation is about 0.85, while for n ranges from 0.2 to 0.5, the value is 0.86. With a spatial correlation value of 0.86, the value of n varying 0.6 to 0.7 and n ranges from 0.8 to 1 have a spatial correlation value of 0.88. This structure is associated with the magnitude of the Rs over the region. In other words, the annual average of the Rs decreases as the value of n increases over West Africa. For instance, the annual mean of Rs over the region is about 268.1 W/m^2; 262.9 W/m^2; 259.3 W/m^2; 253.9 W/m^2 and 249.8 W/m^2 respectively for n equal to 0; 0.3; 0.5; 0.8 and 1. The annual average of the Rs for the n equal to 1 is closer to the observed Rs (244.9 W/m^2), compared with the other values over the region. This suggests that a value of n close to 0 has a low absorption, while a value of n greater than 0.7 has a strong water absorption. These findings are in line with the findings of Chou and Arking (1981) that the value of n close to 0 is seen as weak absorption, while a value of n equal to 0.8 indicates strong absorption (Chou and Arking, 1981). From these results, it is also clear that n equal to 1 indicates strong absorption and that it gives better results when simulating the Rs over West Africa (Table 4.2). However, there are notable biases within the values. Nonetheless, the biases of n greater than 0.7 have lower biases over the study domain with a maximum bias of 15 W/m^2 (over the Guinean zone) and a minimum bias of -5 W/m^2 (over the Sahel zone). Despite those biases, including the correction of the water absorption in the Dudhia scheme (i.e. DudhiaM scheme) improves the simulation of the Rs over the West African region.

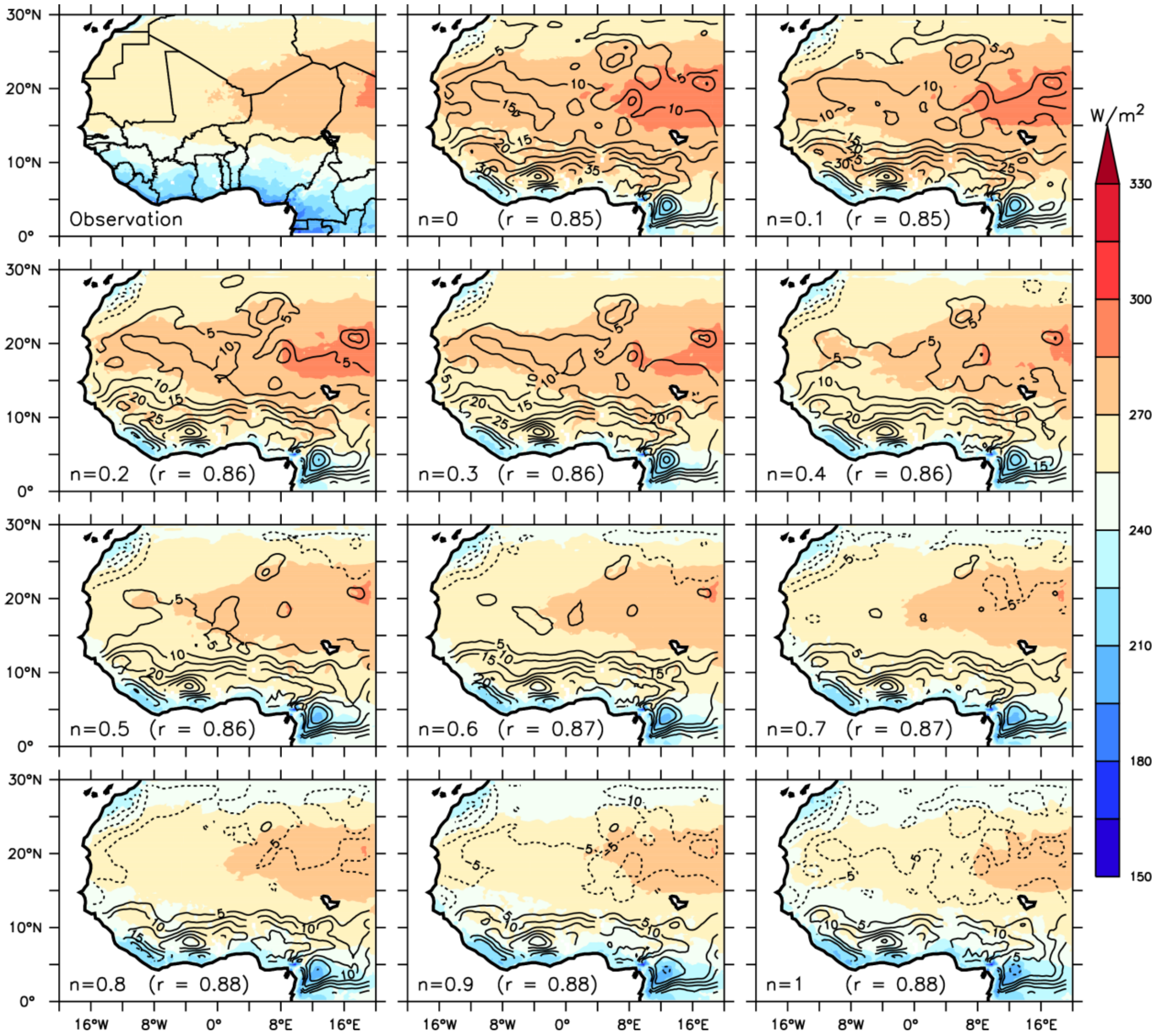

Figure 4.20: Spatial distribution of the downward shortwave radiation (Rs) over West Africa of the variation of *n* values simulations.

Table 4.2: Statistical analysis between the observed Rs and the different simulations of n values.

	West Africa			Guinea			Savannah			Sahel		
n	RMSE	BIAS	MAE	RMSE	BIAS	MAE	RMSE	BIAS	MAE	RMSE	BIAS	MAE
0	60.41	23.7	33.97	81.65	31.7	45	69.2	28	37.5	50.6	14.1	27.9
0.1	59.62	22.6	33.36	79.83	30.1	43.8	69.1	27.4	37.2	49.2	13	27.3
0.2	57.25	20.3	32.08	77.67	28.1	42.5	66.2	24.7	35.7	48.3	10.7	26.7
0.3	54.98	18.5	30.9	76.36	26.3	41.8	62.9	22.7	34	46.5	9.09	25.8
0.4	53.86	16.9	30.09	73.73	24.2	40.2	62.2	21.2	33.3	46.4	7.82	25.7
0.5	52.19	14.8	29.14	71.87	21.6	39.4	60.5	19.4	32.6	45.7	5.93	25.3
0.6	50.66	13.2	28.36	69.97	21	38.3	59.6	17.6	32	44.4	3.7	24.7
0.7	48.99	11.3	27.39	68.55	18.8	37.3	57	15.3	30.6	43.6	2.33	24.2
0.8	47.28	9.03	26.51	66.39	16.8	36	55.3	13	29.8	43.3	0	24.1
0.9	46.52	7.12	26.09	65.16	14.4	35.3	55.5	11.5	29.9	43	-2	24.1
1	45.06	5.26	25.38	63.23	12.5	34.3	52.7	9.38	28.6	42.6	-3.6	24

b. Temporal distribution of the downward shortwave radiation

Figure 4.21 presents the temporal distribution of the diurnal and annual cycle of different $\boldsymbol{n}$ values simulations and the observation. Panel (a-d) shows the observed diurnal cycle of the downward shortwave radiation (Rs) compared to the different WRF modified shortwave radiation schemes under different n values over West Africa and in its different zones. Same for Panel (e-h), but for the annual cycle of Rs.

Most of the n value simulations perform better under cloudless conditions than under cloudy conditions over West Africa (Figure 4.21). Under cloudless conditions (i.e. in the Sahel zone), most of the simulations follow the diurnal cycle and pick up the maximum of the Rs (Figure 4.21 g). Also, the maximum of the Rs (at 1200 UTC) increases, as the value of n decreases. For lower water absorption (n equal to 0), the maximum Rs is 930.4 W/m^2, and the strong water absorption (n equal to 1) Rs reaches about 875.9 W/m^2, which matches the observed value (874.5 W/m^2). An equivalent result can be seen through the seasonal variability of the Rs over the Sahel zone, where n equal to exhibits better results than the other n values. Nonetheless, some n values underestimates the magnitude of the Rs in November, December, January and February, while some (0.6, 0.7 and 0.8) capture Rs well vis-à-vis the observations. This may be due to dusty conditions during these months over the Sahel zone, or it may be that the absorption of water is very high during those months. Conversely, under cloudy conditions in the Guinean zone, the difference between the observed maximum Rs and the n equal to 1 is about 91 W/m^2, while for n equal to 0 the difference is 151.5 W/m^2. The annual cycle over the Guinean zone evinces a similar result, where n equal to 1 shows good results. However, while the observations indicate that the maximum Rs occurs in March and the minimum in August, all the n values in the simulations show the maximum in February and the minimum in September. Moreover, the simulations capture the maximum and the minimum trend of the observed Rs over the Savannah zone. Overall, n equal to 1 in the simulations denotes a good pattern and magnitude of the Rs over the entire region as well as the three different zones.

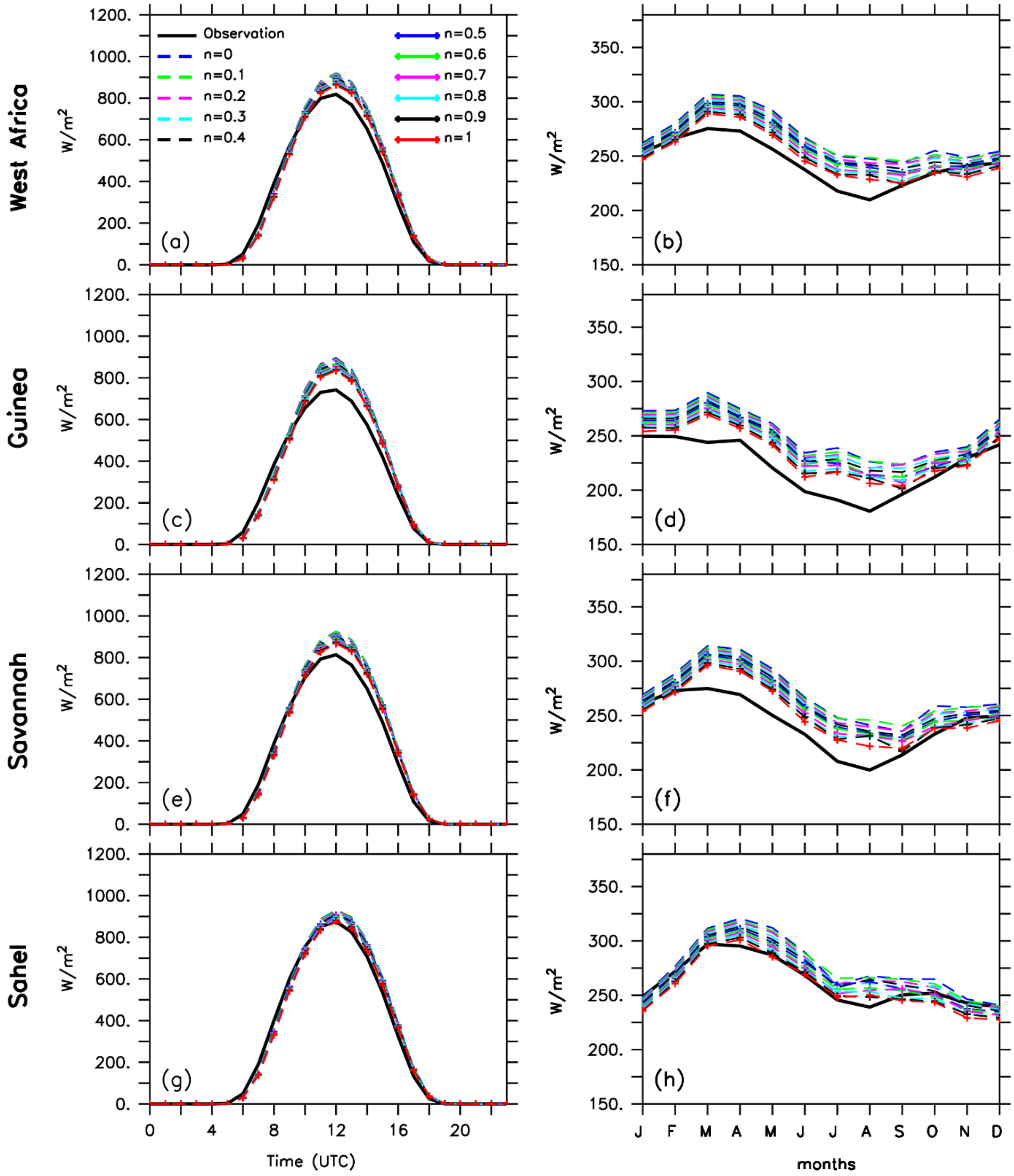

Figure 4.21: Temporal distribution of the diurnal and annual cycle of different *n* values simulations and the observation.

4.3.2 Long-term simulation of the WRF model

4.3.2.1 Spatial distribution of the downward shortwave radiation

Figure 4.22 displays the spatial distribution of the downward shortwave radiation (Rs) of the observation, the WRF Dudhia shortwave radiation (Dudhia) and the modified one (DudhiaM). We mapped the spatial distribution of the Rs with the Dudhia, DudhiaM schemes and the observation under different seasons and the annual mean. The contour lines depict the difference between the observed Rs and both simulations. The value in bracket specifies the spatial correlation between the observation and the WRF DudhiaM and the WRF Dudhia shortwave radiation.

The long-term simulations (25 years) of the seasonal average and the annual average of the DudhiaM and the Dudhia scheme agree when it comes to simulating the observed Rs over West Africa (Figure 4.22). In line with the observations, both simulations identify two major clusters of the Rs over the region. During the September-October-November (SON) and December-January-February (DJF) seasons, the Rs generally has a low value, whereas in March-April-May (MAM) and June-July-August (JJA), it has a high value. Moreover, the two simulations agree on the south-north gradient of the observed Rs. However, the long-term simulation of the DudhiaM exceeds the performance of the WRF Dudhia scheme in simulating the Rs over the region. Most of the seasonal averages of the DudhiaM outperform those of the Dudhia scheme. For instance, over the entire study domain, the magnitude of the Rs in the MAM season in respect of the Dudhia scheme (301.3 W/m^2) is high than that of the DudhiaM (279.7 W/m^2), which is closer to the observed Rs (271.7 W/m^2). In the SON season, while the observed Rs shows an average of 243.5 W/m^2, the Dudhia and the DudhiaM schemes indicate a value of 259.9 W/m^2 and 240.6 W/m^2 respectively. Similarly, the DudhiaM scheme (242 W/m^2) shows a better result than the Dudhia scheme (261.4 W/m^2) in simulating the observed Rs (229.9 W/m^2) during the JJA season. For the DJF season, the DudhiaM scheme (250.7 W/m^2) underestimates the observed Rs (255.2 W/m^2), while the Dudhia scheme (266.8 W/m^2) overestimates it. Overall, the annual average of the Rs over West Africa performs better under the DudhiaM scheme than under the WRF Dudhia scheme, with a difference of -19.2 W/m^2 in simulating the observed Rs (249.9 W/m^2). Additionally, the DudhiaM simulates the spatial pattern of the observed Rs better than the WRF Dudhia scheme.

The contour lines depict less biases in the DudhiaM scheme than in the WRF Dudhia scheme (Figure 4.22). However, these biases differ over the seasons and across the different zones. We denote high biases in the JJA season over the different zones. High biases occur in the Guinean zone, while low biases occur in the Sahel zone for all the seasons. For example, in the Guinean zone, the Dudhia scheme has an average bias of 40.67 W/m^2, whereas in the DudhiaM, we have an average bias of 22.19 W/m^2 in the JJA season. For the same season, over the Sahel zone, we have a bias of 21.66 W/m^2 and 1.5 W/m^2 respectively in the Dudhia and DudhiaM schemes. Over the Sahel zone, in the MAM season, the DudhiaM (-1.8 W/m^2) gives less average bias than the Dudhia scheme (20.74 W/m^2); similar results are found over the Guinean zone, where the results of DudhiaM (13.74 W/m^2) exceed those of the Dudhia scheme (32.59 W/m^2). Moreover, high biases occur in both the MAM and the JJA seasons, while low biases occur in both the SON and the DJF seasons. The results lead to a similar conclusion, where there is still a challenge to parameterise clouds in NWP. Nonetheless, the Dudhia scheme has higher biases than the DudhiaM. The results confirm that there is a good reason for using the DudhiaM rather than the Dudhia scheme in simulating the Rs over West Africa.

Additionally, the annual mean of the average bias of the Dudhia scheme (22.27 W/m^2) has a higher value than the DudhiaM (3.21 W/m^2) over the West African domain.

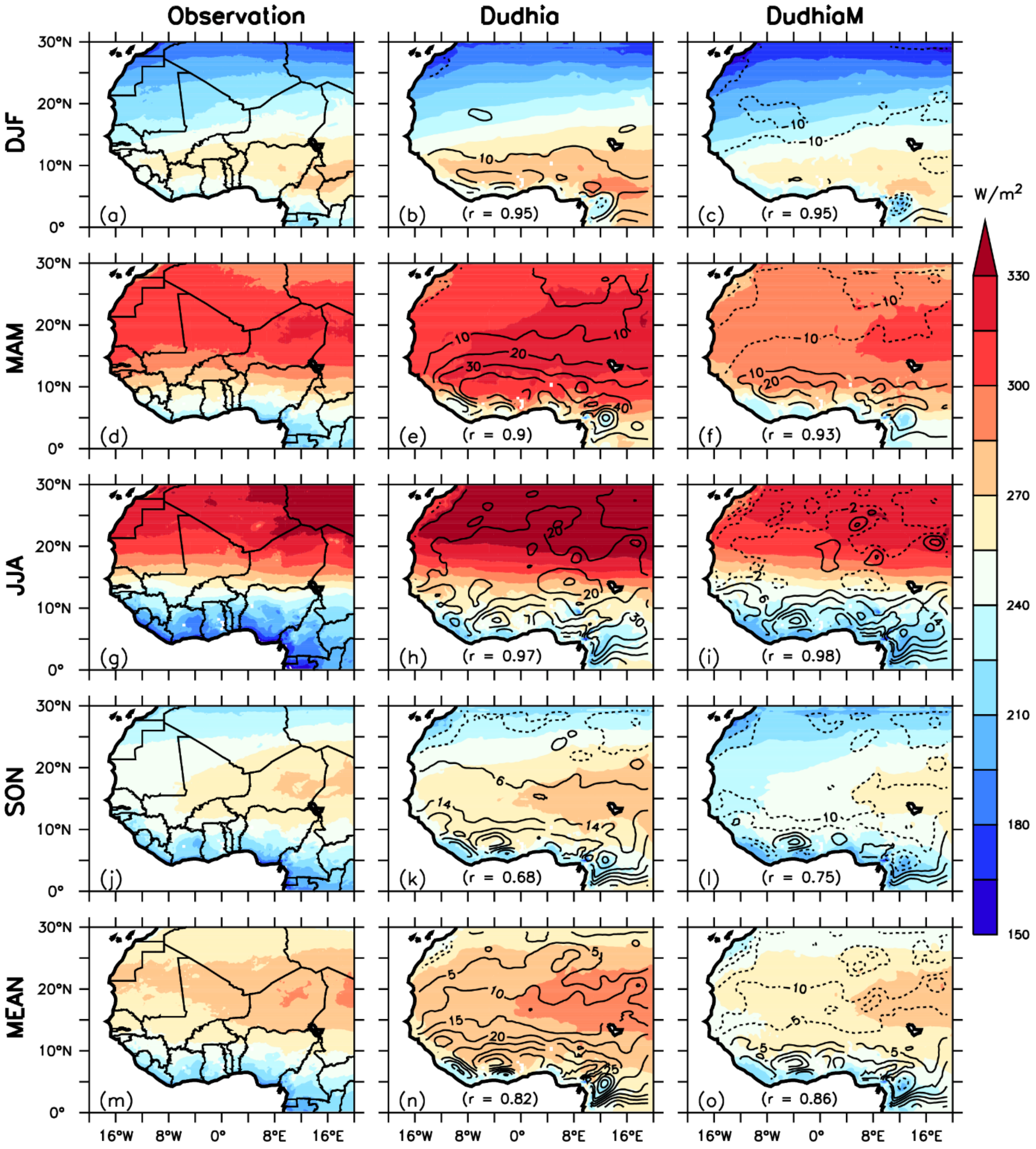

Figure 4.22: Spatial distribution of the downward shortwave radiation (Rs) of the observation, the WRF Dudhia shortwave radiation (Dudhia) and the modified one (DudhiaM).

4.3.2.2 Temporal distribution of the downward shortwave radiation

Figure 4.23 shows the Dudhia modified shortwave radiation scheme (DudhiaM), the WRF Dudhia shortwave radiation scheme and the observation. Note: Panel (a-d): Annual cycle of the Rs; Panel (e-h): inter-annual variability of Rs; Panel (i-l): monthly mean climatology of the Rs; and Panel (m-p): boxplot of the Rs.

The long-term simulations also capture well the annual cycle of the observed Rs over West Africa (Figure 4.23a-d). Both simulations reflect the maximum and the minimum of the observed Rs over each zone. However, there are some differences between the one-year simulation and the long-term simulation. The long-term simulation shows a better pattern in simulating the observed Rs than the one-year simulation over the region and the three zones. We have lower biases in the long-term simulation than in the one-year simulation. For example, over the Guinean zone, the maximum of the DudhiaM (264.1 W/m^2), rather than the Dudhia scheme (282.7 W/m^2), in the long-term simulation is closer to the maximum of the observed Rs (261.8 W/m^2) than that of the one-year simulation of the DudhiaM (265.5 W/m^2) or the Dudhia (291.1 W/m^2) scheme and the observed Rs (249.6 W/m^2). Nevertheless, over the Sahel zone, the biases are almost constant in both cases (long-term and short-term simulations). In the long-term simulation, the maximum of the Rs in the DudhiaM scheme (301 W/m^2), the Dudhia scheme (322 W/m^2), and the observations (297.1 W/m^2) is almost similar to the DudhiaM scheme (301.2 W/m^2), the Dudhia scheme (323.9 W/m^2), and the observations (302.7 W/m^2) in the short-term simulation. We have the same findings throughout the year. This suggests that the short-term and long-term simulation of Rs gives almost the same results, with a maximum bias of 5 W/m^2 over the Sahel zone, whereas, over the Guinean zone, the biases have reduced in the long-term simulation of the Rs. Nonetheless, the simulation of DudhiaM overtakes that of the Dudhia scheme throughout the year across the different zones. In sum, the DudhiaM improves the simulation of the seasonal cycle by simulating the long-term Rs better than the WRF Dudhia scheme over the West African region.

The DudhiaM also surpasses the Dudhia scheme in simulating the inter-annual variability of the observed Rs over West Africa (Figure 4.23e-h). Both schemes follow the pattern of the observed Rs. However, the Dudhia scheme in general overestimates the Rs over the West African region and the different zones. We have high biases over the Guinean zone and low biases over the Sahel zone. Conversely, the DudhiaM scheme accurately captures the pattern and even the magnitude of the inter-annual variability of the Rs over the whole West African domain. Also, the DudhiaM scheme exhibits a better pattern in respect of the observed Rs than the Dudhia scheme over the Savannah zone. A similar result has been obtained over the Guinean zone. Nonetheless, over the Sahel zone, the DudhiaM scheme underestimates the observed Rs but these biases are much closer to the 0 than the bias of the Dudhia scheme. In addition, the DudhiaM and the Dudhia schemes both capture the temporal monthly mean of the observed Rs with a high correlation value (r=0.95; Figure 4.23i-l). Nevertheless, the DudhiaM underestimates the month of August, while the Dudhia scheme overestimates the maximum Rs (in April) throughout the years. Over the Savannah zone, both simulations failed to capture the minimum of the observed Rs, but the DudhiaM shows a good temporal pattern with the observations (r=0.88). Like the Savannah zone, the Guinean zone exhibits a similar tendency with a high temporal correlation of the DudhiaM (0.86). Overall, the DudhiaM scheme shows its capability in simulating the inter-annual variability and the monthly mean climatology of the Rs over West Africa.

The boxplot of the Dudhia scheme exhibits high values in the monthly mean of the observed Rs over West Africa and its three zones (Figure 4.2m-p). Over the subcontinent, most of the 25% of the value of Rs (258.1 W/m^2) of the Dudhia scheme is almost close to the 75 % of the observed Rs (262.1 W/m^2). The maximum of the Dudhia scheme (315.28 W/m^2) exceeds that of the observations (289.88 W/m^2), while the minimum subceeds (203.43 W/m^2) the observed Rs (206.79 W/m^2). Notwithstanding, the DudhiaM scheme demonstrates the ability to capture the 25% (239.7 W/m^2), the 75% (250.1 W/m^2), the minimum (182.44 W/m^2) and the maximum (284.11 W/m^2) of the observed Rs across the whole of West Africa. Nevertheless, both schemes are skewed towards the left, while the observed Rs is almost well distributed. However, the observed, the DudhiaM and the Dudhia schemes all follow the Gaussian distribution of the Rs over the Sahel zone. The median of the DudhiaM scheme (258.8 W/m^2) is closer to the observed Rs (263.3 W/m^2) than is the Dudhia scheme (279.1 W/m^2). Similarly, with regard to the maximum of Rs, where the DudhiaM scheme indicates a magnitude of 309.93 W/m^2, the observation shows a value of 312.87 W/m^2 and the Dudhia scheme has a magnitude of 332.89 W/m^2. The DudhiaM scheme (214.74 W/m^2) underestimates the minimum of the observed Rs (226.52 W/m^2), while the Dudhia scheme (231.79 W/m^2) captures it correctly. The same results are obtained over the Savannah zone, where the DudhiaM scheme has a higher minimum than the observations, although it gives better results than the Dudhia scheme. In contrast, over the Guinean zone, the DudhiaM scheme (182.44 W/m^2) and the observations (173.01 W/m^2) have smaller biases than the Dudhia scheme (212.33 W/m^2). So too for the maximum, where the difference between the DudhiaM scheme and the observations is about 1.89 W/m^2, whereas the bias in relation to the Dudhia scheme is 23.09 W/m^2. All things considered, the DudhiaM scheme has shown an ability to capture the 25%, the median, the 75% and the maximum of the observed Rs better than the Dudhia scheme.

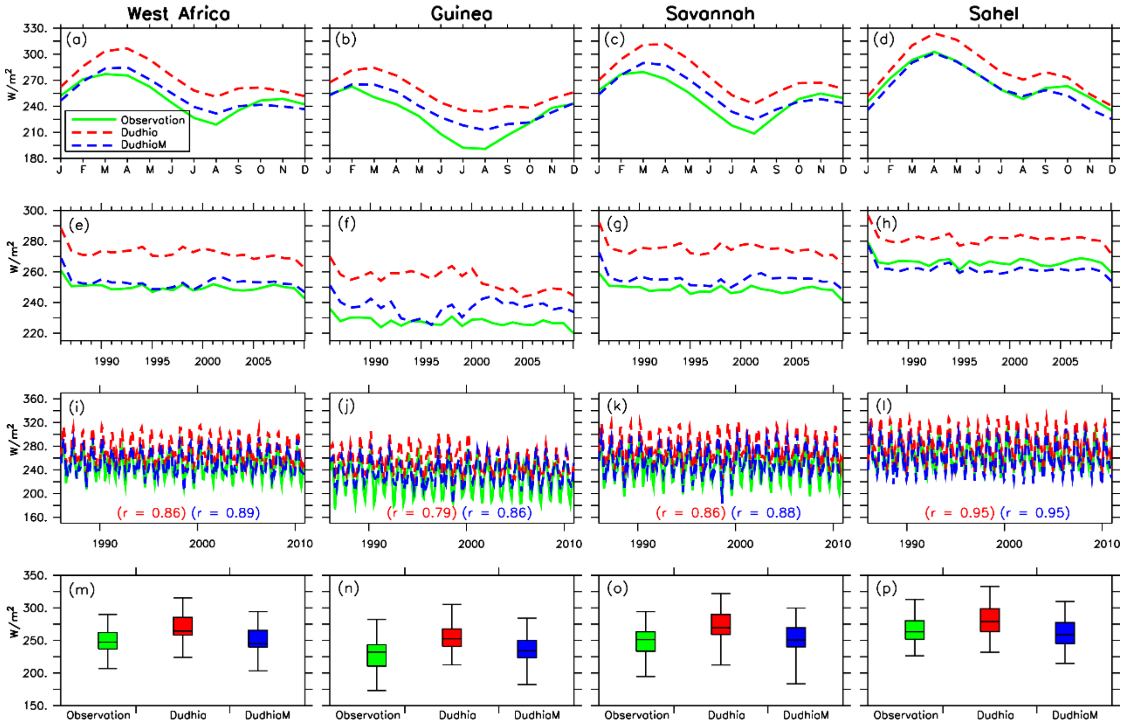

Figure 4.23: The Dudhia modified shortwave radiation scheme (DudhiaM), the WRF Dudhia shortwave radiation scheme and the observation.

4.4 Summary

We have evaluated the WPD and PVP computed from the Rmean and their related variables to the observations. The Rmean is able to capture the spatial distribution of the Ws, Rs, Ts, Rh, WPD and PVP over West Africa with few biases. The Rmean projects a general increase of WPD and a general decrease of PVP over the West Africa region. The results also showed that most of the WRF shortwave radiation schemes are able to simulate the Rs over West Africa and its three zones, but the Dudhia scheme outperforms the other schemes. The development of an algorithm based on Dudhia scheme exhibits accurate results than the default Dudhia WRF radiation scheme. Chapter 5 presents the conclusions.

CHAPTER FIVE: CONCLUSION AND RECOMMENDATIONS

5.1 Conclusion

Firstly, in this study, we have studied the projected changes in wind power density (WPD) at various GWLs under the RCP8.5 climate change scenarios. Eleven multi-model multi-ensemble simulations from CORDEX RCMs were analysed for the projections under different GWLs (GWL1.5, GWL2.0, GWL2.5 and GWL3.0). The RCM simulations downscaled eight GCM simulations for past and future climates. Due to a lack of sufficient station data over West Africa, the GCM and RCM simulations were compared with reanalysis datasets (ERAINT and ERA20C). The capability of the simulations to reproduce the PDF of daily surface wind over the available four stations was examined. The results of the study can be summarised as follows:

- The CORDEX RCMs generally perform better than the GCMs in reproducing the probability distribution of surface wind speed over three of the four stations, but the RCMs overestimate the annual wind speed over the stations and perform worse than the GCMs in this regard.
- The three datasets (RCMs, GCMs, and reanalysis) agree on the spatial distribution of annual wind speed and WPD over West Africa, where they all feature the lowest wind speed and WPD in the Guinean zone and the strongest wind speed and WPD in the Sahel zone.
- While the RCMs ensemble mean suggests that 87% of the cities are viable and suitable for potential wind power generation in the historical climate, the reanalysis dataset indicates that only 27% (i.e. four cities: Kano (Nigeria), Niamey (Niger), Ouagadougou (Burkina Faso), and Dakar (Senegal) are suitable). None of the cities in the Guinean and Savannah zones are suitable.

- However, given that the RCMs have a tendency to overestimate the annual wind speed, they might have overestimated the WPD over these cities.
- The RCMs project an increase in monsoon wind speed and wind power potential over West Africa. The magnitude of these changes increases with increasing GWLs.

However, the increase in the WPD from global warming is not sufficient to make the cities with low WPD (i.e. below the viable threshold in the historical climate) viable for wind power generation under warmer climates.

Secondly, to understand the potential impacts of climate change on the PVP over West Africa, we have also analysed fourteen RCM simulations from the CORDEX dataset at specific GWLs under the RCP8.5 climate scenario. The capability of the simulations to reproduce the climate variables (i.e. solar radiation, ambient air temperature, wind speed, and relative humidity) that would influence the efficiency of the solar panel cells was evaluated by comparing the simulations with the observations (SARAH and CRU) and the reanalysis data. The projected changes in PVP (i.e. ΔPVP) and in the climate variables (i.e. ΔRs, ΔTs, ΔWs and ΔRh) were obtained at four GWLs (1.5°C, 2.2°C, 2.5°C, 3.0°C), and the spatio-temporal relationship between the ΔPVP and the variables of ΔRs, ΔTs, ΔWs and ΔRh was examined. The relative contribution of each component in Equation (14) to ΔPVP was analysed. The results of the study can be summarised as follows:

- The CORDEX simulation ensemble mean reproduces well the spatial distribution of the climate variables (Rs, Ts, Ws and Rh) and PVP over West Africa, but it underestimates Rs over most parts of West Africa (especially over the eastern Sahel zone), while overestimating it over the western Sahel zone.

- The ensemble mean captures the annual cycle of the climate variables and PVP over each climate zone. For all the variables, the simulation ensemble spread encloses the observed curves. In agreement with the observations, the simulations show that the seasonal cycle of PVP is controlled by the monsoon system.
- The CORDEX simulations projected a decrease in PVP over the whole of West Africa and indicate the magnitude of the increases with the increasing GWLs. The decrease in PVP is mainly due to projected solar dimming and increased regional temperature following global warming. However, the spatial distribution of ∆PVP is more influenced by ∆Rs than it is by ∆Ts.
- The annual cycle of ∆PVP shows an increase trend in PVP during the arrival of the monsoon system over each zone because, as a result of global warming, the onset of the monsoon system features stronger winds, drier conditions, less cloudiness, and more radiation. The budget of ∆PVP shows that, during the arrival of monsoon system, the magnitude of ∆Rs.PVP (positive) is more than that of ∆Ts.PVP (negative), especially at GWL1.5.
- More than 75% of the simulations agree on the decrease in PVP over most of the selected countries, especially at GWL3.0. The maximum decrease is projected over Niger.

However, in order to understand how Numerical Weather Prediction (NWP) can simulate the downwelling SW solar radiation (Rs) over West Africa, we used the WRF model to see its capability. We did so by testing the sensitivity of the WRF model by using various SW radiation schemes. For this present study, we used the Cam, Dudhia, Goddard, the modified Goddard, and the rrtmg schemes. We also introduced a new scheme (the DudhiaM) by modifying the Dudhia scheme. This was done by integrating the water vapour absorption at all the levels. All the simulations were done over 13 months (December 2009 - December 2010), with one month being discarded. We also tested ten values of the water vapour absorption, which mainly depends on the parameter n. The best modified Dudhia scheme was thus selected and run for 31 years, together with the Dudhia scheme for comparison. Due to the data covering the observed data from SARAH, we were able to analyse 25 years (1986-2010). We can summarise the main results as follows:

- All the WRF SW radiation schemes reproduce the spatial distribution of the observed Rs over West Africa, with some biases in the magnitude of the observed Rs. Among all the WRF schemes, the Dudhia scheme gives the best results, but the modified Dudhia scheme (DudhiaM) even improves on the results of the Dudhia scheme with regard to the spatial distribution of the Rs over West Africa.
- Most of the simulations follow the pattern of the annual mean diurnal cycle and the annual cycle of the observed Rs over West Africa and its different zones. The new Dudhia scheme (DudhiaM) outperforms the WRF SW radiation scheme. In terms of statistical analysis, the value of the RMSE, the MAE and the bias of the DudhiaM even enhancing all the different schemes.
- The sensitivity of the n values of water vapour absorption in the modified Dudhia scheme replicates well the spatial distribution of the observed Rs over West Africa. Nonetheless, the value of n equal to 0 has a low absorption, while n equal to 1 has a strong absorption. Looking at the RMSE and the MAE over the whole domain, the value of n equal to 1 gives a good result.
- The n value simulations also capture the diurnal cycle and the seasonal cycle of the observed Rs. The simulations perform well under cloudless conditions.

Again, the $n = 1$ of the water vapour absorption simulates accurately the annual cycle and the diurnal cycle of the Rs over the West African region.

- The DudhiaM and the Dudhia schemes agree with regard to simulating the observed Rs of the seasonal mean in respect of the long-term simulation (25 years) over West Africa. The two simulations agree on the latitudinal variation of the observed Rs. We classified the Rs into two majors' clusters, viz. the SON and the DJF seasons; the observations and the simulations agree that there is a generally low value in the Rs, but during MAM and JJA, we have a high value. However, the long-term simulation of the DudhiaM indicates good results than the WRF Dudhia scheme in simulating the Rs over West Africa.
- The long-term simulation of the DudhiaM surpasses the Dudhia scheme in simulating the inter-annual variability, the annual mean and the monthly mean of the observed Rs over West Africa and the three zones.
- The DudhiaM scheme more accurately captures the 25%, the 75%, the median and the maximum of the observed Rs than the Dudhia scheme does.

5.2 Limitations of the study

In this study, we evaluated and projected the wind energy potential over West Africa. The extrapolation model used in this study contains some limitations, however. The model underestimates the wind speed under stable conditions and overestimates it under unstable conditions. This could affect the results of the evaluation and the projection of the WPD over West Africa. Another limitation is that the evaluation of surface wind speed is affected by the observed data used in this study. We were only given access to four weather stations among the fifteen countries, which is not statistically significant.

The limitations of this study can be extended to the evaluation of the PV power potential over the region. There are several limitations with the method used to compute the PVP over the region. For instance, we did not consider the aerosols, the spectral distribution of the incident radiation, the angle of incidence of radiation, the amount of cloud cover, and the operational efficiencies of the system components, which can change the results of this study in terms of evaluation and projection. Also, the approach used here to compute the solar cell temperature is based on the empirical equation by TamizhMani *et al.* (2003). This equation was derived from an experiment conducted in Colorado, US, to model the solar cell temperature; the climate on Colorado is very different to that of West Africa. The equation may consequently change the projection of the PVP, if the model was based on the meteorological parameters of the West African region.

The sensitivity of the WRF SW radiation scheme and the change of value in the water vapour absorption have two shortcomings. Firstly, we used only one set of forcing data to simulate the Rs in the WRF model. To obtain robust and consistent information, it is necessary to use other GCMs or data from the reanalysis dataset. Secondly, we evaluated the performance of the WRF shortwave radiation and the modified Dudhia scheme output by means of satellite data. This satellite data may contain some biases vis-à-vis the observed data, which may thus either lead to overestimating or underestimating the true value of the Rs over West Africa.

5.3 Recommendations and future work

The results of this study may be improved in many ways. For instance, the resolution of the CORDEX dataset available for the study (about 50 x 50 km) is too low to resolve all the important local-scale circulations for wind energy. A good simulation of the mesoscale circulations (e.g. sea-breeze, mountain winds) requires a resolution of 2 to

10 km (Abbs and Physick, 1992). However, running the RCMs over the West African domain at that resolution for climate projection studies is computationally challenging. The future CORDEX Phase II dataset intends to provide ultra-high-resolution simulations over selected areas of Africa. The results of the present study may provide guidance on where to focus such simulations in order to study the impacts of global warming on wind energy generation in West Africa. In addition, to avoid the extrapolation of 100 m wind from surface winds, the future CORDEX dataset should archive 100 m wind data and also make hourly wind speed data available to enable an efficient and accurate study of wind energy. Nonetheless, despite the limitations, the present study has shown the viability of various West African cities for wind energy generation, both in the historical climate and in the future climate under various GWLs. The results of the study thus have application in assessing the risk associated with using wind energy generation to improve the quality and quantity of the electricity supply in West Africa.

Additionally, the PVP projection over West Africa is very sensitive to the uptake and removal of atmospheric dusts by dry and wet convective systems (respectively), and thus high-resolution simulations could give a better representation of the convections and their vertical transport of atmospheric dusts. In addition, simulations that account for moisture chemistry in the clouds may also give a better representation of the chemical processes in the clouds. Studies such as those of Jantsch *et al*. (1991) and Zang *et al*. (2016) have shown that the tilting angle of the solar panel also influences the PV efficiency. These were not accounted for in the present study due to data availability in the CORDEX framework So, incorporating such factors into future studies can improve the robustness of the PVP projections. Furthermore, the focus of our study has been on the impact of climate change on PV, but there are other solar panel technologies available, such as concentrating solar power (CSP). Thus, understanding the impacts of climate change on CSP, will help put the results into a better perspective and provide possibly guidelines for a technology that itself creates the least climate change impacts. Nevertheless, the present study has shown that global warming may reduce the PVP in the future, but the maximum decrease is less than 3.8%. So even though PVP is likely to be reduced, it should still be implemented.

Finally, the improved Dudhia scheme developed in this study could be extended in many approaches to evaluate its performance. For instance, it could be used to evaluate the performance of precipitation against the observation values, as well as related subjects, such as onset and cessation of rainfall, which remains a big challenge for researchers in the region. In general, the shortwave radiation constitutes the largest energy input to the climate system (Schwingshackl *et al*., 2018). So, studies associated with the simulation of meridional or zonal wind could be performed to assess the performance of this new scheme. In addition, the application of solar and wind energy for electricity generation in the region could also use this algorithm to assess the solar and wind energy with WRF simulation.

REFERENCES

Abas, N., Kalair, A., and Khan, N. (2015). Review of fossil fuels and future energy technologies. *Futures*, *69*, 31–49.

Abbs, D., and Physick, W. L. (1992). Sea-breeze observations and modeling. *Austr. Meteor. Mag*, *41*, 7–19.

Abdullahi, S. A., Abdul, M., and Joshua, and A. (2017). Impacts of Relative Humidity and Mean Air Temperature on Global Solar Radiations of Ikeja, Lagos, Nigeria. *International Journal of Scientific and Research Publications*, *7*(2), 315–319.

Abiodun, B. J., Adeyewa, Z. D., Oguntunde, P. G., Salami, A. T., and Ajayi, V. O. (2012). Modeling the impacts of reforestation on future climate in West Africa. *Theoretical and Applied Climatology*, *110*(1–2), 77–96.

Ackermann, T., and Söder, L. (2000). Wind energy technology and current status : a review, *4*.

Afiesimama, E. A., Pal, J. S., Abiodun, B. J., Gutowski Jr, W. J., and Adedoyin, A. (2006). Simulation of West African monsoon using the RegCM3. Part I: model validation and interannual variability. *Theoretical and Applied Climatology*, *86*(1–4), 23–37.

Aguilar, C., Herrero, J. and Polo, M. J. (2010). Topographic effects on solar radiation distribution in mountainous watersheds and their influence on reference evapotranspiration estimates at watershed scale. *Hydrology and Earth System Sciences*, *14*(12), 2479.

Arnault, J., Knoche, R., Wei, J. and Kunstmann, H. (2016). Evaporation tagging and atmospheric water budget analysis with WRF: A regional precipitation recycling study for West Africa. *Water Resources Research*, *52*(3), 1544–1567.

Baldauf, M. (2008). Stability analysis for linear discretisations of the advection equation with Runge--Kutta time integration. *Journal of Computational Physics*, *227*(13), 6638–6659.

Baldauf, M. and Schulz, J. P. (2004). Prognostic precipitation in the Lokal-Modell

(LM) of DWD. *Cosmo Newsletter*, *4*, 177–180.

Bazyomo, S. D. Y. B., Agnidé Lawin, E., Coulibaly, O. and Ouedraogo, A. (2016). Forecasted Changes in West Africa Photovoltaic Energy Output by 2045. *Climate*, *4*(4), 53.

Bechtold, P., Bazile, E., Guichard, F., Mascart, P. and Richard, E. (2001). A mass-flux convection scheme for regional and global models. *Quarterly Journal of the Royal Meteorological Society*, *127*(573), 869–886.

Behringer, D. W. (2007). The Global Ocean Data Assimilation System (GODAS) at NCEP. In *Proceedings of the 11th Symposium on Integrated Observing and Assimilation Systems for the Atmosphere, Oceans, and Land Surface*.

Berrisford, P., Dee, D., Fielding, K., Fuentes, M., Kallberg, P., Kobayashi, S. and Uppala, S. (2009). The ERA-interim archive.

Bhattacharya, T., Chakraborty, A. K. and Pal, K. (2014). Effects of ambient temperature and wind speed on performance of monocrystalline solar photovoltaic module in Tripura, India. *Journal of Solar Energy, 2014*.

Bianco, L. (2008). The Weather Research and Forecasting Model WRF. Retrieved January 7, 2019, from http://cires1.colorado.edu/science/groups/pielke/classes/at7500/Bianco_PresentationWRF.pdf

Boden, T. A., Andres, R. J. and Marland, G. (2017). *Global, Regional, and National Fossil-Fuel CO2 Emissions (1751-2014)(V. 2017).*

Bougeault, P. (1985). A simple parameterization of the large-scale effects of cumulus convection. *Monthly Weather Review*, *113*(12), 2108–2121.

Breslow, P. B. and Sailor, D. J. (2002). Vulnerability of wind power resources to climate change in the continental United States. *Renewable Energy*, *27*(4), 585–598. http://doi.org/10.1016/S0960-1481(01)00110-0

Briegleb, B. P. (1992). Delta-Eddington approximation for solar radiation in the NCAR Community Climate Model. *Journal of Geophysical Research: Atmospheres*, *97*(D7), 7603–7612.

Brooks, A. E. (2014). Chapter 18 - Solar Energy: Photovoltaics. In T. M. Letcher (Ed.), *Future Energy (Second Edition)* (Second Edi, pp. 383–404). Boston: Elsevier. http://doi.org/https://doi.org/10.1016/B978-0-08-099424-6.00018-1

Burnett, D., Barbour, E. and Harrison, G. P. (2014). The UK solar energy resource and the impact of climate change. *Renewable Energy*, *71*, 333–343. http://doi.org/10.1016/J.RENENE.2014.05.034

Burpee, R. W. (1972). The origin and structure of easterly waves in the lower troposphere of North Africa. *Journal of the Atmospheric Sciences*, *29*(1), 77–90.

Burton, T., Jenkins, N., Sharpe, D. and Bossanyi, E. (2011). *Wind energy handbook*. John Wiley and Sons.

Buzzi, M., Rotach, M. W., Holtslag, M. and Holtslag, A. A. M. (2011). Evaluation of the COSMO-SC turbulence scheme in a shear-driven stable boundary layer. *Meteorologische Zeitschrift*, *20*(3), 335–350.

Can Şener, Ş. E., Sharp, J. L. and Anctil, A. (2018). Factors impacting diverging paths of renewable energy: A review. *Renewable and Sustainable Energy Reviews*, *81*, 2335–2342. http://doi.org/10.1016/J.RSER.2017.06.042

Chai, T. and Draxler, R. R. (2014). Root mean square error (RMSE) or mean absolute error (MAE)?--Arguments against avoiding RMSE in the literature. *Geoscientific Model Development*, *7*(3), 1247–1250.

Chander, S., Purohit, A., Sharma, A., Arvind, Nehra, S. P. and Dhaka, M. S. (2015). A study on photovoltaic parameters of mono-crystalline silicon solar cell with cell temperature. *Energy Reports*, *1*, 104–109. http://doi.org/10.1016/J.EGYR.2015.03.004

Chandra, S., Agrawal, S. and Chauhan, D. S. (2018). Effect of Ambient Temperature and Wind Speed on Performance Ratio of Polycrystalline Solar Photovoltaic Module: an Experimental Analysis. *International Energy Journal*, *18*(2).

CHEN, W.-D., CUI, F., ZHOU, H., DING, H. and LI, D.-X. (2017). Impacts of different radiation schemes on the prediction of solar radiation and photovoltaic power. *Atmospheric and Oceanic Science Letters*, *10*(6), 446–451. http://doi.org/10.1080/16742834.2017.1394780

Chou, M.-D. and Arking, A. (1981). An efficient method for computing the absorption of solar radiation by water vapor. *Journal of the Atmospheric Sciences, 38*(4), 798–807.

Chou, M.-D. and Lee, K.-T. (1996). Parameterizations for the absorption of solar radiation by water vapor and ozone. *Journal of the Atmospheric Sciences*, *53*(8), 1203–1208.

Chou, M.-D. and Suarez, M. J. (1994). An efficient thermal infrared radiation parameterization for use in general circulation models.

Chou, M.-D. and Suarez, M. J. (1999). A solar radiation parameterization (CLIRAD-SW) for atmospheric studies. *NASA Tech. Memo*, *10460*, 48.

Chou, M.-D., Suarez, M. J., Liang, X.-Z., Yan, M. M.-H. and Cote, C. (2001). A thermal infrared radiation parameterization for atmospheric studies.

Chu, S. and Majumdar, A. (2012). Opportunities and challenges for a sustainable energy future. *Nature*, *488*(7411), 294.

Clack, C. T. M. (2017). Modeling solar irradiance and solar PV power output to create a resource assessment using linear multiple multivariate regression. *Journal of Applied Meteorology and Climatology*, *56*(1), 109–125.

Collins, W. D., Rasch, P. J., Boville, B. A., Hack, J. J., McCaa, J. R., Williamson, D. L., … others. (2004). Description of the NCAR community atmosphere model (CAM 3.0). *NCAR Tech. Note NCAR/TN-464+ STR*, *226*.

Cornforth, R. (2012). Overview of the West African Monsoon 20111. *Weather*, *67*(3), 59–65.

Crook, J. A., Jones, L. A., Forster, P. M. and Crook, R. (2011). Climate change impacts on future photovoltaic and concentrated solar power energy output. *Energy and Environmental Science*, *4*(9), 3101. http://doi.org/10.1039/c1ee01495a

Dale, V. H. (1997). The relationship between land-use change and climate change. *Ecological Applications*, *7*(3), 753–769.

Davies, R. (1982). Documentation of the solar radiation parameterization in the GLAS climate model.

Davy, R., Gnatiuk, N., Pettersson, L. and Bobylev, L. (2017). Climate change impacts on wind energy potential in the European domain with a focus on the Black Sea. *Renewable and Sustainable Energy Reviews*.

de Souza, E. P., Dias, P. L. da S., Plana-Fattori, A. and Chagas, J. C. S. (1997). Absorption of solar radiation by water vapor in the atmosphere. Part II: Sensitivity tests with a general circulation model. *Revista Brasileira de Geof{\'\i}sica, 15*(3), 291–306.

Dee, D. P., Uppala, S. M., Simmons, A. J., Berrisford, P., Poli, P., Kobayashi, S., … others. (2011). The ERA-Interim reanalysis: Configuration and performance of the data assimilation system. *Quarterly Journal of the Royal Meteorological Society, 137*(656), 553–597.

Déqué, M., Calmanti, S., Christensen, O. B., Dell Aquila, A., Maule, C. F., Haensler, A., … Teichmann, C. (2017). A multi-model climate response over tropical Africa at +2 °C. *Climate Services, 7*, 87–95. http://doi.org/10.1016/J.CLISER.2016.06.002

Diagne, M., David, M., Boland, J., Schmutz, N. and Lauret, P. (2014). Post-processing of solar irradiance forecasts from WRF model at Reunion Island. *Solar Energy, 105*, 99–108.

Diallo, I., Giorgi, F., Deme, A., Tall, M., Mariotti, L. and Gaye, A. T. (2016). Projected changes of summer monsoon extremes and hydroclimatic regimes over West Africa for the twenty-first century. *Climate Dynamics*, *47*(12), 3931–3954.

Diallo, I., Sylla, M. B., Giorgi, F., Gaye, A. T. and Camara, M. (2012). Multimodel GCM-RCM ensemble-based projections of temperature and precipitation over West Africa for the early 21st century. *International Journal of Geophysics, 2012*.

Diedhiou, A., Bichet, A., Wartenburger, R., Seneviratne, S. I., Rowell, D. P., Sylla, M. B., … others. (2018). Changes in climate extremes over West and Central Africa at 1.5° C and 2° C global warming. *Environmental Research Letters*.

Diedhiou, A., Janicot, S., Viltard, A. and de Felice, P. (1998). Evidence of two regimes of easterly waves over West Africa and the tropical Atlantic. *Geophysical Research Letters*, *25*(15), 2805–2808.

Dodge, D. M. (2015). First Use of Wind for “Large-Scale” Generation of Electricity. Retrieved May 8, 2015, from www.telosnet.com/wind/

Doherty, O. M., Riemer, N. and Hameed, S. (2014). Role of the convergence zone over West Africa in controlling Saharan mineral dust load and transport in the boreal summer. *Tellus B: Chemical and Physical Meteorology*, *66*(1), 23191.

Doms, G., Förstner, J., Heise, E., Herzog, H. J., Mironov, D., Raschendorfer, M., … others. (2011). A description of the nonhydrostatic regional COSMO model. Part II: physical parameterization. *Deutscher Wetterdienst, Offenbach, Germany*.

Douville, H., Planton, S., Royer, J.-F., Stephenson, D. B., Tyteca, S., Kergoat, L., … Betts, R. A. (2000). Importance of vegetation feedbacks in doubled-CO2 climate experiments. *Journal of Geophysical Research: Atmospheres*, *105*(D11), 14841–14861.

Duah, N. T. and Asamoah, P. K. (2018). Renewable Energy in Africa; Potential, Impact and The Way Forward. *ELEKTRIKA-Journal of Electrical Engineering*, *17*(1), 16–20.

Dubey, S., Sarvaiya, J. N. and Seshadri, B. (2013a). Temperature dependent photovoltaic (PV) efficiency and its effect on PV production in the world--a review. *Energy Procedia*, *33*, 311–321.

Dubey, S., Sarvaiya, J. N. and Seshadri, B. (2013b). Temperature Dependent Photovoltaic (PV) Efficiency and Its Effect on PV Production in the World – A Review. *Energy Procedia*, *33*, 311–321. http://doi.org/10.1016/J.EGYPRO.2013.05.072

Dudhia, I. (2010). WRF Modeling System Overview. Retrieved from http://mce2.org/wmogurme/images/workshops/ASEAN/day2/WRF_overview.pdf

Dudhia, J. (1989). Numerical study of convection observed during the winter monsoon experiment using a mesoscale two-dimensional model. *Journal of the Atmospheric Sciences*, *46*(20), 3077–3107.

Dudhia, J. (1996). A multi-layer soil temperature model for MM5. In *Preprints, The*

Sixth PSU/NCAR mesoscale model users' workshop (pp. 22–24).

Ebinger, J. and Vergara, W. (2011). *Climate impacts on energy systems: key issues for energy sector adaptation*. The World Bank.

ECMWF. (2007). IFS DOCUMENTATION – Cy31r1 Operational implementation 12 September 2006 PART IV: PHYSICAL PROCESSES.

ECREE. (2013). ECOWAS RENEWABLE ENERGY POLICY. Retrieved August 30, 2017, from http://www.ecreee.org/sites/default/files/documents/ecowas_renewable_energy_policy.pdf

ECREEE. (2013). Observatory for Renewable Energy and Energy Efficiency (ECOWREX). Retrieved December 3, 2018, from http://www.ecreee.org/page/observatory-renewable-energy-and-energy-efficiency-ecowrex

ECREEE. (2015). ECOWAs renewable energy Policy. Retrieved September 8, 2018, from http://www.ecreee.org/sites/default/files/documents/ecowas_renewable_energy_policy.pdf

ECREEE. (2016a). Investment Prospectus : General Assessment and perspectives (Ghana). Retrieved April 9, 2018, from http://www.ecreee.org/sites/default/files/presentation_of_action_agendas_and_ip_advancements_by_national_directors_for_energy_-_ghana_-.pdf

ECREEE. (2016b). Investment Prospectus : General assessment and perspectives Liberia. Retrieved April 9, 2018, from http://www.ecreee.org/sites/default/files/presentation_of_action_agendas_and_ip_advancements_by_national_directors_for_energy_-_liberia.pdf

ECREEE. (2016c). Investment Prospectus : General assessment and perspectives Nigeria. Retrieved April 9, 2018, from http://www.ecreee.org/sites/default/files/presentation_of_action_agendas_and_ip_advancements_by_national_directors_for_energy_-_nigeria_-.pdf

ECREEE. (2016d). Investment Prospectus : General assessment and perspectives

Sierra Leone. Retrieved April 9, 2018, from http://www.ecreee.org/sites/default/files/presentation_of_action_agendas_and_ip_advancements_by_national_directors_for_energy_-_sierra_leone_-_benjamin_kamara_director_for_energy.pdf

ECREEE. (2016e). Investment Prospectus : General Assessment and perspectives THE GAMBIA. Retrieved April 9, 2018, from http://www.ecreee.org/sites/default/files/presentation_of_action_agendas_and_ip_advancements_by_national_directors_for_energy_-_gambia_-_kemo_ceesay_director_for_energy.pdf

ECREEE. (2016f). Prospectus d’Investissement : Etat des lieux et perspectives (MALI). Retrieved April 9, 2018, from http://www.ecreee.org/sites/default/files/presentation_of_action_agendas_and_ip_advancements_by_national_directors_for_energy_-_mali.pdf

ECREEE. (2016g). Prospectus d’Investissement : Etat des lieux et perspectives Bénin. Retrieved April 9, 2018, from c:%5CUsers%5CWASCAL%5CDownloads%5CDocuments%5Cpresentation_of_action_agendas_and_ip_advancements_by_national_directors_for_energy_-_benin_-_sakariyou_mahman_director_for_energy.pdf

ECREEE. (2016h). Prospectus d’Investissement : Etat des lieux et perspectives Côte d’Ivoire. Retrieved from http://www.ecreee.org/sites/default/files/presentation_of_action_agendas_and_ip_advancements_by_national_directors_for_energy_-_cote_divoire_-_director_for_energy.pdf

ECREEE. (2016i). Prospectus d’Investissement : Etat des lieux et perspectives GUINEE. Retrieved April 9, 2018, from http://www.ecreee.org/sites/default/files/presentation_of_action_agendas_and_ip_advancements_by_national_directors_for_energy_-_guinea_-_alpa_ibrahima_diallo_director_for_energy.pdf

ECREEE. (2016j). Prospectus d’Investissement : Etat des lieux et perspectives NIGER. Retrieved April 9, 2018, from http://www.ecreee.org/sites/default/files/presentation_of_action_agendas_and_ip _advancements_by_national_directors_for_energy_-_niger_-_niger_issa_maidagi_director_for_energy.pdf

ECREEE. (2016k). Prospectus d'Investissement : Etat des lieux et perspectives Sénégal. Retrieved April 9, 2018, from http://www.ecreee.org/sites/default/files/presentation_of_action_agendas_and_ip_advancements_by_national_directors_for_energy_-_senegal_-_ibrahima_niane_director_for_energy.pdf

ECREEE. (2016l). Prospectus d'Investissement : Etat des lieux et perspectives TOGO. Retrieved April 9, 2018, from http://www.ecreee.org/sites/default/files/presentation_of_action_agendas_and_ip_advancements_by_national_directors_for_energy_-_togo_-_hodabalo_assih_representative_of_director_for_energy.pdf

ECREEE. (2016m). West Africa's Sustainable Energy Market. Retrieved December 3, 2018, from http://www.ecreee.org/sites/default/files/the_renewable_energy_and_energy_efficiency_market_in_west_africa_-_mahama_kappiah_executive_director_ecreee.pdf

ECREEE. (2017). Plano de Ação Nacional no Sector das Energias renováveis (PNAER) de Guiné-Bissau Período 2015-2030. Retrieved November 11, 2018, from http://www.se4all.ecreee.org/sites/default/files/plano_de_acao_nacional_no_sector_das_energias_renovaveis_paner_para_a_guine-bissau.pdf

Edenhofer, O. (2015). *Climate change 2014: mitigation of climate change* (Vol. 3). Cambridge University Press.

Ellabban, O., Abu-Rub, H. and Blaabjerg, F. (2014). Renewable energy resources: Current status, future prospects and their enabling technology. *Renewable and Sustainable Energy Reviews*, *39*, 748–764. http://doi.org/10.1016/J.RSER.2014.07.113

Ettah, E. B., Nawabueze, O. J. and Njar, G. N. (2011). The relationship between solar radiation and the efficiency of solar panels in Port Harcourt Nigeria. *International Journal of Applied Science and Technology, 1*(4).

Fant, C., Schlosser, C. A. and Strzepek, K. (2016). The impact of climate change on wind and solar resources in southern Africa. *Applied Energy, 161*, 556–564.

Fesharaki, V. J., Dehghani, M., Fesharaki, J. J. and Tavasoli, H. (2011). The effect of temperature on photovoltaic cell efficiency. In *Proceedings of the 1stInternational Conference on Emerging Trends in Energy Conservation--ETEC, Tehran, Iran* (pp. 20–21).

Flaounas, E., Bastin, S. and Janicot, S. (2011). Regional climate modelling of the 2006 West African monsoon: sensitivity to convection and planetary boundary layer parameterisation using WRF. *Climate Dynamics*, *36*(5–6), 1083–1105.

Fouquart, Y. and Bonnel, B. (1980). Computations of solar heating of the earth's atmosphere- A new parameterization. *Beitraege Zur Physik Der Atmosphaere, 53*, 35–62.

Gao, L. (2013). *Validation and statistical downscaling of ERA-Interim reanalysis data for integrated applications*. lmu.

Gbobaniyi, E., Sarr, A., Sylla, M. B., Diallo, I., Lennard, C., Dosio, A., … others. (2014). Climatology, annual cycle and interannual variability of precipitation and temperature in CORDEX simulations over West Africa. *International Journal of Climatology*, *34*(7), 2241–2257.

Ghitas, A. E. (2012). Studying the effect of spectral variations intensity of the incident solar radiation on the Si solar cells performance. *NRIAG Journal of Astronomy and Geophysics, 1*(2), 165–171. http://doi.org/10.1016/J.NRJAG.2012.12.013

Ghosh, T. K. and Prelas, M. A. (2011). *Energy resources and systems: volume 2: renewable resources* (Vol. 2). Springer Science and Business Media.

Gilani, S. I.-H., Dimas, F. A. R., Shiraz, M. and others. (2011). Hourly solar radiation estimation using ambient temperature and relative humidity data. *International Journal of Environmental Science and Development, 2*(3), 188–193.

Giorgetta, M. and Wild, M. (1995). *The water vapour continuum and its representation in ECHAM4*. Max-Planck-Institut für Meteorologie.

Giorgi, F. (2010). Uncertainties in climate change projections, from the global to the regional scale. *EPJ Web of Conferences*, *9*, 115–129.

http://doi.org/10.1051/epjconf/201009009

Giorgi, F., Jones, C. and Asrar, G. R. (2009). Addressing climate information needs at the regional level : the CORDEX framework, *58*(July), 175–183.

Gnansounou, E. (2008). Boosting the electricity sector in West Africa: An integrative vision. *International Association for Energy Economics*, *17*, 23–29.

Griffith, J. S., Rathod, M. S. and Paslaski, J. (1981). Some tests of flat plate photovoltaic module cell temperatures in simulated field conditions. In *15th Photovoltaic Specialists Conference* (pp. 822–830).

Gwandu, B. A. L. and Creasey, D. J. (1995). Humidity: A factor in the appropriate positioning of a photovoltaic power station. *Renewable Energy*, *6*(3), 313–316. http://doi.org/10.1016/0960-1481(95)00073-S

Hagemann, S. (2002). An improved land surface parameter dataset for global and regional climate models.

Hall, N. M. J. and Peyrillé, P. (2006). Dynamics of the West African monsoon. In *Journal de Physique IV (Proceedings)* (Vol. 139, pp. 81–99).

Hamdi, R. T. A., Hafad, S. A., Kazem, H. A. and Chaichan, M. T. (2018). Humidity impact on photovoltaic cells performance: A review. *International Journal of Recent Engineering Research and Development (IJRERD)*, *3*(11), 27–37.

Hersbach, H., Poli, P. and Dee, D. (2015). 18 The observation feedback archive for the ICOADS and ISPD data sets.

Herzog, H.-J., Vogel, G. and Schubert, U. (2002). LLM--a nonhydrostatic model applied to high-resolving simulations of turbulent fluxes over heterogeneous terrain. *Theoretical and Applied Climatology*, *73*(1–2), 67–86.

Hewson, E. W. (1975). Generation of power from the wind. *Bulletin of the American Meteorological Society*, *56*(7), 660–675.

Holton, J. R., Wallace, J. M. and Young, J. A. (1971). On boundary layer dynamics and the ITCZ. *Journal of the Atmospheric Sciences*, *28*(2), 275–280.

Hong, S.-Y., Dudhia, J. and Chen, S.-H. (2004). A revised approach to ice microphysical processes for the bulk parameterization of clouds and precipitation.

Monthly Weather Review, *132*(1), 103–120.

Houghton, J. T., Ding, Y., Griggs, D. J., Noguer, M., Van Der Linden, P. J., Dai, X., … Johnson, C. A. (2001). Contribution of working group I to the third assessment report of the intergovernmental panel on climate change. *Climate Change 2001: The Scientific Basis*, *388*.

Houze Jr, R. A. and Betts, A. K. (1981). Convection in GATE. *Reviews of Geophysics*, *19*(4), 541–576.

Huber, I., Bugliaro, L., Ponater, M., Garny, H., Emde, C. and Mayer, B. (2016). Do climate models project changes in solar resources? *Solar Energy*, *129*, 65–84. http://doi.org/10.1016/J.SOLENER.2015.12.016

Hulme, M. (2016). 1.5 C and climate research after the Paris Agreement. *Nature Climate Change*, *6*(3), 222.

Iacono, M. J., Delamere, J. S., Mlawer, E. J., Shephard, M. W., Clough, S. A. and Collins, W. D. (2008). Radiative forcing by long-lived greenhouse gases: Calculations with the AER radiative transfer models. *Journal of Geophysical Research: Atmospheres*, *113*(D13).

Ibrahim, H. and Anani, N. (2017). Variations of PV module parameters with irradiance and temperature. *Energy Procedia*, *134*, 276–285. http://doi.org/10.1016/J.EGYPRO.2017.09.617

International Energy Agency (IEA). (2017). Energy Access Outlook 2017 From poverty to prosperity. Retrieved February 3, 2018, from https://www.iea.org/publications/freepublications/publication/WEO2017SpecialReport_EnergyAccessOutlook.pdf

International Energy Agency (IEA). (2018). Recent trends in solar PV. Retrieved October 12, 2018, from https://www.iea.org/tcep/power/renewables/solar/

IPCC. (2007a). *Climate change 2007-the physical science basis: Working group I contribution to the fourth assessment report of the IPCC* (Vol. 4). Cambridge University Press.

IPCC. (2007b). REPORT OF THE NINETEENTH SESSION OF THE INTERGOVERNMENTAL PANEL ON CLIMATE CHANGE (IPCC) Geneva, 17-20 (am only) April 2002.

Janjić, Z. I. (1994). The step-mountain eta coordinate model: Further developments of the convection, viscous sublayer, and turbulence closure schemes. *Monthly Weather Review*, *122*(5), 927–945.

Jantsch, M., Stoll, M., Roth, W., Kaiser, R., Schmidt, H. and Schmid, J. (1991). The Effect of Tilt Angle and Voltage Conditions on PV System Performance An Experimental Investigation. In *Tenth EC Photovoltaic Solar Energy Conference* (pp. 431–434).

Jerez, S., López-Romero, J. M., Turco, M., Jiménez-Guerrero, P., Vautard, R. and Montávez, J. P. (2018). Impact of evolving greenhouse gas forcing on the warming signal in regional climate model experiments. *Nature Communications*, *9*(1), 1304.

Jerez, S., Tobin, I., Vautard, R., Montávez, J. P., López-Romero, J. M., Thais, F., … others. (2015). The impact of climate change on photovoltaic power generation in Europe. *Nature Communications*, *6*, 10014.

Jiao, Y. and Jones, C. (2008). Comparison studies of cloud-and convection-related processes simulated by the Canadian Regional Climate Model over the Pacific Ocean. *Monthly Weather Review*, *136*(11), 4168–4187.

Johnson, D. L. and Erhardt, R. J. (2016). Projected impacts of climate change on wind energy density in the United States. *Renewable Energy*, *85*, 66–73. http://doi.org/10.1016/j.renene.2015.06.005

Kain, J. S. (2004). The Kain--Fritsch convective parameterization: an update. *Journal of Applied Meteorology*, *43*(1), 170–181.

Kaldellis, J. K., Kapsali, M. and Kavadias, K. A. (2014). Temperature and wind speed impact on the efficiency of PV installations. Experience obtained from outdoor measurements in Greece. *Renewable Energy*, *66*, 612–624.

Kalnay, E., Kanamitsu, M., Kistler, R., Collins, W., Deaven, D., Gandin, L., … others. (1996). The NCEP/NCAR 40-year reanalysis project. *Bulletin of the American Meteorological Society*, *77*(3), 437–471.

Kanamitsu, M., Ebisuzaki, W., Woollen, J., Yang, S.-K., Hnilo, J. J., Fiorino, M. and

Potter, G. L. (2002). Ncep--doe amip-ii reanalysis (r-2). *Bulletin of the American Meteorological Society, 83*(11), 1631–1644.

Kazem, H. A. and Chaichan, M. T. (2015). Effect of humidity on photovoltaic performance based on experimental study. *International Journal of Applied Engineering Research (IJAER), 10*(23), 43572–43577.

Kazem, H. A. and Chaichan, M. T. (2016). The impact of using solar colored filters to cover the PV panel on its outcomes. *Bulletin Journal*, *2*(7), 464–469.

Kazem, H. A., Chaichan, M. T., Al-Shezawi, I. M., Al-Saidi, H. S., Al-Rubkhi, H. S., Al-sinani, K. and Al-Waeli, A. H. A. (2012). Effect of Humidity on the PV Performance in Oman.

Klein, C., Heinzeller, D., Bliefernicht, J. and Kunstmann, H. (2015). Variability of West African monsoon patterns generated by a WRF multi-physics ensemble. *Climate Dynamics*, *45*(9–10), 2733–2755.

Klutse, N. A. B., Ajayi, V. O., Gbobaniyi, E. O., Egbebiyi, T. S., Kouadio, K., Nkrumah, F., … others. (2018). Potential impact of 1.5° C and 2° C global warming on consecutive dry and wet days over West Africa. *Environmental Research Letters*, *13*(5), 55013.

Klutse, N. A. B., Sylla, M. B., Diallo, I., Sarr, A., Dosio, A., Diedhiou, A., … others. (2016). Daily characteristics of West African summer monsoon precipitation in CORDEX simulations. *Theoretical and Applied Climatology*, *123*(1–2), 369–386.

Knippertz, P. and Fink, A. H. (2008). Dry-season precipitation in tropical West Africa and its relation to forcing from the extratropics. *Monthly Weather Review*, *136*(9), 3579–3596.

Knippertz, P., Tesche, M., Heinold, B., Kandler, K., Toledano, C. and Esselborn, M. (2011). Dust mobilization and aerosol transport from West Africa to Cape Verde—a meteorological overview of SAMUM-2. *Tellus B*, *63*(4), 430–447.

Koehl, M., Heck, M., Wiesmeier, S. and Wirth, J. (2011). Modeling of the nominal operating cell temperature based on outdoor weathering. *Solar Energy Materials and Solar Cells*, *95*(7), 1638–1646. http://doi.org/10.1016/J.SOLMAT.2011.01.020

Konstantinidis, E. I. and Botsaris, P. N. (2016). Wind turbines: current status, obstacles, trends and technologies. In *IOP Conference Series: Materials Science and Engineering* (Vol. 161, p. 12079).

Kothe, S., Pfeifroth, U., Cremer, R., Trentmann, J. and Hollmann, R. (2017). A satellite-based sunshine duration climate data record for Europe and Africa. *Remote Sensing*, *9*(5), 429.

Kumi, N. and Abiodun, B. J. (2018). Potential impacts of 1.5° C and 2° C global warming on rainfall onset, cessation and length of rainy season in West Africa. *Environmental Research Letters*, *13*(5), 55009.

Kurtz, S., Whitfield, K., Miller, D., Joyce, J., Wohlgemuth, J., Kempe, M., … Zgonena, T. (2009). Evaluation of high-temperature exposure of rack-mounted photovoltaic modules. In *Photovoltaic Specialists Conference (PVSC), 2009 34th IEEE* (pp. 2399–2404).

Lacis, A. A. and Hansen, J. (1974). A parameterization for the absorption of solar radiation in the earth’s atmosphere. *Journal of the Atmospheric Sciences*, *31*(1), 118–133.

Lavaysse, C., Flamant, C., Janicot, S., Parker, D. J., Lafore, J.-P., Sultan, B. and Pelon, J. (2009). Seasonal evolution of the West African heat low: a climatological perspective. *Climate Dynamics*, *33*(2–3), 313–330.

Lee, J.-Y. and Wang, B. (2014). Future change of global monsoon in the CMIP5. *Climate Dynamics*, *42*(1–2), 101–119.

Lee, R. (2011). The outlook for population growth. *Science*, *333*(6042), 569–573.

Leggett, J., Pepper, W. J., Swart, R. J., Edmonds, J., Meira Filho, L. G., Mintzer, I. and Wang, M. X. (1992). Emissions scenarios for the IPCC: an update. *Climate Change*, 69–95.

Lenderink, G. and Holtslag, A. A. M. (2004). An updated length-scale formulation for turbulent mixing in clear and cloudy boundary layers. *Quarterly Journal of the Royal Meteorological Society*, *130*(604), 3405–3427.

Li, R., Jin, J., Wang, S.-Y. S. and Gillies, R. R. (2014). Significant Impacts of Radiation Physics in the WRF Model on the Precipitation and Dynamics of the

West African Monsoon. *Climate Dynamics*.

Lohmann, U. and Roeckner, E. (1996). Design and performance of a new cloud microphysics scheme developed for the ECHAM general circulation model. *Climate Dynamics*, *12*(8), 557–572.

Louis, J.-F. (1979). A parametric model of vertical eddy fluxes in the atmosphere. *Boundary-Layer Meteorology*, *17*(2), 187–202.

Lurwan, S. M., Mariun, N., Hizam, H., Radzi, M. A. M. and Zakaria, A. (2014). Predicting power output of photovoltaic systems with solar radiation model. In *Power and Energy (PECon), 2014 IEEE International Conference on* (pp. 304–308).

Madlener, R. and Sunak, Y. (2011). Impacts of urbanization on urban structures and energy demand: What can we learn for urban energy planning and urbanization management? *Sustainable Cities and Society*, *1*(1), 45–53. http://doi.org/10.1016/J.SCS.2010.08.006

Mariotti, L., Diallo, I., Coppola, E. and Giorgi, F. (2014). Seasonal and intraseasonal changes of African monsoon climates in 21st century CORDEX projections. *Climatic Change*, *125*(1), 53–65. http://doi.org/10.1007/s10584-014-1097-0

Mavromatakis, F., Makrides, G., Georghiou, G., Pothrakis, A., Franghiadakis, Y., Drakakis, E. and Koudoumas, E. (2010). Modeling the photovoltaic potential of a site. *Renewable Energy*, *35*(7), 1387–1390.

Mba, W. P., Longandjo, G.-N. T., Moufouma-Okia, W., Bell, J.-P., James, R., Vondou, D. A., … others. (2018). Consequences of 1.5° C and 2° C global warming levels for temperature and precipitation changes over Central Africa. *Environmental Research Letters*, *13*(5), 55011.

Mellor, G. L. and Yamada, T. (1982). Development of a turbulence closure model for geophysical fluid problems. *Reviews of Geophysics*, *20*(4), 851–875.

Miller, L. M., Gans, F. and Kleidon, A. (2011). Estimating maximum global land surface wind power extractability and associated climatic consequences. *Earth System Dynamics*, *2*, 1–12.

Mlawer, E. J., Taubman, S. J., Brown, P. D., Iacono, M. J. and Clough, S. A. (1997).

Radiative transfer for inhomogeneous atmospheres: RRTM, a validated correlated-k model for the longwave. *Journal of Geophysical Research: Atmospheres, 102*(D14), 16663–16682.

Moiloa, B. H. E. (2009). Geographical Information Systems for Strategic Wind Energy Site Selection. *Vrije Universiteit Amsterdam Netherlands*.

Monerie, P.-A., Roucou, P. and Fontaine, B. (2013). Mid-century effects of Climate Change on African monsoon dynamics using the A1B emission scenario. *International Journal of Climatology, 33*(4), 881–896.

Monin, A. S. and Obukhov, A. M. F. (1954). Basic laws of turbulent mixing in the surface layer of the atmosphere. *Contrib. Geophys. Inst. Acad. Sci. USSR, 151*(163), e187.

Mooney, P. A., Mulligan, F. J. and Fealy, R. (2011). Comparison of ERA-40, ERA-Interim and NCEP/NCAR reanalysis data with observed surface air temperatures over Ireland. *International Journal of Climatology, 31*(4), 545–557.

Morcrette, J.-J. (1990). Impact of changes to the radiation transfer parameterizations plus cloud optical. Properties in the ECMWF model. *Monthly Weather Review, 118*(4), 847–873.

Moss, R. H., Edmonds, J. A., Hibbard, K. A., Manning, M. R., Rose, S. K., Van Vuuren, D. P., … others. (2010). The next generation of scenarios for climate change research and assessment. *Nature, 463*(7282), 747.

Nakicenovic, N., Alcamo, J., Grubler, A., Riahi, K., Roehrl, R. A., Rogner, H.-H. and Victor, N. (2000). *Special report on emissions scenarios (SRES), a special report of Working Group III of the intergovernmental panel on climate change*. Cambridge University Press.

Nfaoui, H. et al. (1998). Wind characteristics and wind energy potential in Morocco. *Solar Energy, 63*(1), 51–60.

Nicholson, S. E. (2009). A revised picture of the structure of the “monsoon” and land ITCZ over West Africa. *Climate Dynamics, 32*(7–8), 1155–1171.

Nicholson, S. E. (2013). The West African Sahel: A review of recent studies on the rainfall regime and its interannual variability. *ISRN Meteorology, 2013*.

Nicholson, S. E. and Grist, J. P. (2001). A conceptual model for understanding rainfall variability in the West African Sahel on interannual and interdecadal timescales. *International Journal of Climatology: A Journal of the Royal Meteorological Society*, *21*(14), 1733–1757.

Nikulin, G., Jones, C., Giorgi, F., Asrar, G., Büchner, M., Cerezo-Mota, R., … others. (2012). Precipitation climatology in an ensemble of CORDEX-Africa regional climate simulations. *Journal of Climate*, *25*(18), 6057–6078.

Njoku, H. O. (2013). Solar photovoltaic potential in Nigeria. *Journal of Energy Engineering*, *140*(2), 4013020.

NOAA. (2018). THE NOAA ANNUAL GREENHOUSE GAS INDEX (AGGI). Retrieved November 28, 2018, from https://www.esrl.noaa.gov/gmd/aggi/aggi.html

O'Hirok, W. and Gautier, C. (2003). Absorption of shortwave radiation in a cloudy atmosphere: Observed and theoretical estimates during the second Atmospheric Radiation Measurement Enhanced Shortwave Experiment (ARESE). *Journal of Geophysical Research: Atmospheres*, *108*(D14).

Olukan, T. A. and Emziane, M. (2014). A Comparative Analysis of PV Module Temperature Models. *Energy Procedia*, *62*, 694–703. http://doi.org/10.1016/J.EGYPRO.2014.12.433

Oreskes, N. (2004). The scientific consensus on climate change. *Science*, *306*(5702), 1686.

Otth, D. H. and Ross, R. G. (1983). Assessing photovoltaic module degradation and lifetime from long term environmental tests. In *29th Institute of Environmental Sciences Technical Meeting, Los Angeles, CA* (pp. 121–126).

Ouammi, A., Sacile, R. and Mimet, A. (2010). Wind energy potential in Liguria region, *14*, 289–300. http://doi.org/10.1016/j.rser.2009.07.006

Palmer, T. N. (2016). A personal perspective on modelling the climate system. *Proc. R. Soc. A*, *472*(2188), 20150772.

Panagea, I. S., Tsanis, I. K., Koutroulis, A. G. and Grillakis, M. G. (2014). Climate change impact on photovoltaic energy output: the case of Greece. *Advances in*

Meteorology, *2014*.

Pandian, P. K. and Iyappan, L. (2012). DEVELOPING A GEOSPATIAL BASED APPROACH TO LOCATE WIND FARMS IN POLLACHI TALUK, TAMIL NADU, INDIA.

Panjwani, M. K. and Narejo, G. B. (2014). Effect of humidity on the efficiency of solar cell (photovoltaic). *International Journal of Engineering Research and General Science*, *2*(4), 499–503.

Parker, D. J. and Diop-Kane, M. (2017). *Meteorology of tropical West Africa: The forecasters' handbook*. John Wiley and Sons.

Parker, D. J., Thorncroft, C. D., Burton, R. R. and Diongue-Niang, A. (2005). Analysis of the African easterly jet, using aircraft observations from the JET2000 experiment. *Quarterly Journal of the Royal Meteorological Society*, *131*(608), 1461–1482.

Patel, M. R. (2005). *Wind and solar power systems: design, analysis, and operation*. CRC press.

Patt, A., Pfenninger, S. and Lilliestam, J. (2013). Vulnerability of solar energy infrastructure and output to climate change. *Climatic Change*, *121*(1), 93–102.

Penick, T. and Louk, B. (1998). Photovoltaic power generation. *Final Report Presented to Gale Greenleaf on December*, *4*, 1998.

Pfeifroth, U., Sanchez-Lorenzo, A., Manara, V., Trentmann, J. and Hollmann, R. (2018). Trends and Variability of Surface Solar Radiation in Europe Based On Surface-and Satellite-Based Data Records. *Journal of Geophysical Research: Atmospheres*, *123*(3), 1735–1754.

Pinker, R. T., Zhang, B. and Dutton, E. G. (2005). Do satellites detect trends in surface solar radiation? *Science*, *308*(5723), 850–854.

Plana-Fattori, A., de Souza, E. P. and Chagas, J. C. S. (1997). Absorption of solar radiation by water vapor in the atmosphere. Part I: A comparison between selected parameterizations and reference results. *Revista Brasileira de Geof{\'\i}sica*, *15*(3), 275–290.

Poli, P., Hersbach, H., Tan, D., Dee, D., Thepaut, J.-N., Simmons, A., … others. (2013). *The data assimilation system and initial performance evaluation of the ECMWF pilot reanalysis of the 20th-century assimilating surface observations only (ERA-20C)*. European Centre for Medium Range Weather Forecasts.

Possner, A. and Caldeira, K. (2017). Geophysical potential for wind energy over the open oceans. *Proceedings of the National Academy of Sciences*, *114*(43), 11338–11343.

Powers, J. G., Klemp, J. B., Skamarock, W. C., Davis, C. A., Dudhia, J., Gill, D. O., … others. (2017). The weather research and forecasting model: Overview, system efforts, and future directions. *Bulletin of the American Meteorological Society*, *98*(8), 1717–1737.

Price, T. J. (2005). James Blyth—Britain's first modern wind power pioneer. *Wind Engineering*, *29*(3), 191–200.

Rahim, M., Yoshino, J., Doi, Y. and Yasuda, T. (2012). Effects of global warming on the average wind speed field in Central Japan. *Journal of Sustainable Energy and Environment*, *3*(4).

Ramaswamy, V. and Freidenreich, S. M. (1991). Solar radiative line-by-line determination of water vapor absorption and water cloud extinction in inhomogeneous atmospheres. *Journal of Geophysical Research: Atmospheres*, *96*(D5), 9133–9157.

Ramel, R., Gallée, H. and Messager, C. (2006). On the northward shift of the West African monsoon. *Climate Dynamics*, *26*(4), 429–440. http://doi.org/10.1007/s00382-005-0093-5

Randall, D. A., Wood, R. A., Bony, S., Colman, R., Fichefet, T., Fyfe, J., … others. (2007). Climate models and their evaluation. In *Climate change 2007: The physical science basis. Contribution of Working Group I to the Fourth Assessment Report of the IPCC (FAR)* (pp. 589–662). Cambridge University Press.

Rechid, D., Raddatz, T. J. and Jacob, D. (2009). Parameterization of snow-free land surface albedo as a function of vegetation phenology based on MODIS data and applied in climate modelling. *Theoretical and Applied Climatology*, *95*(3–4), 245–255.

Ren, D. (2010). Effects of global warming on wind energy availability. *Journal of Renewable and Sustainable Energy*, *2*(5), 52301.

REN21. (2018). RENEWABLES 2018 GLOBAL STATUS REPORT. Retrieved October 12, 2018, from http://www.ren21.net/wp-content/uploads/2018/06/17-8652_GSR2018_FullReport_web_final_.pdf

Riahi, K., Rao, S., Krey, V., Cho, C., Chirkov, V. and Fischer, G. (2011). RCP 8 . 5 — A scenario of comparatively high greenhouse gas emissions, 33–57. http://doi.org/10.1007/s10584-011-0149-y

Ricard, J. L. and Royer, J. F. (1993). A statistical cloud scheme for use in an AGCM. In *Annales Geophysicae* (Vol. 11, pp. 1095–1115).

Ritter, B. and Geleyn, J.-F. (1992). A comprehensive radiation scheme for numerical weather prediction models with potential applications in climate simulations. *Monthly Weather Review*, *120*(2), 303–325.

Saha, S., Moorthi, S., Wu, X., Wang, J., Nadiga, S., Tripp, P., … others. (2014). The NCEP climate forecast system version 2. *Journal of Climate*, *27*(6), 2185–2208.

Samuelsson, P., Kourzeneva, E. and Mironov, D. (2010). The impact of lakes on the European climate as simulated by a regional climate model.

Sass, B. H., Rontu, L. and Räisänen, P. (1994). *HIRLAM-2 radiation scheme: Documentation and tests*. HIRLAM.

Savijärvi, H. (1990). Fast radiation parameterization schemes for mesoscale and short-range forecast models. *Journal of Applied Meteorology*, *29*(6), 437–447.

Schleussner, C.-F., Lissner, T. K., Fischer, E. M., Wohland, J., Perrette, M., Golly, A., … others. (2016). Differential climate impacts for policy-relevant limits to global warming: the case of 1.5 C and 2 C. *Earth System Dynamics*, *7*, 327–351.

Schlichting, H. and Gersten, K. (2000). Boundary Layer Theory Springer-Verlag. *Berlin, Heidelberg*.

Schulz, J. P., Dümenil, L., Polcher, J., Schlosser, C. A. and Xue, Y. (1998). Land surface energy and moisture fluxes: Comparing three models. *Journal of Applied*

Meteorology, *37*(3), 288–307.

Schwingshackl, C., Hirschi, M. and Seneviratne, S. I. (2018). Global contributions of incoming radiation and land surface conditions to maximum near-surface air temperature variability and trend. *Geophysical Research Letters*, *45*(10), 5034–5044.

Schwingshackl, C., Petitta, M., Wagner, J. E., Belluardo, G., Moser, D., Castelli, M., … Tetzlaff, A. (2013). Wind effect on PV module temperature: Analysis of different techniques for an accurate estimation. *Energy Procedia*, *40,* 77–86. http://doi.org/10.1016/j.egypro.2013.08.010

SE4ALL. (2015). Plan d'Action National de l'Initiative Energie Durable Pour Tous « SE4ALL ». Retrieved April 9, 2018, from https://www.se4all-africa.org/fileadmin/uploads/se4all/Documents/Country_AAs/Burkina_Faso_Agenda_d'Action_de_L'initiative_Energie_Durable_Pour_Tous.pdf

Silang, A., Uy, S. N., Dado, J. M., Cruz, F. A., Narisma, G., Libatique, N. and Tangonan, G. (2014). Wind energy projection for the Philippines based on climate change modeling. *Energy Procedia*, *52,* 26–37.

Sirisamphanwong, C. and Sirisamphanwong, C. (2013). The Effect of Photon Flux Density and Module Temperature on Power Output of Photovoltaic Array. *Energy Procedia, 34,* 430–438. http://doi.org/10.1016/J.EGYPRO.2013.06.771

Skamarock, W. C., Klemp, J. B., Dudhia, J., Gill, D. O., Barker, D. M., Wang, W. and Powers, J. G. (2005). *A description of the advanced research WRF version 2*.

Skoplaki, E., Boudouvis, A. G. and Palyvos, J. A. (2008). A simple correlation for the operating temperature of photovoltaic modules of arbitrary mounting. *Solar Energy Materials and Solar Cells*, *92*(11), 1393–1402. http://doi.org/10.1016/J.SOLMAT.2008.05.016

Skoplaki, E. and Palyvos, J. A. (2009). On the temperature dependence of photovoltaic module electrical performance: A review of efficiency/power correlations. *Solar Energy*, *83*(5), 614–624. http://doi.org/10.1016/J.SOLENER.2008.10.008

Smithers, J. and Smit, B. (1997). Human adaptation to climatic variability and change. *Global Environmental Change, 7*(2), 129–146. http://doi.org/10.1016/S0959-

3780(97)00003-4

Stephens, G. L. and Tsay, S.-C. (1990). On the cloud absorption anomaly. *Quarterly Journal of the Royal Meteorological Society*, *116*(493), 671–704.

Stöckli, R. and Stöckli, R. (2013). *The HelioMont surface solar radiation processing*. Bundesamt für Meteorologie und Klimatologie, MeteoSchweiz.

Strandberg, G., Bärring, L., Hansson, U., Jansson, C., Jones, C., Kjellström, E., … Ullerstig, A. (2015). *CORDEX scenarios for Europe from the Rossby Centre regional climate model RCA4*. SMHI.

Stull, R. B. (2012). *An introduction to boundary layer meteorology* (Vol. 13). Springer Science and Business Media.

Sultan, B. and Gaetani, M. (2016). Agriculture in West Africa in the Twenty-first Century: climate change and impacts scenarios, and potential for adaptation. *Frontiers in Plant Science*, *7*.

Sylla, M. B., Diallo, I. and Pal, J. S. (2013). West African monsoon in state-of-the-science regional climate models. *Climate Variability—Regional and Thematic Patterns*, *10*, 55140.

Sylla, M. B., Elguindi, N., Giorgi, F. and Wisser, D. (2016). Projected robust shift of climate zones over West Africa in response to anthropogenic climate change for the late 21st century. *Climatic Change*, *134*(1), 241–253. http://doi.org/10.1007/s10584-015-1522-z

Sylla, M. B., Gaye, A. T., Jenkins, G. S., Pal, J. S. and Giorgi, F. (2010a). Consistency of projected drought over the Sahel with changes in the monsoon circulation and extremes in a regional climate model projections. *Journal of Geophysical Research*, *115*(D16), D16108. http://doi.org/10.1029/2009JD012983

Sylla, M. B., Gaye, A. T., Jenkins, G. S., Pal, J. S. and Giorgi, F. (2010b). Consistency of projected drought over the Sahel with changes in the monsoon circulation and extremes in a regional climate model projections. *Journal of Geophysical Research Atmospheres*, *115*(16), 1–9. http://doi.org/10.1029/2009JD012983

Sylla, M. B., Giorgi, F., Pal, J. S., Gibba, P., Kebe, I. and Nikiema, M. (2015). Projected changes in the annual cycle of high-intensity precipitation events over

West Africa for the late twenty-first century. *Journal of Climate*, *28*(16), 6475–6488.

Sylla, M. B., Giorgi, F., Ruti, P. M., Calmanti, S. and Dell'Aquila, A. (2011). The impact of deep convection on the West African summer monsoon climate: a regional climate model sensitivity study. *Quarterly Journal of the Royal Meteorological Society*, *137*(659), 1417–1430.

Sylla, M. B., Nikiema, P. M., Gibba, P., Kebe, I. and Klutse, N. A. B. (2016). Climate Change over West Africa: Recent Trends and Future Projections. In *Adaptation to Climate Change and Variability in Rural West Africa* (pp. 25–40). Springer.

TamizhMani, G., Ji, L., Tang, Y., Petacci, L. and Osterwald, C. (2003). Photovoltaic module thermal/wind performance: long-term monitoring and model development for energy rating. In *NCPV and Solar Program Review Meeting Proceedings, 24-26 March 2003, Denver, Colorado (CD-ROM).*

Tang, C., Morel, B., Wild, M., Pohl, B., Abiodun, B. and Bessafi, M. (2018). Numerical simulation of surface solar radiation over Southern Africa. Part 1: Evaluation of regional and global climate models. *Climate Dynamics*. http://doi.org/10.1007/s00382-018-4143-1

Taylor, K. E. (2005). Taylor diagram primer. *Work. Pap*, 1–4.

Taylor, K. E., Stouffer, R. J. and Meehl, G. A. (2012). An overview of CMIP5 and the experiment design. *Bulletin of the American Meteorological Society*, *93*(4), 485–498.

The World Bank. (2018a). Access to electricity (% of population). Retrieved November 30, 2018, from https://data.worldbank.org/indicator/EG.ELC.ACCS.ZS

The World Bank. (2018b). Population, total. Retrieved November 30, 2018, from https://data.worldbank.org/indicator/SP.POP.TOTL

The World Bank. (2018c). Regional Power Trade in West Africa Offers Promise of Affordable, Reliable Electricity. Retrieved December 3, 2018, from https://www.worldbank.org/en/news/feature/2018/04/20/regional-power-trade-west-africa-offers-promise-affordable-reliable-electricity

Tiedtke, M. (1989). A comprehensive mass flux scheme for cumulus parameterization in large-scale models. *Monthly Weather Review, 117*(8), 1779–1800.

Tiedtke, M. (1993). Representation of clouds in large-scale models. *Monthly Weather Review*, *121*(11), 3040–3061.

Tiedtke, M. (1996). An extension of cloud-radiation parameterization in the ECMWF model: The representation of subgrid-scale variations of optical depth. *Monthly Weather Review, 124*(4), 745–750.

Tobin, I., Vautard, R., Balog, I., Bréon, F.-M., Jerez, S., Ruti, P. M., … Yiou, P. (2015). Assessing climate change impacts on European wind energy from ENSEMBLES high-resolution climate projections. *Climatic Change*, *128*(1–2), 99–112.

Tompkins, A. M. (2002). A prognostic parameterization for the subgrid-scale variability of water vapor and clouds in large-scale models and its use to diagnose cloud cover. *Journal of the Atmospheric Sciences, 59*(12), 1917–1942.

Touati, F. A., Al-Hitmi, M. A. and Bouchech, H. J. (2013). Study of the effects of dust, relative humidity, and temperature on solar PV performance in Doha: comparison between monocrystalline and amorphous PVS. *International Journal of Green Energy*, *10*(7), 680–689.

Touré, N., Konaré, A. and Silué, S. (2012). Intercontinental transport and climatic impact of Saharan and Sahelian dust. *Advances in Meteorology, 2012*.

UNFCCC. (2015). Paris Agreement: essential elements. Retrieved September 3, 2017, from http://unfccc.int/paris_agreement/items/9485.php

USAID. (2018a). Burkina Faso POWER AFRICA FACT SHEET. Retrieved April 9, 2018, from https://www.usaid.gov/powerafrica/burkina-faso

USAID. (2018b). Senegal POWER AFRICA FACT SHEET. Retrieved April 9, 2018, from https://www.usaid.gov/powerafrica/senegal

van Vuuren, D. P., Edmonds, J., Kainuma, M., Riahi, K., Thomson, A., Hibbard, K., … Rose, S. K. (2011). The representative concentration pathways: an overview. *Climatic Change*, *109*(1), 5. http://doi.org/10.1007/s10584-011-0148-z

Vilar (ed) (2012). Renewable energy in western africa: situation, experiences and tendencies. Retrieved December 3, 2018, from www.ecreee.org/sites/default/files/renewable_energy_in_west_africa_0.pdf

Vitousek, P. M., Mooney, H. A., Lubchenco, J. and Melillo, J. M. (1997). Human domination of Earth's ecosystems. *Science, 277*(5325), 494–499.

Walker, R. P. and Swift, A. (2015). *Wind energy essentials: Societal, economic, and environmental Impacts*. John Wiley and Sons.

Wang, Q., Wu, S., Zeng, Y. and Wu, B. (2016). Exploring the relationship between urbanization, energy consumption, and CO2 emissions in different provinces of China. *Renewable and Sustainable Energy Reviews, 54*, 1563–1579. http://doi.org/10.1016/J.RSER.2015.10.090

Wild, M., Folini, D., Henschel, F., Fischer, N. and Müller, B. (2015). Projections of long-term changes in solar radiation based on CMIP5 climate models and their influence on energy yields of photovoltaic systems. *Solar Energy, 116*, 12–24. http://doi.org/10.1016/J.SOLENER.2015.03.039

Wild, M., Gilgen, H., Roesch, A., Ohmura, A., Long, C. N., Dutton, E. G., … Tsvetkov, A. (2005). From dimming to brightening: Decadal changes in solar radiation at Earth's surface. *Science*, *308*(5723), 847–850.

Williamson, L. E., Connor, H. and Moezzi, M. (2009). Climate-proofing energy systems. *Helio International*.

Zang, H., Guo, M., Wei, Z. and Sun, G. (2016). Determination of the optimal tilt angle of solar collectors for different climates of china. *Sustainability*, *8*(7), 654.

Zdanowicz, T., Rodziewicz, T. and Waclawek, M. Z. (2003). Effect of air mass factor on the performance of different type of PV modules. In *Proceedings of the 3rd World Conference on Photovoltaic Energy Conversion* (pp. 2019–2022).

Zempila, M.-M., Giannaros, T. M., Bais, A., Melas, D. and Kazantzidis, A. (2015). Evaluation of WRF shortwave radiation parameterizations in predicting Global Horizontal Irradiance in Greece. *Renewable Energy*, *86*, 831–840.

Zhang, C., Woodworth, P. and Gu, G. (2006). The seasonal cycle in the lower troposphere over West Africa from sounding observations. *Quarterly Journal of the Royal Meteorological Society*, *132*(621), 2559–2582.

Zweibel, K. and Hersch, P. (1984). *Basic photovoltaic principles and methods*. Van Nostrand Reinhold Company.